Development of an Electromagnetic Sensor for in Pipeline Inspection and Asset Management for the Water Industry

Mamadou Adama Diallo

A thesis submitted in partial fulfilment of the requirements of Liverpool John Moores University for the degree of Doctor of Philosophy (PhD)

January 2015

Abstract

In the UK, the Water Services Regulation Authority (OFWAT), estimates that for all the water and sewage companies there was over 3,365 Ml/d (megalitres per day) of water leakage in the reported period 2010 and 2011, which was still at 3094.21 Ml/day in the 2013 review. Leakage estimates do not include water siphoned illegally through unaccounted connections worsened as asset management of buried utility services has been overlooked for years. With the asset management programme framework (AMP6) due to come into effect in April 2015, water companies are expected to get more out of their existing infrastructure and making considerable investment while keeping bills reasonable for customers. Improving the management of these assets is therefore a priority, as effective asset management enables companies to reduce cost, through leakage management, to plan investments and repairs, and to evaluate operational risks by better fault prediction rather than the current reactive approach.

This research focuses on the water distribution network as an asset that include leaks and pipe infrastructure with different materials and diameters. A novel method for leak detection and asset management using an electromagnetic sensor has been developed. Trials in the laboratory showed the sensor is capable of detecting pipe types and conditions thus improving leak detection and asset management in the water industry without extensive digs and modification to existing access valves within the network for system deployment. Furthermore, the sensor would potentially benefit the gas industry by modifying the frequency of operation to match gas filled cylindrical metal structures.

Acknowledgement

I would like to thank all those who contributed in the completion of this thesis. My supervisory team; Dr Andy Shaw, for giving me the opportunity to work on this research but also for his guidance and calm when I have been in panic mode because plans seem to be scrambling, Dr Steve Wylie and Prof Ahmed Al'Shamma'a for all the guidance and support.

I extend my gratitude to the unlimited resourcefulness of Dr Jeff Cullen and Dr Alex Mason for advice on testing antennas and programming microcontrollers.

I do not forget Alan Smith and Steve Horan from the engineering workshop without whom my prototype might have "drowned" and the administrative team; Elizabeth Hoare for sorting all the paperwork, Dr Montserrat Ortoneda Pedrola and Dr Nina Wylie for chasing those last minute orders.

The UK Technology Strategic Board (TSB) for partially funding this project.

I would like to thank my Guinean and Lithuanian families for their continuous support, especially my dad Mamadou Bailo, Tonton Cherif and Tonton Soumano in Conakry to whom I am eternally grateful.

I also wish to thank my friends Dr L. Coulibaly and Illa for their time.

And last but not least, I thank my wife Sigita for her unfaltering love and understanding during these years.

Table of contents

Figures Lists

List of Table

Chapter 1: Introduction

1.1 Introduction

Leakage is considered to be any *'loss of water from the supply network, which escapes other than through controlled action'* [1]. Illegal and unaccounted connections in the water distribution network are part of these losses and water companies would financially benefit from a system that is able to offer a means to manage these assets. Utility companies such as water and electricity companies are highly dependent on the correct management of their most important asset, their distribution network.

In a country with considerable rainfall, the number of drought alerts, hose pipe bans and environmental regulations has put the 22 companies, working in the provision of water and or sewerage related services in the UK, under great pressure. Leak detection has been at the forefront of this strategy and various types of equipment are employed to find and manage leaks. Leakage not only results in water wastage but also in the inefficient use of energy required to pump the water around.

The amount of water leakage in the distribution network varies from region to region around the world. In Canada, water leakage was estimated to be as high as 35 or 45% [2] while in much better maintained networks such as in the Netherlands, this is as low as 3-7% [3]. In the UK, the Water Services Regulation Authority (OFWAT), estimates that for all the water and sewage companies there was over 3,365 Ml/d (megalitres per day) of water leakage in the reported period 2010 and 2011 [4], which is about 30%. In the 2013 review, the leakage level was still at 3094.21 Ml/day [5]. Leaks are inherent to any water network, however their volume should be within the sustainable economical level of leakage (SELL) threshold which determines the annual leakage target individually set by the water utilities companies and agreed

by the water regulator OFWAT. The total leakage is estimated by summing the potable water losses from the treatment plants to the customer's stop tap provided by the water companies. Table 1 shows a 5 year leakage targets for the companies in England and Wales.

Table 1: Company estimates leakage target – megalitres per day (Ml/d) [6]

	2010-11	2011-12	2012-13	2013-14	2014-15
Water and sewerage companies					
Anglian	212	212	211	211	211
Dŵr Cymru	190	188	186	185	184
Northumbrian-North East	150	147	144	141	141
Northumbrian-Essex & Suffolk	66	66	66	66	66
Severn Trent	483	474	468	456	453
South West	84	84	84	84	84
Southern	83	93	90	89	88
Thames	674	673	673	673	673
United Utilities	464	464	464	463	463
Wessex	71	71	71	71	71
Yorkshire	297	297	297	297	297
Water only companies					
Sembcorp Bournemouth	22	22	22	22	21
Bristol	52	51	50	49	49
Cambridge	14.0	14.0	14.0	14.0	14.0
Dee Valley	10.2	10.2	10.2	10.2	10.2
Portsmouth	30	30	30	30	30
South East	95	95	94	94	93
South Staffordshire	74	74	74	74	74
Sutton & East Surrey	25	25	25	25	25
Veolia Water Central	185	185	185	185	185
Veolia Water East	5.1	5.1	5.1	5.1	5.1
Veolia Water South East	7.9	7.8	7.7	7.6	7.5
Industry	**3,294**	**3,288**	**3,271**	**3,252**	**3,245**

Twort [7] wrote "distribution losses comprise leaks from mains, joints, valves, hydrants and washouts, and leaks from service pipes upstream of consumers' meters or boundary stopcocks". Leakage estimates do not include water siphoned illegally through unaccounted connections. The number of leaks in the network is worsened as asset management of buried utility services has been overlooked for years. There are still considerable portions of the network after trunk mains, that the water companies do not have records of [8]. This is because they were laid at a time

when the need of an accurate location was not seen as a priority. It is estimated that there are over 1.5 million km of combined water, sewer, gas and electricity services [9] of which, according to a Water UK estimate in 2008, there are 408,500 kilometres of pipes that form the water supply network in the UK [10]. With the expansion of urban areas and the increasing density of the population in these areas, a multitude of utility services are being installed. The result of this oversight is financial loss, poor service management, longer down times in the event of failure and potentially a health and safety issue for maintenance crews digging to improve or restore services. In certain areas, these unaccounted branches are sometimes discovered by chance or while investigating faults. Currently, water companies rely on reactive management in that customers notify the network of issues. Improving the management of their asset is therefore a priority as effective asset management enables companies to reduce leakage, plan investments and repairs as well as evaluate operational risks.

Despite new figures submitted by water companies to the water regulator, which showed that most were hitting the estimated leakage target. The House of Lords' Science and Technology Committee said that the "level of leakage is unacceptably high" [11] while Wu [12] estimates this wastage to be over 15% of the water produced in the UK. Fixing leaks often requires digging in urban areas, causing street congestion with a social and economic impact estimated at £667.2million [13] or £4.2billion [14] or even £5.5billion [15] per year. Regardless of which estimate is most accurate, the statutory undertakers as set by the New Roads and Street Works Act of 1991 (NRSW) are under even more pressure with the revised charges for the occupation of the highway [16]. To be able to protect and better manage the

network, a pre-emptive approach is necessary to address potential issues before they become major failures and to also find previously unrecorded pipe types and branches. It is therefore necessary to detect, identify by type, diameter and the condition of these assets without extensive excavations.

Reliable leak detection and asset management tools are required for the water industry to comply with regulations and satisfy the public demand for reduced water leakage. Several research groups are looking into, this and many solutions have been proposed. However, these have to various extents yielded poor results in field trials so far. The project, Mapping the Underworld [17] is a national initiative to accurately locate and identify the UK buried utility infrastructure with the Subsurface Utility Engineering in the US [8] advocating the use of multi-sensors and multi-frequencies as identified by Sterling [18] in the “Utility locating technologies: a summary of responses to a statement of need distributed by the federal laboratory consortium for technology transfer”.

Different techniques have been researched for leak detection including [19] using finite-difference time-domain (FDTD) method analysis to model the use of ground penetrating radar, while Castaldo [20] used time domain reflectometry that requires two wires at equal distance to be attached along the pipeline to be monitored thus requiring new pipe infrastructure to be laid.

Inari [21] developed a pig-like optical inspection tool for pipe walls with a ±0.1mm resolution for corrosion detection which used a circular optical pattern allowing a full circumferential inspection of the inner wall for defects in real time. However, practical tests showed that it was necessary to clean the pipe internal walls first [21]. Another similar pig concept was developed by NDT systems & Services in Germany

[22]. This ultrasonic tool allowed a full circumferential inspection of 0.5m to 1.4m diameter inner pipe walls over hundreds of kilometres. This modular pig design has a recording unit that stores the data collected for later processing; making it unsuitable for real-time inspection and the additional drawback is the likelihood of it becoming stuck as well as build-up on inner pipe walls affecting the ultrasonic.

A Qatar group [23] developed an acoustic wireless sensor which transmitted data to static relay stations in real-time. The system detects leakage by sensing the noise level in underground water pipelines. Results on an unburied plastic pipe showed a signal amplitude variation with the simulated leakage magnitude. Another solution is the SmartBall [24], a free flowing aluminium ball that uses acoustics technology to detect leaks in pipes that have a 150mm or larger diameter. The data is recorded and then post processed after retrieving the ball. It should be noted that regardless of these results, pig and free flowing wireless sensors tend to get stuck in the pipelines due to bends and mineral build up in the internal pipe walls, making them very difficult to locate and retrieve without excavation.

Reported results for these techniques have been inconsistent due to environmental noise, poor knowledge of pipe location and the requirement for the system to be integrated into the pipeline installation phase.

LJMU has been researching a non-destructive method of detecting leaks using electromagnetic waves. A proof of concept using an antenna connected to a vector network analyzer (VNA) through a coaxial cable showed that electromagnetic waves were able to detect leaks [25] in water distribution mains. The present research will address the need of the water industry for an asset management sensor using electromagnetic waves. This will also be used for leak detection purposes in order

to reduce the cost to the water companies and to minimise the number of dry digs. The electromagnetic sensor will be deployed into the water pipeline through existing bore hydrants utilising a deployment system developed by our project partner JD7[1] without the need to convert these traditional access points.

1.2 Aims and objectives

The main aim of this research is to develop a non-destructive inspection sensor using electromagnetic waves for leak detection and asset management for the water industry. The sensor will be capable of detecting leaks, differentiating between pipe types and diameters, as well as detecting branches connected to the pipe under test.

This project will:

- Review the current techniques used to localise leaks and manage the pipeline infrastructure.
- Investigate the propagation of electromagnetic waves in a water filled pipe to determine the asset type and/or condition.
- Design various antennas to determine the best antenna design for the sensor making better use of the objective above.
- Develop a graphical user interface (GUI) software to compare and identify pipeline features in real time. For cost saving, the user interface should allow operators to use the sensor system with minimal training.
- Develop a sensor prototype with embedded electronics capable of detecting and localising leaks or asset within a known range. The size of the sensor

[1] JD7 - is a specialized technology provider focused on Pipeline Assessments and Inspection solutions for all utility sectors. www.jd7.co.uk

should fit in the Ø118mm standard water distribution pipe.

- Evaluate the performance of the electromagnetic sensor prototype.

1.3 Research methodology and thesis structure

To achieve the aim and objectives stated in section 1.2, the following thesis methodology and structure was used.

Chapter 1, this starts by assesses the extent of water leakage through publicly available data collected by the water authorities and regulatory bodies before moving onto the literature review. This review considers both academic and industry research. It discusses existing leak detection methods and ongoing industry research, including their limitations and uses sources from leak detection companies, conference papers and journals focusing on the use of non-destructive methods for leak detection and asset management, as well as books addressing electromagnetic wave propagation in cylindrical structures and antenna design.

In chapter 2, the theory of electromagnetic waves will be reviewed and simulations of the standard DN100 water distribution, pipe modelled using CAD software, will be presented. These simulations examine the electromagnetic propagation properties. This chapter also includes the results of experimental tests which were carried out to verify the findings.

Chapter 3, expands on the models and experiments in chapter 2 and includes the antenna theory required for the design. The sensor design requirements provided by the industrial partners, in term of the deployment technique used by JD7 and the pipeline characteristics of old networks, will be considered for the selection of the antenna type using antenna theory through modelling and experimentation. The fundamental characteristics of the antennas are explored for a pipeline environment

filled with water. The chosen antenna will then be tested in the laboratory facility which consists of sections of pipes that represent those encountered in over 40% the UK water network. In addition, a water proof sensor housing is designed and tested to assess performance.

In chapter 4, experiments in leak detection using nylon rings of different thickness to simulate cracks on the pipe, and another setup with different pipe materials inserted to simulate asset management will be carried out in the laboratory. An antenna prototype connected to a VNA will be used both in the laboratory experiments and at a test site that will be provided by United Utilities[2]. The findings in this chapter will be used to shape the sensor prototype design in chapter 6.

Chapter 5 discusses the development of the sensor system to interpret the frequency sweeps generated, at this stage of the design by the VNA, and to distinguish from each of the frequency responses. The frequency sweep data gathered for the various pipe types and conditions will be stored in a database, which will then be used to match frequency responses acquired during the current test. The design of the user interface will be based on a traffic light system with minimal input requirement from the operator and applying existing analysis method within the software. The analysis used will look at different technics to compare series of data analysis with each other to identify best fit. Finally a conceptual design of the sensor system will be created based on these requirement and all the knowledge gathered in the previous chapters.

In chapter 6, components will be identified to work within the required frequency

[2] Responsible for the provision and maintenance of water supply in the UK North West region. www.unitedutilities.com

range so that a prototype can be constructed that will replicate the functionality of the VNA, by generating a frequency sweep and measuring the reflected power. An incremental design method will be adopted allowing the functionality of individual modules to be experimentally verified before integration into the full design. Off-the-shelf components will be used to test the functionality of the sensor assembly before a printed circuit board using surface mount components, is designed to fit into a water proof prototype casing in line with the dimensions set by the industrial partners. The operational performance of the fully integrated prototype is then tested using the lab rig and the results are discussed.

Finally, chapter 7 describes the novelty and benefit of the developed sensor system and reviews the main findings of the research. The thesis will be completed by proposing future work to further improve the electromagnetic sensor system.

The development methodology is summarised in Figure 1.

.

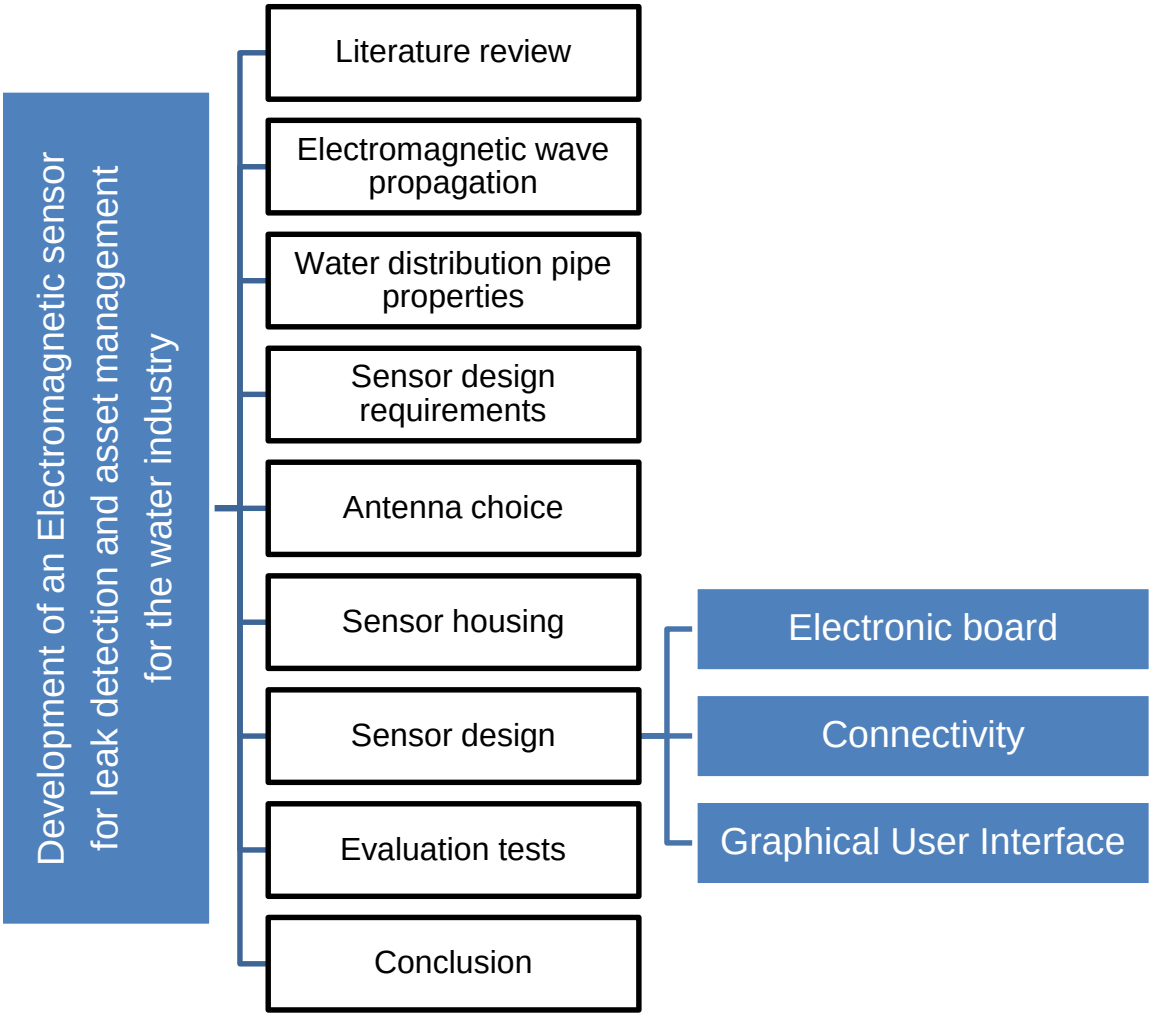

Figure 1: Development methodology

1.4 Current trend in leak detection

Companies around the globe utilise various techniques and systems to find and manage leaks within the water distribution network, while numerous other experimental methods are under development. According to the regulator OFWAT [26], water companies mainly use the minimum night flow and total integrated flow methods to estimate leakage on their network in defined zones called District Metered Areas (DMA). With the minimum night flow, water entering and leaving the zones is measured hourly at night while the total integrated flow method relies on

the balance of water used and the water supplied over an extended period. However, with just over 40% of consumers metered [27] these approaches heavily rely on estimates that may not reflect the true state of the network as both methods incorporate the volume of water used.

1.4.1 Pressure Reduction

Water loss reduction has been traditionally achieved using pressure management. This is done by the creation of district metered areas (DMAs) with pressure reducing valves (PRVs) and or pressure maintaining valves (PMVs) thus managing the flow of the water into the zone depending on the pressure threshold set or detected, effectively managing their asset by pressure reduction.

It is proven that, subject to variations, a 1% pressure reduction will result in 1.15% decrease in leakage. However, the level of this reduction is limited, otherwise, certain appliances such as combi boilers may malfunction when the minimum design water pressure is not provided[28].

1.4.2 Listening devices

Listening devices have been used in the vicinity of suspected leaks to determine their location for decades. The low cost leak detection stick is a metal rod with a wooden or plastic ear piece, as shown in Figure 2 (a).This device is applied against the ground, directly above a pipe, to pick up noise propagated through the soil by the vibrations produced by the leak.

(a) (b)

Figure 2: Operator with (a) listening stick [29] and (b) digital listening device [30]

Its efficiency, however relies heavily on the operator's hearing and experience. However, a more high tech solution is to use a modern version with piezoelectric components, as shown in Figure 2 (b), which amplifies the detected vibrations created by any escaping water. Regardless, inspection holes are still required to pinpoint the leak. Even though these devices are electronically simple, the operator must be experienced enough to distinguish environmental noise from leakage noise produced by pressurised water escaping through cracks.

1.4.3 Ground Penetrating Radar

Ground penetrating radar (GPR) is a non-destructive method of detecting leaks in buried utilities. The device sends radio waves to probe buried objects and uses the reflected electromagnetic pulses to build an underground map of the surveyed area. It still requires inspection holes to be dug at regular intervals to pinpoint any suspected leak. The system efficiency is greatly affected by voids, soil conditions [31], such as moisture level, and the type of buried pipeline under inspection. The

ground penetrating radar is more suitable for mapping pipeline infrastructure and locating buried objects rather than for leak detection.

Figure 3: Operator with (a) handheld [32] and (b) wheeled GPR [33]

1.4.4 Other leak detection methods:

In the laboratory, Miller [34] injected nitrogen (‘nitrogen flush’) into a pipe at 1.7 bar to improve the leak detection between two external acoustic emission sensors placed on the pipe, by creating periodic air and water/nitrogen disturbances. Meanwhile, Hudaini [35] proposed a cross-correlation function method to estimate the time delay of induced signals in order to locate the leak between two simultaneously recorded signals using hydrophones. Furthermore, Wan [36] reported laboratory tests using a power spectrum analysis method of the raw acoustic data to detect leaks in pipes of a boiler system, while Yang [37] used approximate entropy to separate a leak signal with environmental noise achieving a 92.5% correct detection rate but field tests showed the method to be sensitive to noise from other sources in the vicinity of the pipe location area such as building work or road traffic.

Other systems investigated include low-frequency quasi-static electromagnetic fields created by the introduction of a low frequency current, in the region of Hz to kHz [17], and leak prediction software such as the WaterGems Darwin Optimisation package by Bentley Systems [12] which applies a genetic algorithm to identify leakage hotspots in a district metered area. Bimpas [38] proposed the use of a 2.45GHz continuous wave sensor used above ground over the pipe path. This sensor makes use of the Doppler shift generated by electromagnetic waves hitting water escaping through a leak. It was unable however to efficiently detect leaks in pipes buried deep underground or in wet soils due to the high attenuation of the electromagnetic wave.

1.5 Summary

The ageing state of the water distribution network in the UK and around the world due to the limitations of existing and proposed new leak detection systems combined with public and regulators pressure have been driving the water companies to seek for a reliable technology that will allow them to pinpoint leaks and reduce water wastage through the correct identification of existing buried asset without extensive excavation. It is this need that has prompted the development of a novel electromagnetic wave based sensor technology for asset management and leak detection in real-time.

The next chapter will look into the properties of the standard ductile iron cement lined pipe that makes the majority of existing water distribution network and the theory of electromagnetic waves as well as their propagation within these circular structures.

Chapter 2: Electromagnetic waves in the water distribution pipe

The use of an electromagnetic wave sensor as a tool for water industry asset management is novel. The propagation of electromagnetic waves in standard water distribution pipes will be studied and the minimum frequency of propagation will be determined for both an empty pipe and a water filled pipe.

2.1 Water distribution pipe

In the UK, the majority of water distribution pipes are ductile iron cement lined (DICL) and polyvinylchloride (PVC) all approved by the Drinking Water Inspectorate (DWI) and governed by the BS EN 545 standard. The DN100 refers to a DICL pipe with an outer diameter of 118, and is shown in

and a 5mm (-1.5mm tolerance) thick cement liner [39], typically distributed in 5.2m or 6m lengths. These pipes are made to withstand the internal pressure created by the water flow, and external load due to backfill and road traffic over ground. In the present document, the DN100 pipe will be referred to by Ø118 mm pipe.

The outside wall of the iron has a zinc coating which then is painted with an epoxy coating to protect against abrasion and erosion giving a longer lifespan to the pipe.

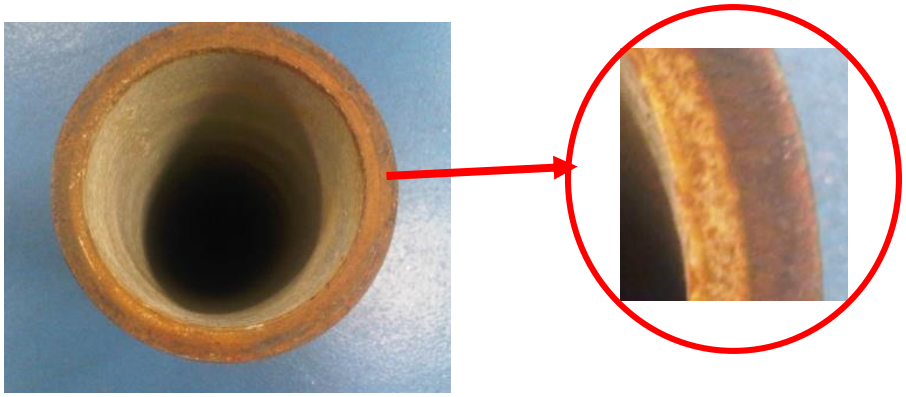

Figure 4: Ductile iron with 2 layers zoomed

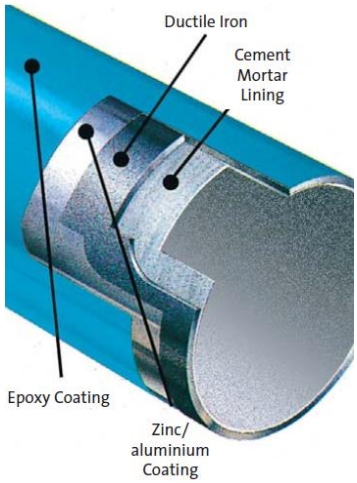

Figure 5: Typical layers in the ductile iron pipe design [40]

As the iron and zinc/aluminium coating are electrically conductive, the pipe can be considered as a circular waveguide. Electromagnetic wave propagation in a circular waveguide was therefore considered next.

2.2 Electromagnetic waves

The diameter of the pipe limits the propagation of very low frequencies.

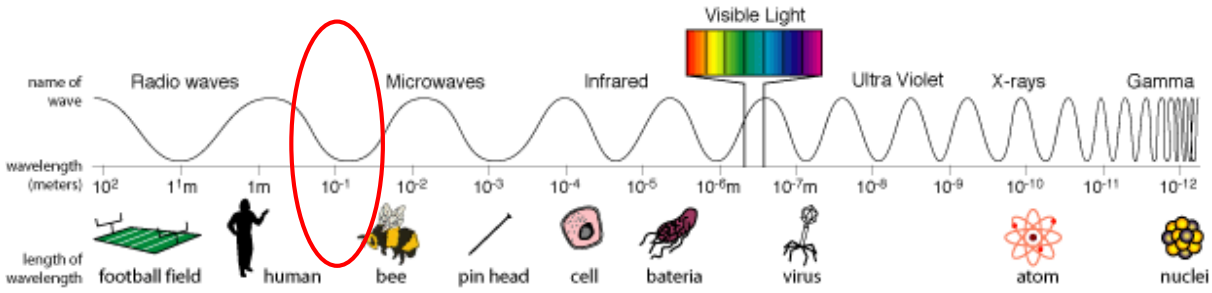

Figure 6: Electromagnetic Spectrum [41]

The microwave range will therefore be used in this project, the wavelength of interest is between $0.3\text{m}\ (1\text{GHz})$ to $0.03\text{m}\ (10\text{GHz})$, as shown in Figure 6.

Electromagnetic waves always have two components: the electrical field E and the magnetic field H. These two fields in a time-variation situation are linked by

Maxwell's equations.

2.3 Maxwell's equations

Electromagnetic field theory was developed by James Clerk Maxwell [1831-1879]. Maxwell developed the electromagnetic field theory based on Ampere's law, Faraday's law and Gauss' law to produce four integral equations now known as Maxwell equations. These are listed in Table 2.

Table 2: Maxwell equations [42]

Differential Form	Integral Form	Significance
$\nabla \times \mathbf{E} = -\frac{\partial \boldsymbol{B}}{\partial \boldsymbol{t}}$	$\oint_{\boldsymbol{c}} \boldsymbol{E}.\boldsymbol{dl} = -\frac{\boldsymbol{d\Phi}}{\boldsymbol{dt}}$	Faraday's law
$\nabla \times \boldsymbol{H} = \boldsymbol{J} + \frac{\partial \boldsymbol{D}}{\partial \boldsymbol{t}}$	$\oint_{\boldsymbol{c}} \boldsymbol{H}.\boldsymbol{dl} = \boldsymbol{I} + \int_{\boldsymbol{s}} \frac{\partial \boldsymbol{D}}{\partial \boldsymbol{t}}.\boldsymbol{ds}$	Ampere's circuital law
$\nabla.\boldsymbol{D} = \boldsymbol{\rho}$	$\oint_{\boldsymbol{s}} \boldsymbol{D}.\boldsymbol{ds} = \boldsymbol{Q}$	Gauss's law
$\nabla.\boldsymbol{B} = \mathbf{0}$	$\oint_{\boldsymbol{s}} \boldsymbol{B}.\boldsymbol{ds} = \mathbf{0}$	No isolated magnetic charge

Where:

$\mathbf{E}$ electrical field intensity	$\boldsymbol{B}$ magnetic flux density
$\boldsymbol{t}$ time	$\mathbf{H}$ magnetic field intensity
$\boldsymbol{\Phi}$ magnetic flux	$\mathbf{D}$ electric flux density
$\boldsymbol{l}$ segment length	$\boldsymbol{\rho}$ charge density
$\boldsymbol{s}$ surface	$\boldsymbol{J}$ current density
$\boldsymbol{Q}$ charge	

2.4 Propagation of electromagnetic waves

For a wave propagating in the *z* direction in a linearly polarised plane, E and H are given by the Maxwell equations as:

$$E_x = E_0 e^{(j\omega t-\gamma z)} \quad (1)$$

$$H_y = H_0 e^{(j\omega t-\gamma z)} \quad (2)$$

ω being the angular frequency expressed as ω = 2πf were *f* is the frequency in hertz. These two equations take into account the propagation constant γ [43].

$$\gamma=\alpha+j\beta \quad (3)$$

Were α is the attenuation constant and β is the phase constant.

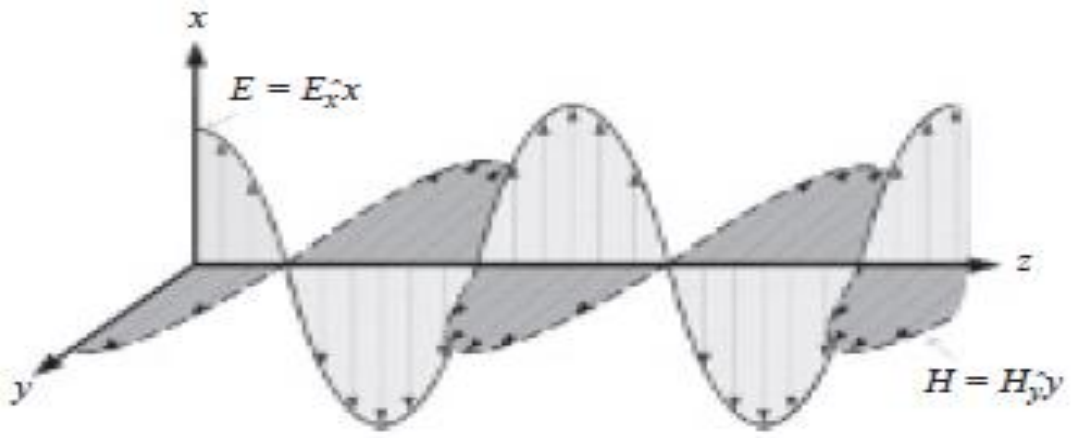

Figure 7: Electromagnetic wave travelling in the z direction [44]

The propagation of electromagnetic waves in a lossy medium is different from its propagation in lossless medium due to the conductivity σ of the dielectric.

When propagating in a lossy medium, the amplitude of the electromagnetic fields decrease exponentially as $e^{-\alpha z}$ with the propagation distance z, where α is the attenuation constant. In a lossy dielectric medium, the electrical field E and the magnetic field H are not in phase along the propagation path. Meanwhile, in a lossless dielectric medium, both fields are in phase and perpendicular to each other.

In free space, electromagnetic waves have a velocity [42] of $c_{vacuum} = 29979245ms^{-1}$. They are linked to the permittivity and permeability of free space by equation (4) [42]

$$c_{vacuum} = \frac{1}{\sqrt{\varepsilon_0 \mu_0}} \qquad (4)$$

ε_0=8.854×10^{-12} F/m, the permittivity of free space

μ_0=4π×10^{-7} H/m, the permeability of free space

For lossless dielectrics, the electromagnetic wave velocity is reduced by a factor of $\sqrt{\varepsilon_r \mu_r}$ where ε_r is the relative permittivity and μ_r the relative permeability of the medium in which the wave is propagating. For water, the relative permittivity and the relative permeability are respectively $\varepsilon_r = 81$ and $\mu_r = 0.9999$ [45] at 15^{o}c.

Thus the EM velocity in water $c_{water}\ (C)$ is given by equation (5):

$$c_{water} = \frac{c_{vacuum}}{\sqrt{\varepsilon_r \mu_r}} \qquad (5)$$

Therefore, the velocity of the electromagnetic wave $c_{water} = 33310000ms^{-1}$

Water pipe as a waveguide

Electromagnetic waves may propagate in a conductive hollow shell such as the standard ductile iron pipe used in the water distribution network.

In a circular waveguide, above the cut-off frequency, electromagnetic waves may propagate in a number of modes: the transverse electric TE with a null longitudinal electric-field and the transverse magnetic TM with a null longitudinal magnetic-field. In all the experiments, the Ø118mm pipe in Figure 4 will be used, including the bigger Ø170mm diameter pipe version as they constitute 40-60% of all installed pipes for potable water distribution in the UK with a standard wall thickness to up to 5mm.

Above the cut-off frequency, electromagnetic waves are able to propagate through empty metal pipes of any cross section, thus acting as a waveguiding structure.

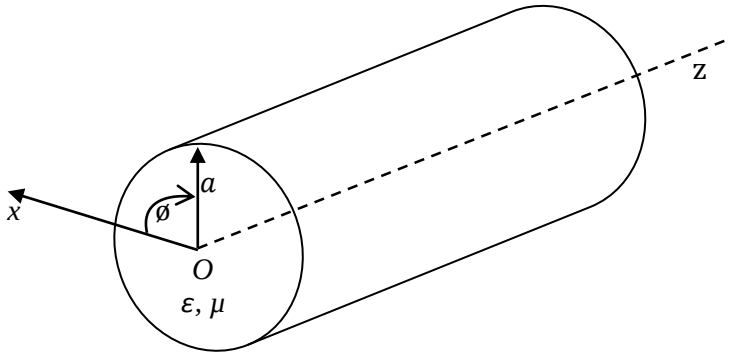

Figure 8: Circular waveguide [42]

Figure 8 shows a metallic waveguide of radius a along the z direction. The enclosed medium has characteristic parameters, ε and μ.

A circular waveguide can propagate transverse electromagnetic waves (with E_z=0 and H_z=0), if the wavelength is very much smaller than the radius, but it can also support the transverse magnetic (TM) modes and the transverse electric (TE) modes at low frequencies both have a longitudinal component; electric-field and magnetic-field respectively, and each characteristic cut-off frequency as a lower limit [42].

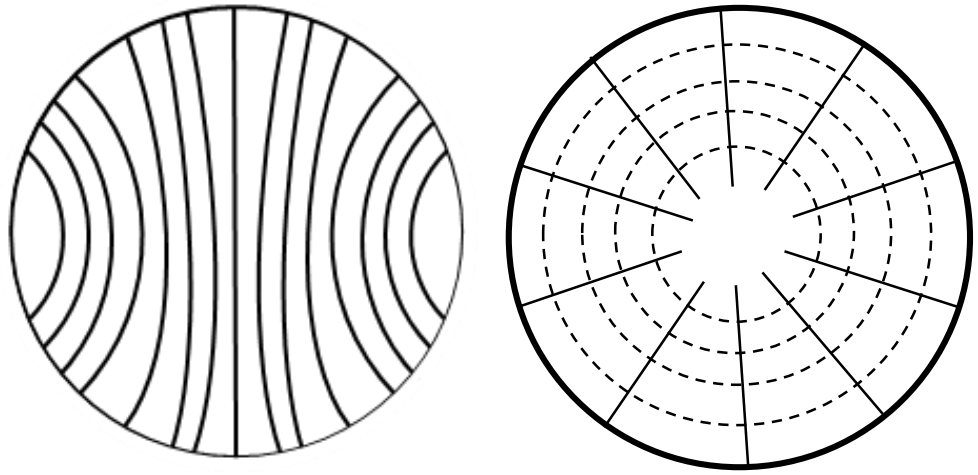

TE_{11} TM_{01}

Figure 9: TE_{11} and TM_{01} fields configuration in a circular waveguide [46]

The electric and the magnetic field configurations of the two dominant modes in a circular waveguide cross section are shown in Figure 9.

However, a transverse electromagnetic TEM wave can exist in a dielectric filled waveguide if there is an axial [42] [43] such as a coaxial transmission line. These operate at all frequencies (ignoring losses at high frequency) down to dc.

TM and TE will be the only modes that will be considered in this project due to the absence of inner conductor in water pipelines and the focus on RF frequency range.

Propagation within cylindrical waveguide relies on electric field reflection from the conductive wall, and these produce modes whose properties are dependent on involving roots of the Bessel function of the first kind, $J_m(u)$ [43] and its derivative $J'_m(u)$.

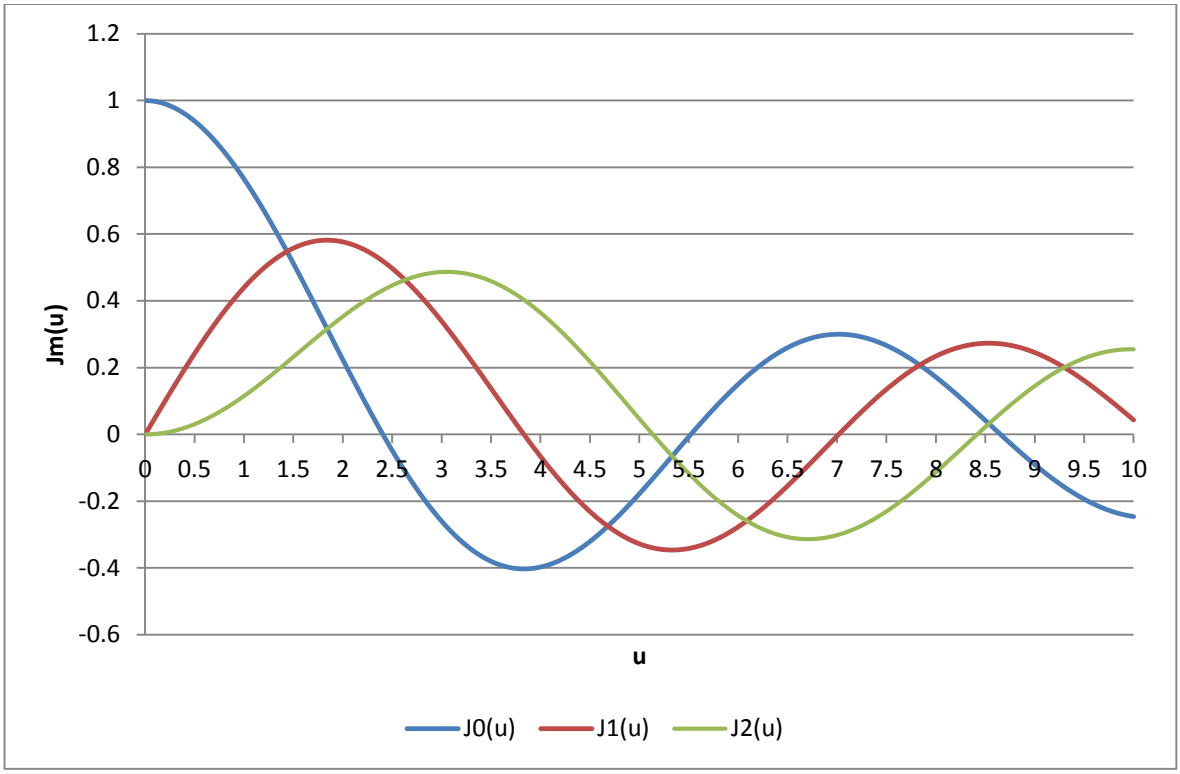

Figure 10: Bessel function of the first kind

Figure 10 shows $J_m(u)$ oscillations for some values of m. It should be noted that $J_0(u)$=1 when u=0 the zeroth order while $J_m(0)$=0 for all m except when $m = 0$. Furthermore, $\mathrm{J_m(u)}$ are oscillations with decreasing amplitude [42].

$$\boldsymbol{J_m(u) = 0, \quad u = x_{mn}} \qquad (6)$$

$$\boldsymbol{J'_m(u) = 0, \quad u = x'_{mn}} \qquad (7)$$

For TM modes,

$$f_{c,mn} = \frac{x_{mn}}{2\pi a\sqrt{\varepsilon\mu}} \qquad (8)$$

For TE modes,

$$f_{c,mn} = \frac{x'_{mn}}{2\pi a\sqrt{\varepsilon\mu}} \qquad (9)$$

μ permeability, ε permittivity, a pipe radius, x_{mn} root value of the Bessel function, x'_{mn} root value of the derivative of the Bessel function, $f_{c,mn}$ cut-off frequency, m

and n constants ($m = 0,1,2, \ldots$ and $n = 1,2,3, \ldots$).

Table 3: Some root value of the Bessel function [43]

	x_{mn}		
m / n	0	1	2
1	2.405	3.832	5.136
2	5.52	7.016	8.417
3	8.654	10.173	11.62

	x'_{mn}		
m / n	0	1	2
1	3.832	1.841	3.054
2	7.016	5.331	6.706
3	10.173	8.536	9.969

In the pipe, the lowest cut-off frequency for the TE mode is TE_{11} while for the TM mode, it is TM_{01} determined by the lowest root values for each function shown in red in the table above. However, TE_{11} is the true dominant mode as it yields the lowest cut-off frequency. These Bessel function solutions in Table 3 will be used in the calculations to determine the minimum cut-off frequency below which there is no propagation.

The effective internal pipe radius a and the available length used for this experiment are shown in Table 4 below:

Table 4: Pipe dimensions

Pipe Type	Internal Radius	Length
Cast iron	52mm	720mm

The cut-off frequencies are calculated using the smallest values in Table 3 to derive the two dominant modes for TE_{mn} and TM_{mn} :

$$(f_c)_{11}^{TE^z} = \frac{1.8412}{2\pi a\sqrt{\mu\varepsilon}} \qquad (10)\ [46]$$

$$(f_c)_{01}^{TM^z} = \frac{2.405}{2\pi a\sqrt{\mu\varepsilon}} \qquad (11)\ [46]$$

Where $(f_c)_{11}^{TE^z}$ and $(f_c)_{01}^{TM^z}$ are the corresponding cut-off frequencies for the TE11

and the TM01 modes respectively, a is the radius of the pipe, and z is the direction of propagation which will be along the length of the pipe.

As well as the surrounding dielectric, the wavelength of the propagating waves is also dependent on the radius of the guide. In free space, the wavelength is:

$$\lambda = \frac{c}{f_{11}} = 3.413a \qquad [43]$$

$$\lambda = \frac{c}{f_{01}} = 2.612a$$

However, the wavelength of the waves that exist inside a waveguide λ_g is expressed by:

$$\boldsymbol{\lambda_g = \frac{\lambda}{\sqrt{1-\left(\frac{f_c}{f}\right)^2}}} \qquad \text{when} \quad \boldsymbol{f > f_c = (f_c)_{mn}} \qquad (12)\ [46]$$

And the phase constant β along the z axis of the wave is

$$\beta_z = \frac{2\pi}{\lambda}\sqrt{1-\left(\frac{f_c}{f}\right)^2} \qquad (13)\ [46]$$

With a sample pipe of radius 52mm, the theoretical cut-off frequencies in the empty pipe are calculated using the solutions from the Bessel function and shown in Table 5. The cut-off frequencies shown in red correspond to the dominant modes.

Table 5: Some cut-off frequencies (GHz) in air for the Ø118mm pipe

	TM_{01}	TM_{11}	TM_{21}	TM_{02}	TM_{12}	TM_{22}	TM_{03}	TM_{13}	TM_{23}
x_{mn}	2.405	3.832	5.136	5.520	7.016	8.417	8.654	10.173	11.620
$f_{c,mn}$	2.204	3.512	4.708	5.060	6.431	7.715	7.932	9.325	10.651
	TE_{01}	TE_{11}	TE_{21}	TE_{02}	TE_{12}	TE_{22}	TE_{03}	TE_{13}	TE_{23}
x'_{mn}	3.832	1.841	3.054	7.016	5.331	6.706	10.173	8.536	9.969
$f_{c,mn}$	3.512	1.687	2.799	6.431	4.886	6.147	9.325	7.824	9.138

For waves propagating in the pipe, the wavelength at frequencies above the cut-off frequencies is calculated using equation (12). The calculated wavelength for

frequencies above the dominant modes TE_{11} and TM_{01} set respectively at 1.75GHz and 2.5GHz are 670.6mm and 611.7mm inside the empty waveguide.

The velocity of electromagnetic waves is reduced by interaction with the medium, as described by equation (14).

$$c_{medium} = \frac{c_{vacuum}}{\sqrt{\varepsilon_r \mu_r}} \quad (14)$$

Where ε_r is the relative permittivity and μ_r is the relative permeability.

For water, the relative permittivity and the relative permeability are respectively $\varepsilon_r = 81$ and $\mu_r = 0.9999$ [45] at 15°c.

Therefore, the velocity of the electromagnetic wave in water is $c_{water} = 33310000 ms^{-1}$.

Using equation (14), the cut-off frequencies in water are shown in Table 6.

Table 6: Some calculated cut-off frequencies (MHz) in water for the Ø118mm pipe

	TM_{01}	TM_{11}	TM_{21}	TM_{02}	TM_{12}	TM_{22}	TM_{03}	TM_{13}	TM_{23}
X_{mn}	2.405	3.832	5.136	5.520	7.016	8.417	8.654	10.173	11.620
$f_{c,mn}$	245.19	390.68	523.62	562.77	715.29	858.13	882.29	1037.15	1184.68

	TE_{01}	TE_{11}	TE_{21}	TE_{02}	TE_{12}	TE_{22}	TE_{03}	TE_{13}	TE_{23}
X'_{mn}	3.832	1.841	3.054	7.016	5.331	6.706	10.173	8.536	9.969
$f_{c,mn}$	390.68	187.69	311.36	715.29	543.50	683.69	1037.15	870.26	1016.36

There will be no wave propagation below the cut-frequency shown in red in the table.

Table 7: Calculated cut-off frequencies (MHz) in ascending order

Mode	TE_{11}	TM_{01}	TE_{21}	TM_{11}	TM_{21}	TE_{12}	TE_{22}	TE_{02}/TM_{12}	…
Frequency	187.69	245.19	311.36	390.68	523.62	543.50	683.69	715.29	…

As the radius a increases, the cut-off frequency decreases. Hence, for the second

most used pipe in the water distribution network, the Ø170mm pipe, which has an internal radius of 78.7mm, the cut-off frequencies for TE_{11} and TM_{01} are respectively 124MHz and 162MHz in a water filled pipe.

In water filled pipes, the minimum frequency to be used with the Ø118mm should be above 187.69MHz while the Ø170mm requires just above 124MHz.

2.5 Scattering parameters

Experimentally testing the wave propagation inside the pipeline will require the use of antennas to transmit and receive the waves. The signal strength is observed through the reflection and transmission coefficients measured inside the pipe; which will introduce the concept of scattering or s-parameters. These two antenna ports are modelled in a two port network in Figure 11 and energy propagation can be quantified using the two dimension scattering matrix. A two port device is represented as:

Figure 11: A two port network [47]

The s-parameters matrix of this network is shown below:

$$S = \begin{bmatrix} S_{11} & S_{12} \\ S_{21} & S_{22} \end{bmatrix} \qquad [47]$$

S_{11} and S_{22} are the reflection coefficients from port 1 and port 2 respectively. While S_{12} and S_{21} are the transmission coefficients from port 2 to port 1, and from port 1 to port 2 respectively.

This matrix connects the input power wave to the output power wave:

$$\begin{bmatrix} b_1 \\ b_2 \end{bmatrix} = \begin{bmatrix} S_{11} & S_{12} \\ S_{21} & S_{22} \end{bmatrix} \begin{bmatrix} a_1 \\ a_2 \end{bmatrix} \qquad [44]$$

Where a_1 and a_2 are the incident voltage wave amplitudes, and b_1 and b_2 are the reflected voltage wave amplitudes.

If port 1 and port 2 are alternatively terminated with a matched impedance, the resulting reflection and transmission coefficients of the network of the 2 ports will be as the following:

$S_{11} = b_1/a_1$ – Reflection coefficient at port 1

$S_{21} = b_2/a_1$ – Transmission coefficient from port 1 to port 2

$S_{12} = b_1/a_2$ – Transmission coefficient from port 2 to port 1

$S_{22} = b_2/a_2$ – Reflection coefficient at port 2

2.6 Wave propagation modelling

In this section, the electromagnetic wave behaviour in the empty pipe and the water filled pipe will be shown. The propagation only takes place when the operating frequency is above the cut-off frequency. The transmission in the Ø118mm pipeline acting as a waveguide will be modelled with two ports to determine the frequency of propagation using the s-parameter S_{21} and show the electromagnetic field distribution in the pipe above the cut-off frequency.

This step was achieved by modelling and simulating a cylindrical waveguide of the same radius as the pipe with perfect conducting walls using ANSYS's high frequency structure simulator (HFSS) software version 13 [45] which uses the finite element method to solve Maxwell equations for complex structures.

The cylinder was drawn with two wave ports at each end to transmit the signal and receive the signal respectively. These wave ports were excited and the transmission curve was plotted as well as the electric and magnetic field distribution.

Using a wave port at each end of the pipe section ensures that the propagating wave is not reflected and the pipe section does not act as a cavity.

The results of the pipe simulations in Figure 12 through Figure 15, show the field distribution for an empty pipe (air) and for a fresh water filled pipe with both the TE_{11} and TM_{01} modes.

In HFSS, a frequency sweep was set from the cut-off frequency of the dominant mode TE_{11} to a frequency below the TM_{01} mode in order to ensure transmission within the TE_{11} mode only.

In air, the electrical and magnetic fields distribution is plotted for the TE_{11} in Figure 12.

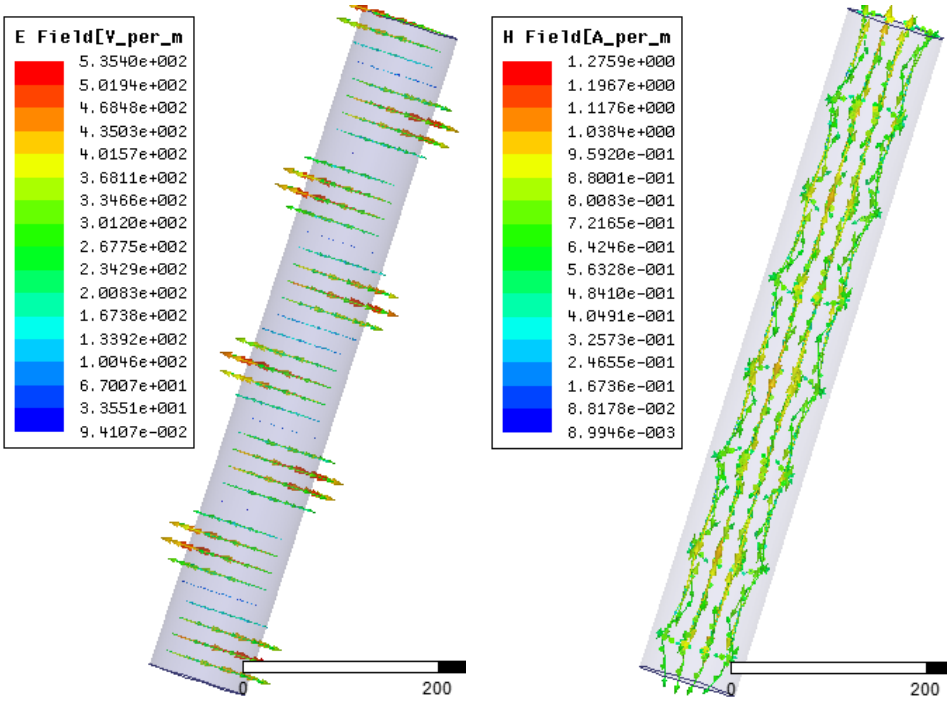

Figure 12: TE_{11} in air

For transmission in the TM_{01} mode, the frequency is above 2.2GHz and below the next mode. The electromagnetic field distribution is shown in Figure 13.

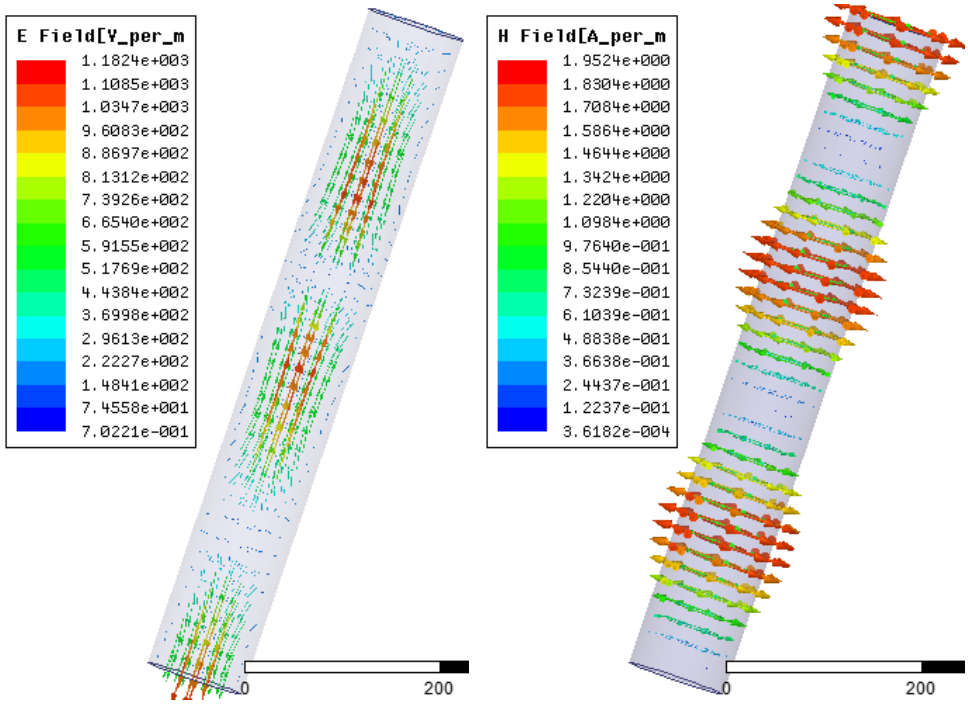

Figure 13: TM_{01} in air

Both figures of the field distribution for the air filled pipe above showed no wave attenuation.

After the simulation using the empty pipe, it was filled with fresh water.

Taking into account the reduction factor $\sqrt{\varepsilon_r \mu_r}$ in the medium of propagation, in water, the frequency was set 300MHz to cover both modes.

The electromagnetic fields from the simulations are shown in Figure 14 and Figure 15.

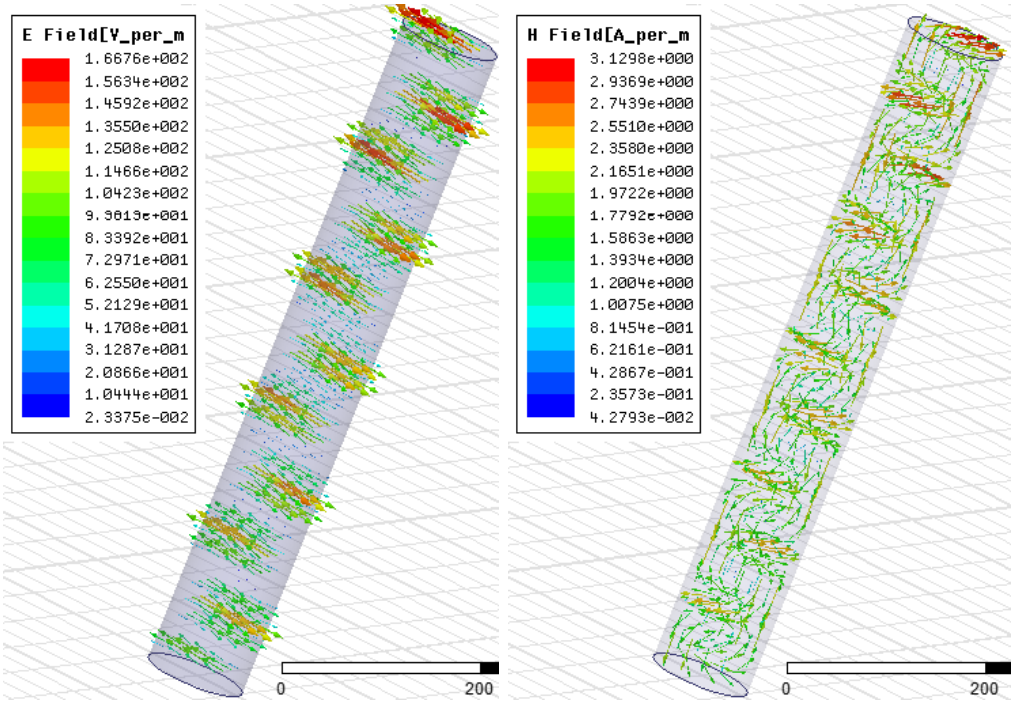

Figure 14: TE_{11} in water

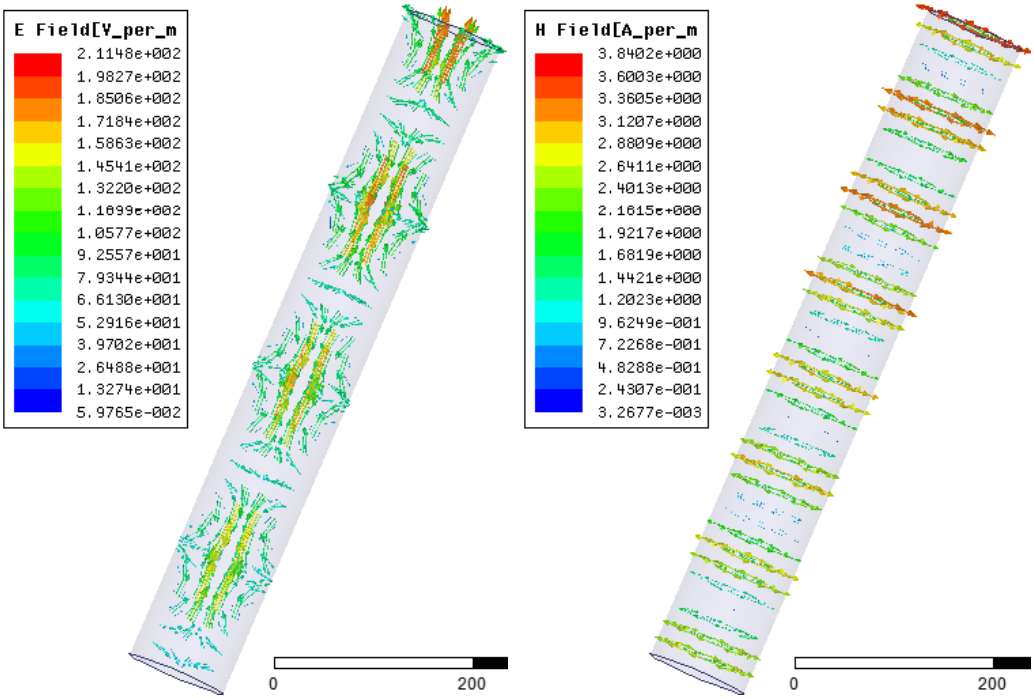

Figure 15: TM_{01} in water

When the pipe is filled with water, the electromagnetic waves propagate but at a velocity of only $3.3x10^{7}m^{-1}$ due to the water permittivity.

Both in the TE_{11} and TM_{01} mode, signal attenuation is observed as the wave propagates away from the excited port.

The modelling results showed the pipe used for water distribution satisfies the properties of a circular waveguide and various electromagnetic propagation modes are possible.

2.7 Wave propagation experimental test

To compare the theory to the actual pipe, measurements were taken on an experimental setup using two equivalent common, loops and monopole antennas, with a Ø118mm cast iron potable water pipe section. Figure 16 - Figure 18 show the equipment used for the experiment.

Figure 16: A vector network analyser - Rhode & Schwarz ZVL-3GHz

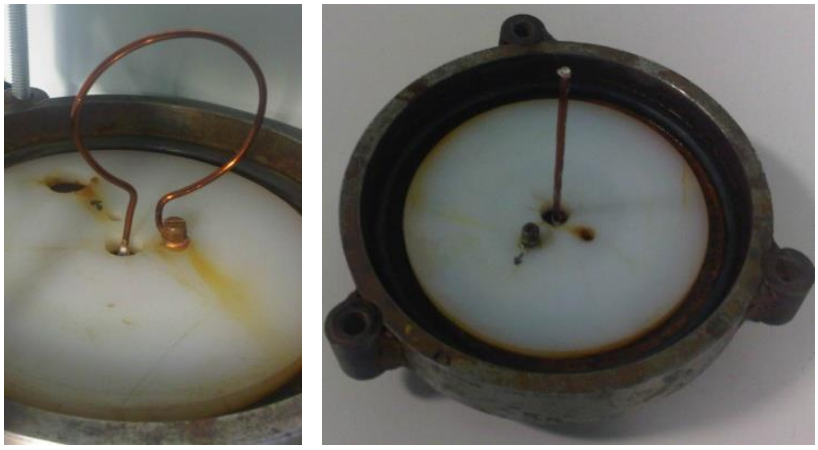

Figure 17: Loop and monopole antenna

Figure 18: Full setup with the Ø118mm pipe

Two caps at each end of a 720mm cast iron pipe section with the same antenna type at each end were connected to ports 1 and 2 of a Rhode & Schwarz ZVL-3GHz [48] vector network analyzer (VNA) to measure the transmit a signal and measure its reflected power.

The electromagnetic wave is generated on port 1 and received on port 2. The transmission S_{21} is plotted against frequency in Figure 19.

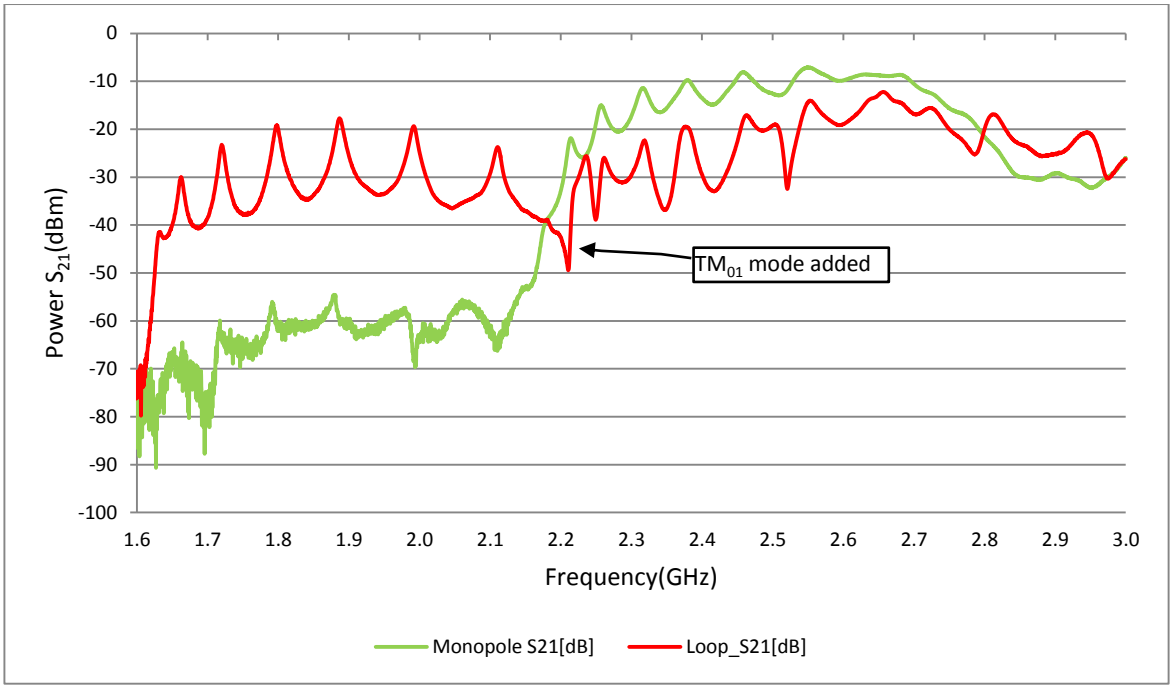

Figure 19: Cut-off frequency in the empty pipe

In the empty pipe, for the loop antenna, the measured transmission starts around 1.63GHz while the monopole starts around 2.18GHz. These transmissions are slightly below the theoretical cut-off frequency calculated. This discrepancy may be explained by the dielectric properties of the mortar lining.

The loop antenna transmitted the signal in air in the TE with the TM mode starting at 2.208 GHz shown in Figure 19, while the monopole antenna transmitted much better from the TM mode above the calculated 2.204GHz (TM_{01}) which is the cut-off frequency of this mode shown in Table 5. This effect is due to the fact that the loop antenna is more sensitive to the magnetic field [49].

The experiment above was repeated with the pipe filled with fresh water.

Due to water dielectric properties, higher frequency range transmission was not observed during the experiment due to high attenuation.

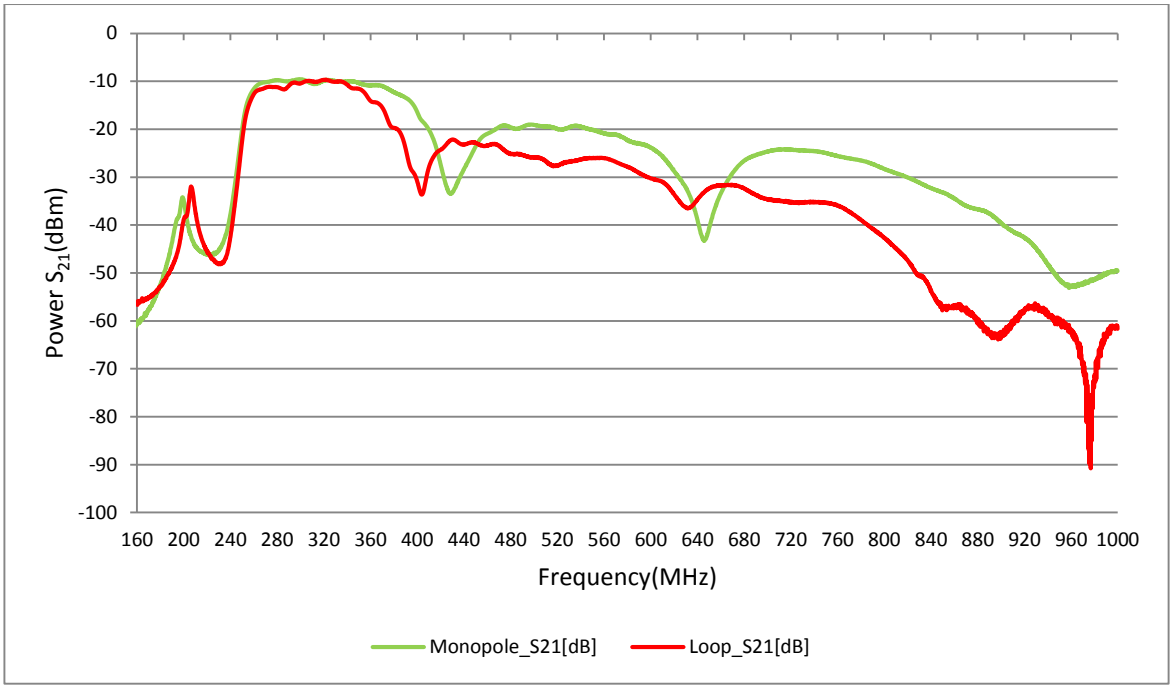

Figure 20: Cut-off frequency in the water pipe

When the pipe was filled with fresh water, the cut-off frequencies are expected to be lowered by a factor of $\sqrt{\mu_r \varepsilon_r}$.

In water, the cut-off frequencies are:

$$f_{11} = 1.841 \frac{c_{water}}{2\pi a} \quad (15)$$

$$f_{11} = 1.841 \times (3.331 \times 10^7 / 2\pi \times 0.05205) = 187.45MHz$$

$$f_{01} = 2.405 \frac{c_{water}}{2\pi a} \quad (16)$$

$$f_{01} = 2.405 \times (3.331 \times 10^7 / 2\pi \times 0.05205) = 244.88MHz$$

Compared to the 222MHz measured frequency, in water both the loop and the monopole antenna transmitted from the TE mode with a theoretical cut-off frequency of 187.51MHz. Both antennas couple with the electric and magnetic fields and give a S_{21} value of -10dBm between 227MHz and 351MHz while attenuation was observed as shown in Figure 20.

The cut-off frequencies for the HFSS model, calculated and experimentally

measured have shown that the standard Ø118mm cast iron pipe, widely used for water distribution, satisfies the properties of a circular waveguide based on the propagation of the electromagnetic modes TE_{11} and TM_{01}.

Electromagnetic waves will propagate differently in non-metallic pipes due to the material's ability to reflect the waves. Metal are highly reflective because their mobile electrons will not sustain an electric field component parallel to the surface. In the case of plastics, reflections will occur due to the difference in permittivity of the pipe medium and water but transmission through the pipe wall is possible.

2.8 Summary

The modelling and experiments carried out in this chapter have shown that the ductile iron cement lined standard water distribution pipe acts as a circular waveguide due to its electrically conductive shell. Each pipe radius has a minimum frequency below which there is no wave propagation. In a circular waveguide, the dominant electromagnetic wave propagation mode is the transverse electric TE_{11}, which correspond to the lowest cut-off frequency. The cut-off frequency of the water filled pipe was shown to be 187.69MHz. This value will be the minimum frequency for the sensor to cover both the Ø118mm and Ø170mm pipes. In the next chapter, the selection and design process of the appropriate antenna for the sensor will be described.

Chapter 3: Antenna design

The choice of the antenna is governed by its ability to be integrated into a sensor case which must comply with the form and size restrictions imposed by the stakeholders. Due to this size constraint, the sensor will be built around a single antenna which will transmit a signal and detect the amount that is reflected using the reflection coefficient at port 1, as described in the two port network theory in the preceding chapter.

The wave quantity measured from the antenna is the scattering parameter S11, which with just a source at port 1 is the reflection coefficient Γ expressed by:

$$\Gamma = \frac{b}{a} \qquad (17)\ [50]$$

Γ is the ratio of the incident power a to the reflected power b. The scattering parameter S11 is a quantity measured from a one-port device as illustrated in Figure 21:

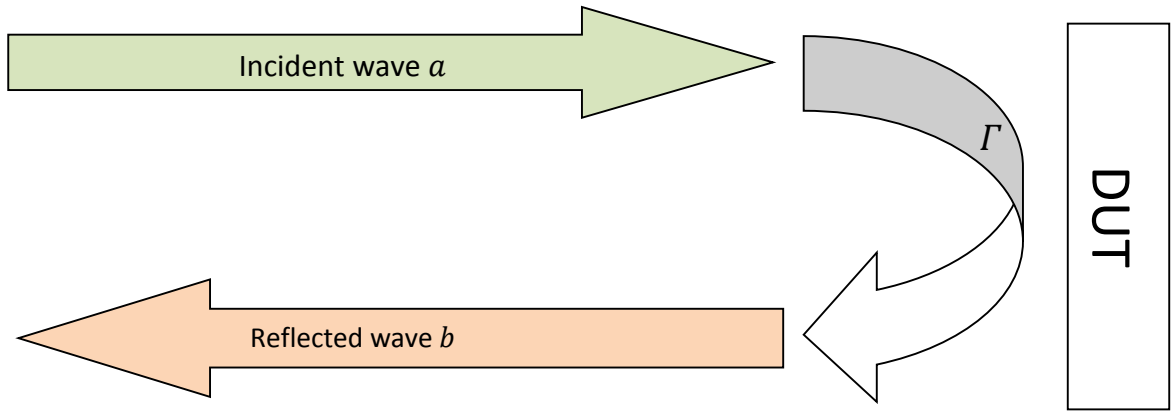

Figure 21: One-port device with incident and reflected waves [50]

In this illustration, the incident wave is partially reflected by the device under test (DUT) back to the source.

This reflection coefficient is a complex quantity derived from the complex impedance Z of the DUT using:

$$\Gamma = \frac{z-1}{z+1} \qquad (18)$$

With $z = \frac{Z_D}{Z_0}$ where Z_0 is the reference impedance, typically 50Ω.

The return loss RL is a measure of how much power is delivered from a transmission line to a load expressed in decibels:

$$RL = 10\log_{10}\left(\frac{P_{in}}{P_{ref}}\right) dB \qquad (19) [51]$$

The power reflected P_{ref} cannot be higher than the incident power P_{in}.

In this document, the magnitude of S_{11}in dB versus frequency will be referred to as the return loss calculated as:

$$\mathrm{S}_{11}(dB) = 20\log_{10}|\mathrm{S}_{11}|$$

Along the return loss parameter, bandwidth will be considered.

The bandwidth of an antenna is the range of frequencies, in relation to the centre frequency, over which the power dissipation is high. A narrow bandwidth should be an advantage, as any structural change to the shell of the water distribution pipe should affect the frequency and amplitude of the spectrum.

3.1 Antennas

There are numerous types of antennas and the most popular are categorised into wire-type made with conducting wires, aperture type widely used in high frequency applications and antenna arrays which are geometric arrangement of multiple radiating elements to form a single antenna [44]. For example, the dipole, loop and helical antennas are all classed in the wire-type antenna category. In this group, the most familiar antenna is the Yagi-Uda antenna used for domestic TV reception. Horn and microstrip antennas as well as reflectors are part of the aperture group.

The choice of the antenna type to use for this project is limited by the 100mm

maximum length of the sensor body set by the industrial partners and its ability to fit in a standard water distribution pipe. Therefore three antenna types, a loop, a monopole and a patch, were considered for this research because they are common antennas for the frequency range needed and are potentially easier to integrate into the sensor. Antennas with resonant frequencies in free space above the cut-off frequency of the pipe, will be designed and simulated. These antennas will be tested and experimented with and their performance compared.

3.1.1 Loop antenna

The diameter (d) of the loop antenna was chosen based on the results from a previous LJMU project [52]. The maximum size of the antenna is bound by the maximum diameter of the sensor body imposed by water industry stakeholders. The size was set in order to allow the sensor to be inserted inside water pipes through existing hydrants in the distribution network. Due to the insertion angle and mineral deposit build up over time, the maximum antenna diameter allowed was estimated to be 28mm.

The circumference of a loop antenna is expressed with equation (20). For a one wavelength loop of 28mm diameter antenna, λ the wavelength is equal to C the circumference of the loop antenna ($\lambda = C$).

$$\lambda = C = \pi \times d \qquad (20)\ [53]$$

$$\lambda = C = \pi \times 28mm = 87.96mm$$

This antenna is classed as an electrically large loop antenna with a non-uniform current.

The wavelength is linked to the frequency by equation (21):

$$f = \frac{c}{\lambda} \qquad (21)$$

$$f = \frac{2.99792 \times 10^8}{0.08796} = 3408 \times 10^6 = 3.4GHz$$

With the calculated frequency, a resonant loop antenna was then modelled and simulated in HFSS and its output shown in Figure 22.

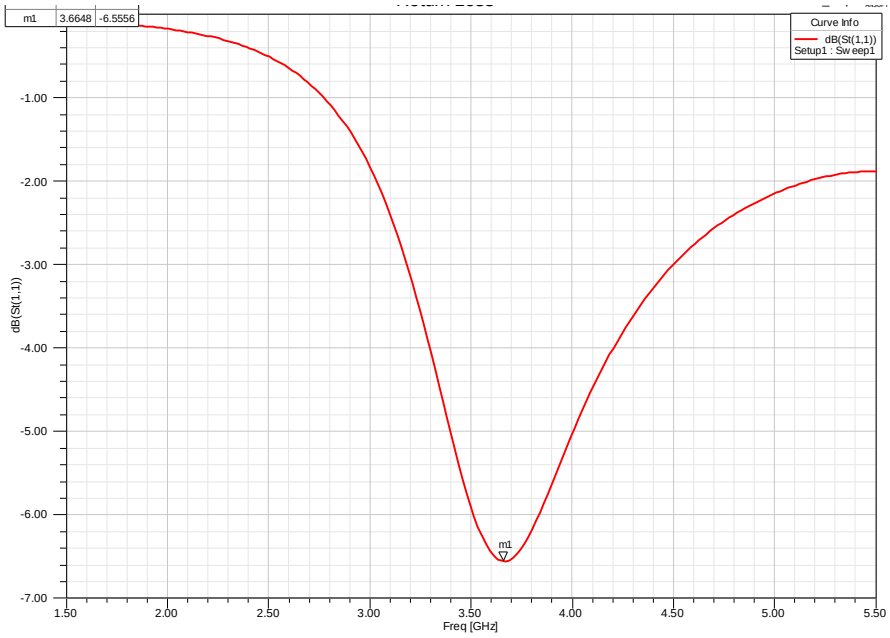

Figure 22: Loop S11 in air

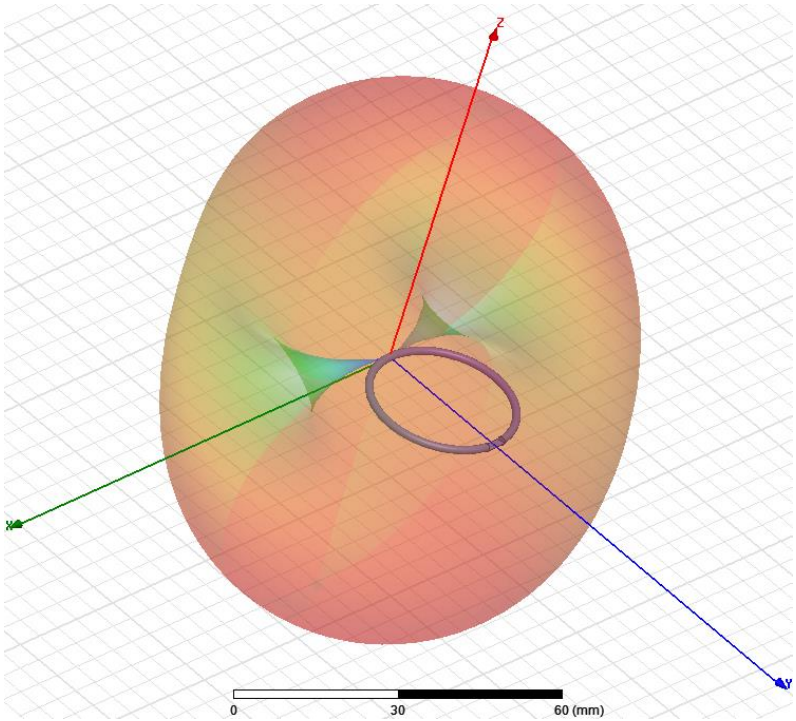

Figure 23: Large loop radiation field

This loop satisfies the electrically large loop property because the circumference $C = 2\pi a$ is more than $\frac{\lambda}{3}$ ($C = 2\pi \times 28 > 175.92/3$). It is stated that when the loop circumference is almost equal to the wavelength, the maximum radiation fields shift by 90º ($\theta = 0$ and π) on it axis perpendicular to the plane loop [44] as shown in the 3D radiation plot in Figure 23.

As this is an electrically large loop, the current along the circumference of the antenna is non-uniform and is better expressed by a Fourier series:

$$\mathrm{I}(\emptyset') = \mathrm{I}_0 + 2\sum_{\mathrm{n}=1}^{\mathrm{M}} \mathrm{I}_\mathrm{n} \cos(\mathrm{n}\emptyset') \qquad (22)\ [54]$$

The Q factor of the antenna is calculated using equation (23):

$$\mathrm{Q} = \frac{\mathrm{f}_0}{\Delta \mathrm{f}_{\mathrm{HP}}} \qquad (23)\ [55]$$

f_0 the centre frequency

$\Delta \mathrm{f}_{\mathrm{HP}}$ the bandwidth at half power

While its directivity D is given by equation (24):

$$\mathrm{D} = 0.68\mathrm{C}_\lambda \qquad (24)\ [53]$$

Where C_λ is the loop circumference.

A loop of this size was then designed and experimentally tested to evaluate its return loss.

Figure 24: 28mm loop antenna

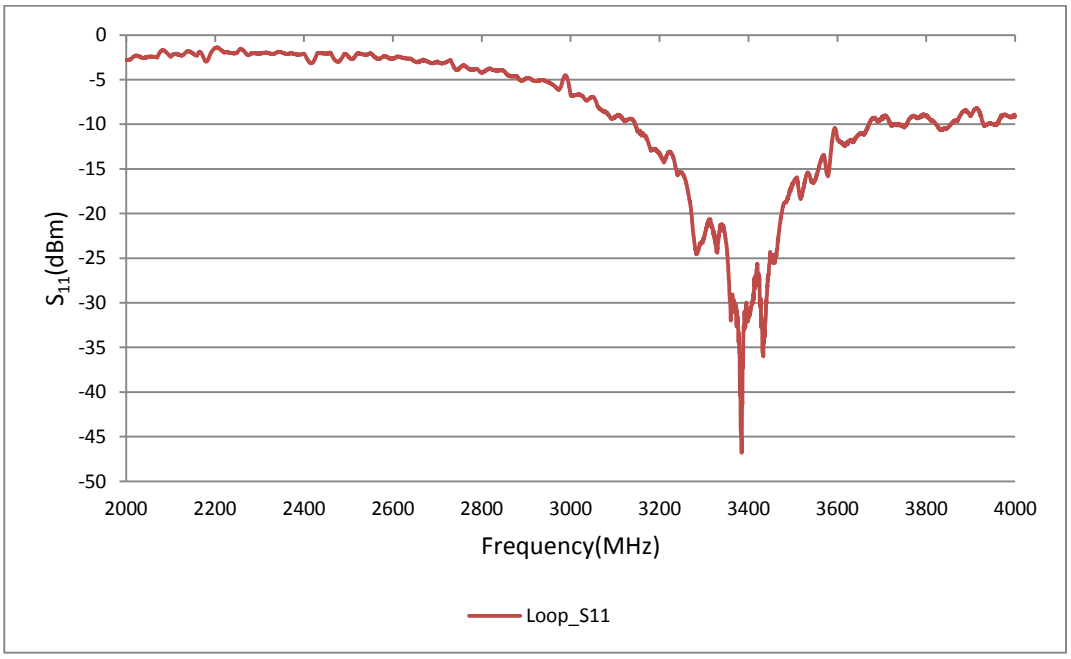

Figure 25: 28mm loop antenna S11 in air

S_{11} is plotted against frequency in Figure 25. The resonant frequency was 3.3769GHz, which is very close to the theoretical frequency of 3.4GHz with a 525MHz bandwidth at -10dBm.

3.1.2 Monopole antenna

A monopole with equivalent properties this loop antenna, was modelled in HFSS to

determine its return loss and radiation pattern for comparison. This monopole antenna was $\frac{\lambda}{4}$ long with a ground plane and was also designed to resonate at 3.4GHz.

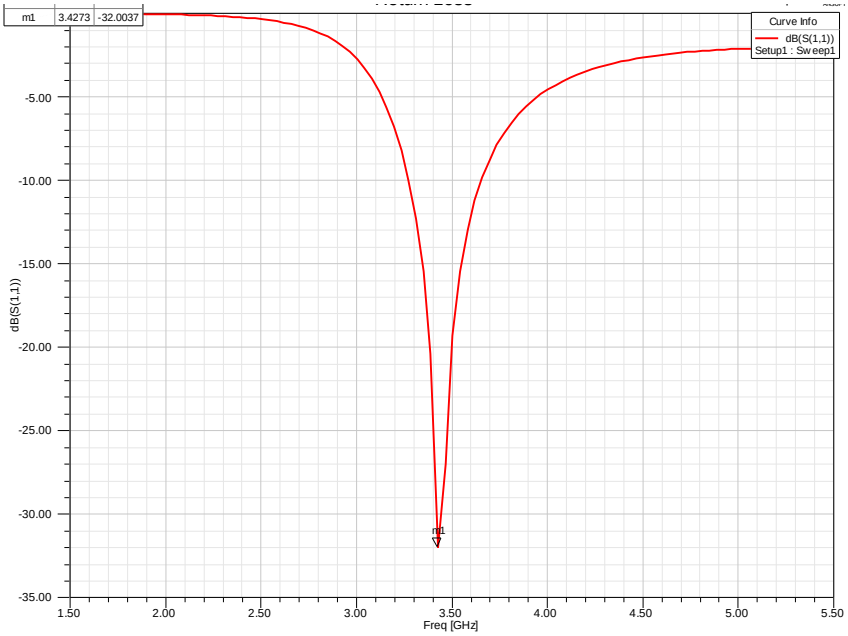

Figure 26: Monopole S11 in air

In air, the simulated monopole had a high return loss but a smaller bandwidth of 400MHz as shown in Figure 26.

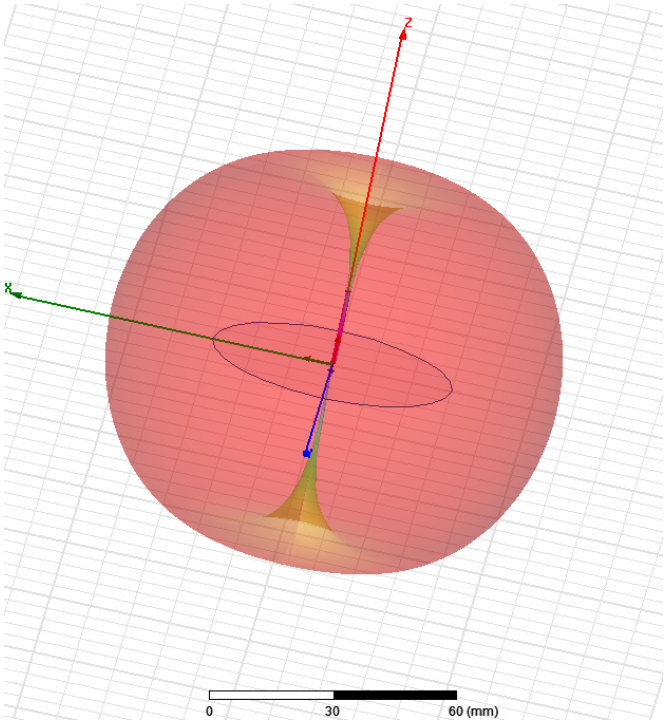

Figure 27: λ/4 monopole radiation pattern

Meanwhile, the radiation of the monopole antenna is omni-directional and based on its radiation pattern, this antenna would be perfect for the purpose of covering the full circumference of the internal pipe.

A $\frac{\lambda}{4}$ monopole was constructed and tested. Its resonant frequency in Figure 29 is 50MHz lower than the target frequency. This could be tuned using a larger ground plane.

Figure 28: λ/4 Monopole antenna

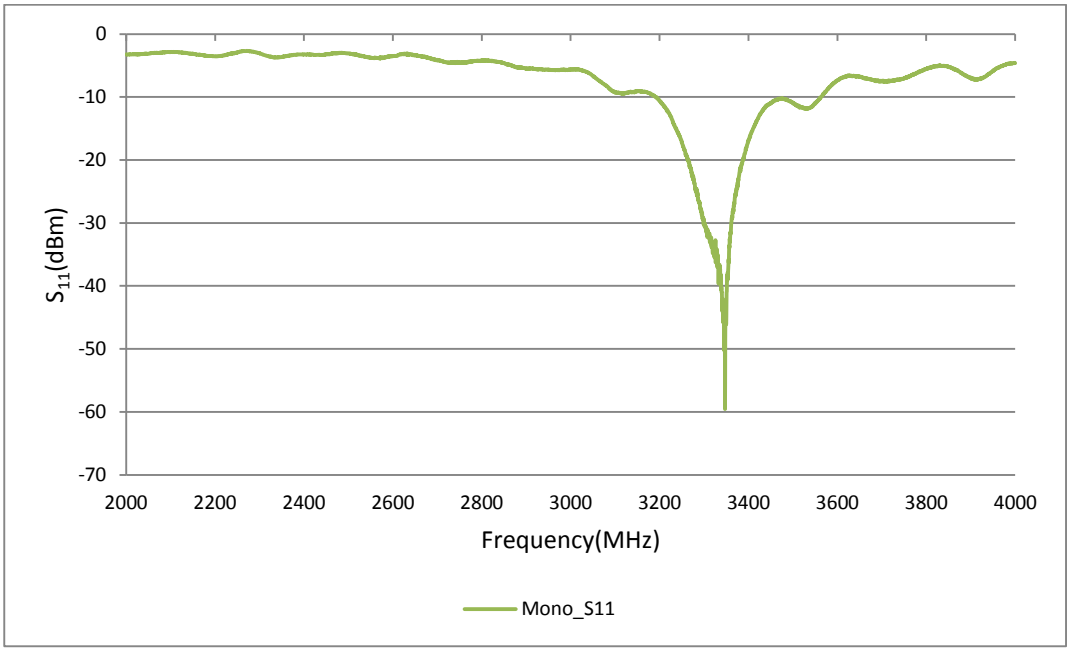

Figure 29: Monopole S11 in air

Despite having the appropriate radiation characteristics and bandwidth of 225MHz, however, this antenna was considered to be too fragile and mechanically unsuitable for integration into the proposed sensor case.

3.1.3 Patch antenna

The third type of antenna to be investigated was the patch antenna. This antenna

was considered due to its rigidity, mechanical strength and directivity.

In order to check the suitability of this type of antenna for our sensor, a patch equivalent to the previous antennas was designed and modelled in HFSS.

To design the patch antenna, the PCB characteristics below were used with the patch antenna design parameters [44]. The following parameters of the double sided copper clad epoxy glass FR4 [56] PCB board were known through the datasheet: permittivity $\varepsilon_r = 4.3$ and thickness $d = 1.588mm$.

The width of the patch (W) was determined using:

$$W = \frac{1}{2f_r\sqrt{\varepsilon_0\mu_0}}\sqrt{\frac{2}{\varepsilon_r+1}} \qquad (25)$$

Using the electromagnetic wave propagation in air, $W = 27.1mm$

The length of the patch antenna is

$$L = \frac{1}{2f_r\sqrt{\varepsilon_{reff}}\sqrt{\varepsilon_0\mu_0}} - \Delta L \qquad (26)$$

Where

$$\varepsilon_{reff} = \frac{\varepsilon_r+1}{2} + \frac{\varepsilon_r-1}{2\sqrt{1+\frac{12d}{W}}} \qquad (27)$$

and

$$\Delta L = \frac{0.412d(\varepsilon_{reff}+0.3)\left(\frac{W}{d}+0.264\right)}{(\varepsilon_{reff}-0.258)\left(\frac{W}{d}+0.8\right)} \qquad (28)$$

These equations gave L = 20.84mm

A microstrip $\frac{\lambda}{4}$ transformer was used to match the impedance of the patch to the 50Ω impedance of the source. This industry standard characteristic impedance specifies the ratio of voltage to current for a single travelling wave. Matching the impedance between the input and the output maximises the transmitted power.

Equations (29) through (34) were used:

$$Z_a = 90\frac{{\varepsilon_r}^2}{\varepsilon_r - 1}\left(\frac{L}{W}\right)^2 \quad (29)$$

$$Z_T = \sqrt{50 Z_a} \quad (30)$$

$$Z_0 = \frac{60}{\varepsilon_r}\ln\left(\frac{8d}{w_T} + \frac{w_T}{4d}\right) \quad (31)$$

$$\varepsilon_{re} \approx \frac{\varepsilon_r + 1}{2} + \frac{\varepsilon_r - 1}{2\sqrt{1 + \frac{12d}{w_T}}} \quad (32)$$

$$\frac{\lambda}{4} = \frac{\lambda_0}{4\sqrt{\varepsilon_{re}}} \quad (33)$$

$$Z_0 = \frac{120\pi}{\sqrt{\varepsilon_r}\left(\frac{w_m}{d} + 1.393 + 0.667\ln\left(\frac{w_m}{d} + 1.44\right)\right)} = 50\Omega \quad (34)$$

The transition line width and length were $w_T = 0.187mm$ and $\frac{\lambda}{4} = 13.15mm$ respectively, while the microstrip feed width was $w_m = 2.41mm$.

The patch return loss and radiation pattern are shown below.

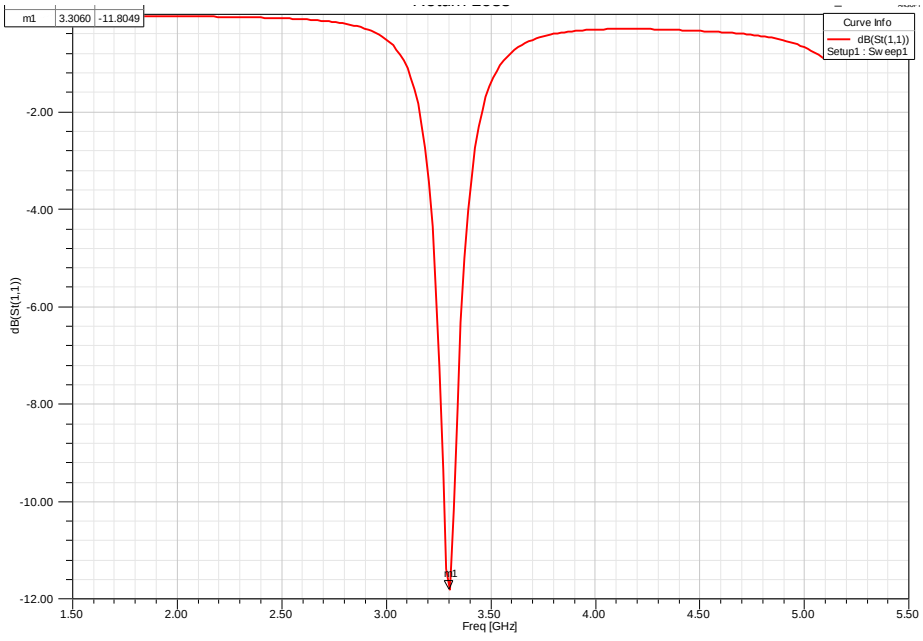

Figure 30: Patch S11 in air

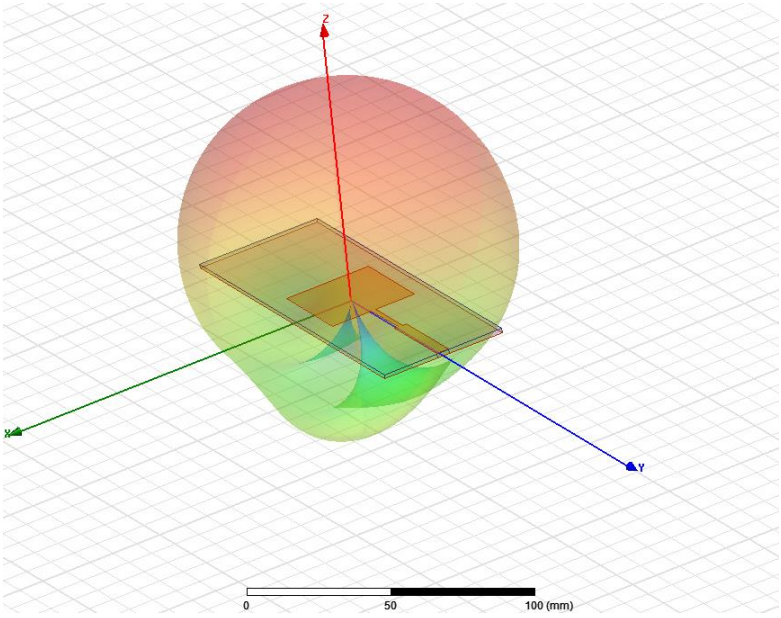

Figure 31: Radiation pattern

The strongest radiation field is perpendicular to the surface of the patch antenna and its bandwidth, shown in Figure 30, is much smaller compared to the monopole. The patch was then constructed, Figure 32, and tested. Its return loss is shown in Figure 33.

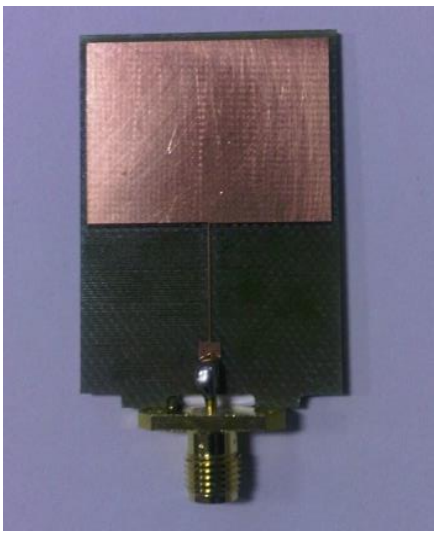

Figure 32: Patch antenna using transition line with λ/4 transformer

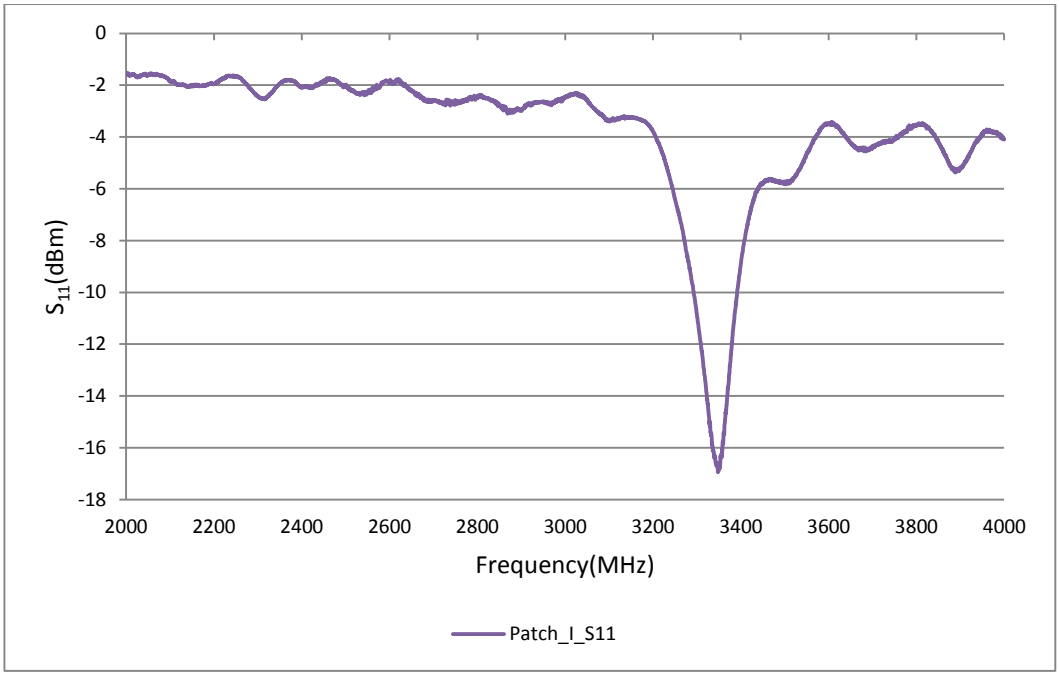

Figure 33: Patch antenna S11 in air

Testing this patch antenna showed that the measured frequency was 3.35GHz which was lower than the design frequency. In Figure 32, the quarter-wave matching transition line width is a $0.18mm$.

This strip width- $W_T = 0.18mm$ - is very thin thus creating a practical challenge as cutting this dimension accurately with the existing CNC router equipment available in the laboratory is very difficult. To minimize potential failures in manufacturing, a different type of feed was chosen for the patch, the inset feed.

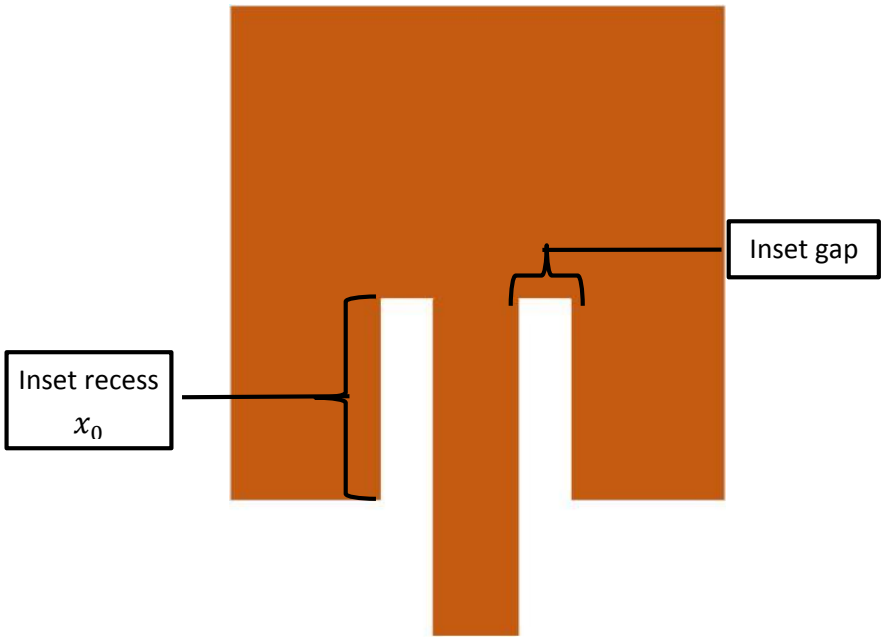

Figure 34: Microstrip antenna with inset feed line

The dimensions of the inset feed cutting into the patch, as shown in Figure 34, were found using equation (35) and optimised in HFSS.

$$R_{in}(x = x_0) = R_{in}(x = 0)cos^2\left(\frac{\pi}{L}x_0\right) \qquad (35)\ [44]$$

$$x_0 = 7.6mm$$

HFSS was used to optimise the antenna inset gap and depth of the cut into the patch. Different inset gaps were tried and the resonant frequency compared in Figure 35.

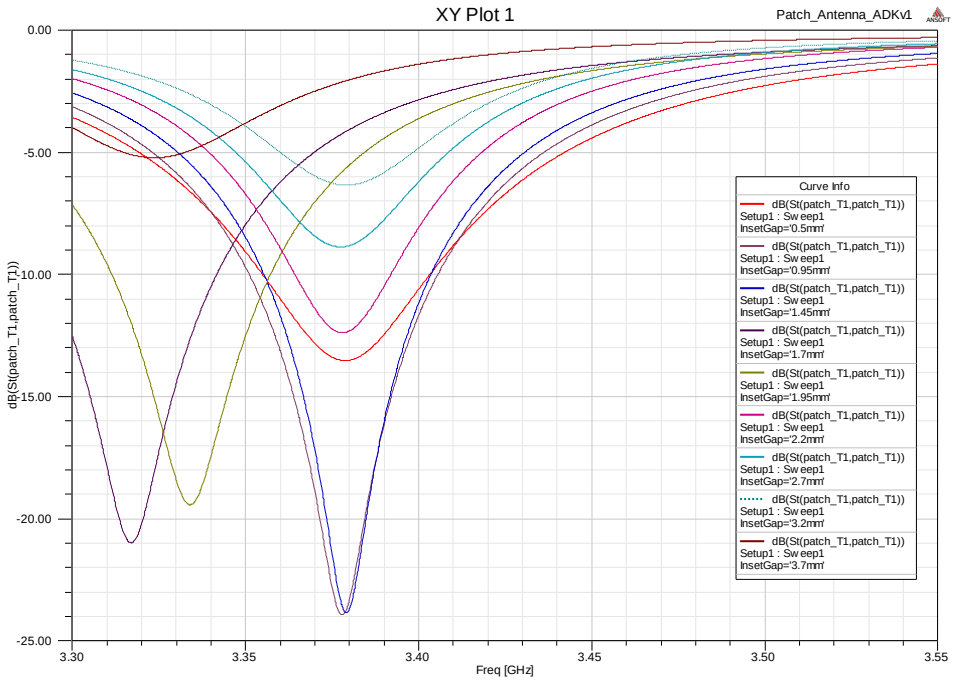

Figure 35: Return loss from Inset gap size

The values listed in Table 8 show that 1.45mm is the optimum inset gap for matching at 3.4GHz.

Table 8: Inset gap optimisation frequency and return loss results

Inset Gap (mm)	0.5	0.95	1.45	1.7	1.95	2.2	2.7	3.2	3.7
Resonant Frequency (GHz)	3.3787	3.3779	3.3791	3.3169	3.3339	3.3779	3.3774	3.3791	3.3236
Return loss (dB)	-13.53	-23.92	-23.83	-20.97	-19.42	-12.38	-8.88	-6.32	-5.23

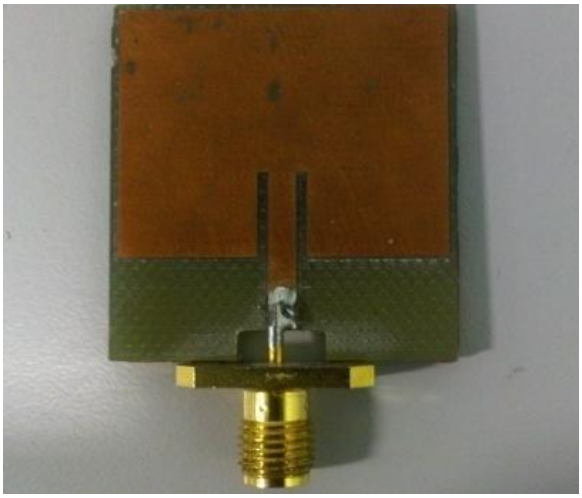

Figure 36: Patch antenna using transition inset feed

After designing the patch antenna from the calculations and the HFSS optimisation, the inset gap was found to be best at 1.45mm while the inset cut into the patch is 6.9mm. The constructed patch antenna in Figure 36 inset gap and recess were, however, measured to be 1mm and 7mm respectively.

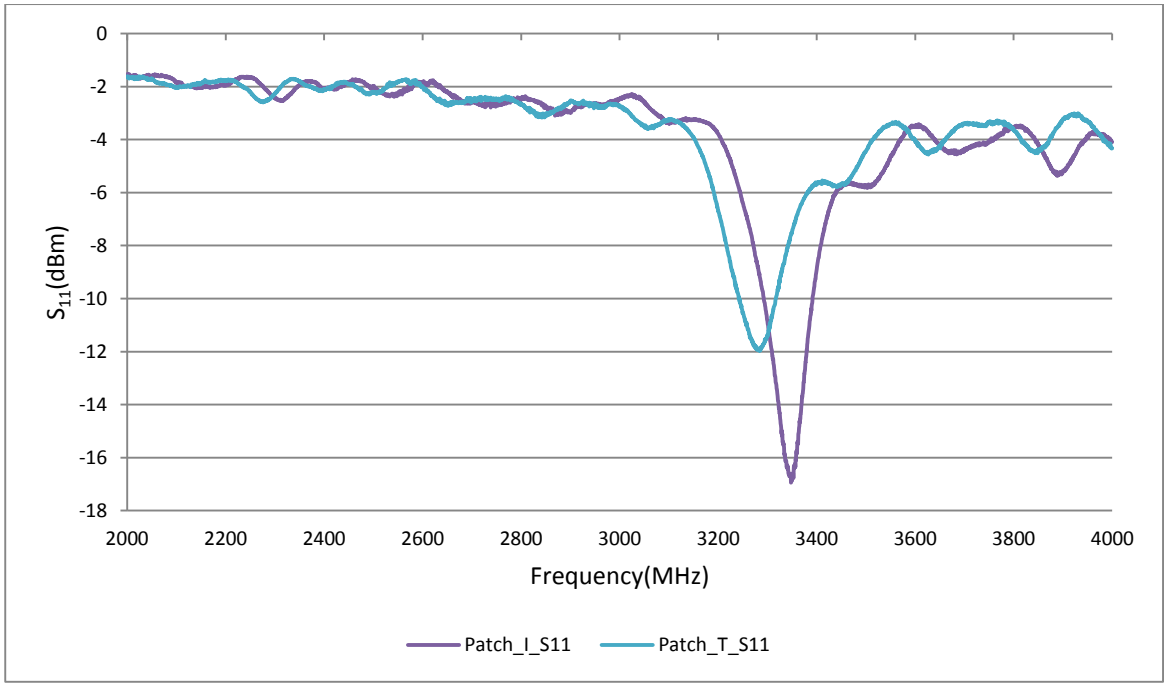

Figure 37: Patch antenna return loss in air

The two patch antennas were compared in Figure 37 and the results showed measured frequency was closer to the 3.4GHz target frequency for the inset type antenna (Patch_I_S11) with a better return loss than the transition line (Patch_T_S11) type. However, as shown by the HFSS radiation pattern simulation, the patch antenna will not cover the internal wall full circumference due to its directivity.

Despite the shortcoming of the patch antenna in terms of directivity, the single patch antenna was evaluated in the pipe filled with water and results showed very poor return loss as shown in Figure 38. Within the range of frequency measured, the different sections of the test rig returned frequency responses very similar to each other thus unusable for this purpose.

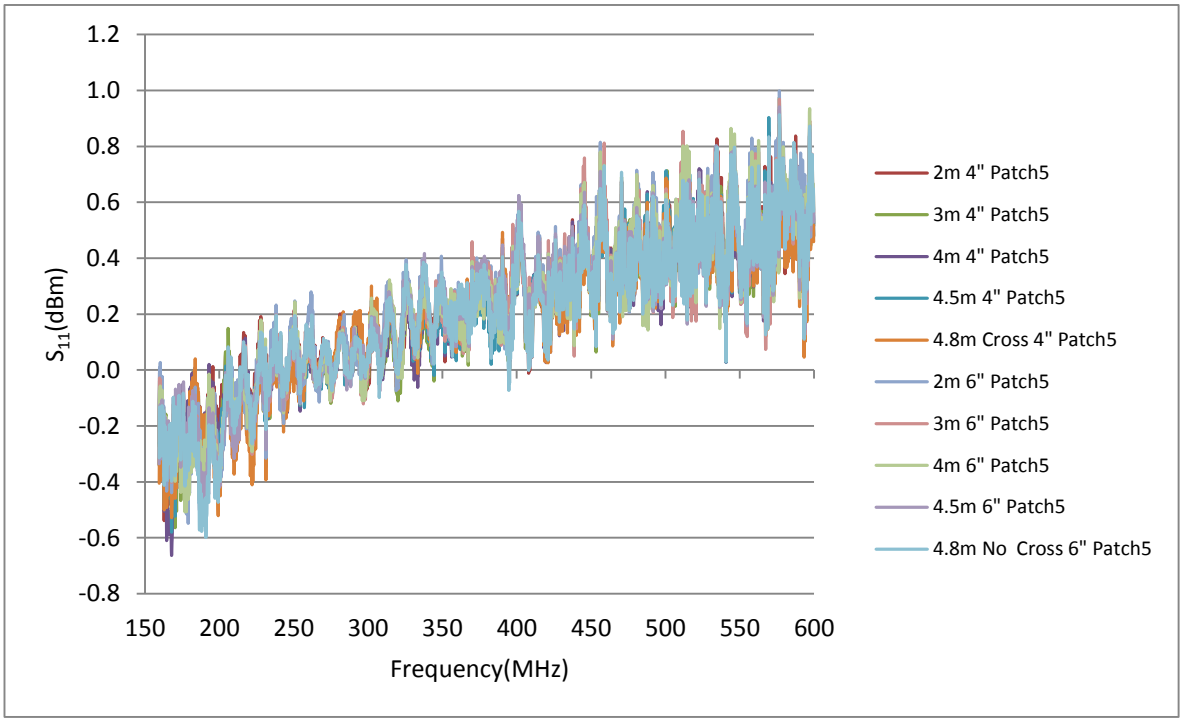

Figure 38: Test with patch antenna

The patch antenna results in water make it unsuitable for this environment application.

3.2 Choosing the antenna

For the purpose of this project, multiple antenna types, shown in Figure 39, were designed and tested on the rig.

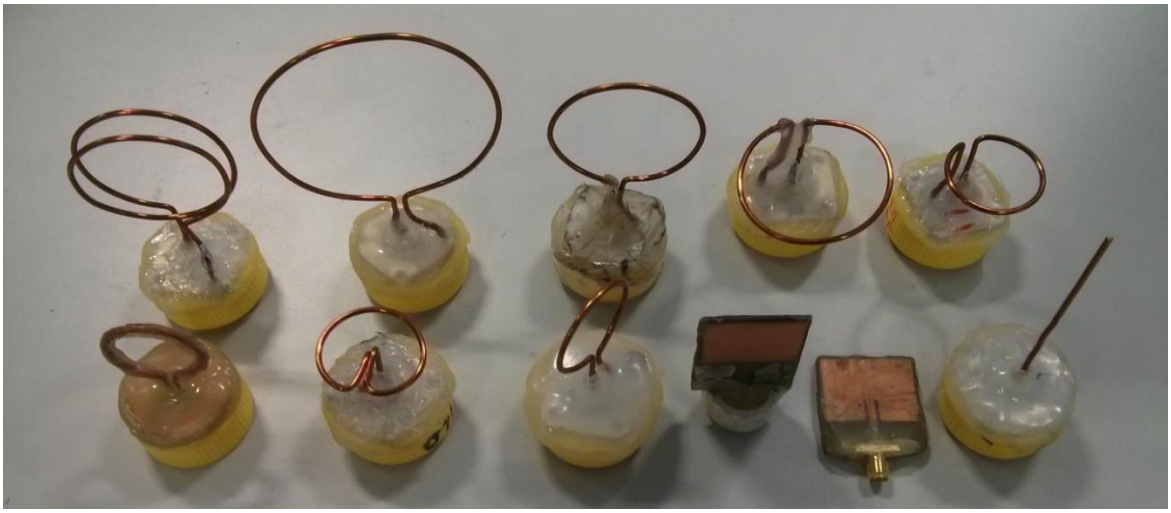

Figure 39: Set of antennas tested in the laboratory rig

However, the patch antenna with its poor return loss in water was rejected and the monopole antenna was discarded as it is more prone to physical damage and could not be integrated to the intended sensor casing which is based on the shape and dimensions provided by the stakeholders.

Therefore, considering the electrical and the physical characteristics of the different antennas, the loop antenna was chosen. Moreover, in water, experimental tests showed a better coefficient of reflection with a size small enough to fit in the pipe and within the sensor size constraint.

The loop antenna was retested with the standard Ø118mm water distribution pipe. To conform to the desired sensor casing shape, the straight loop was bent 90^{o} to test for its usability with the sensor. These two 28mm loop antennas were mounted on two caps (as shown in Figure 18) acting as the ground plane on each end of 720mm long Ø118mm pipe section filled with water.

(a) (b)

Figure 40: 28mm diameter a) straight loop and b) 90^{o} bent loop

The two ends were then connected to a vector network analyzer to measure the transmission S21 in order to compare the performance of the standard straight loop antenna and the 90^{o} bent version.

The graph in Figure 41 shows S21 for the loops when the pipe was filled with water.

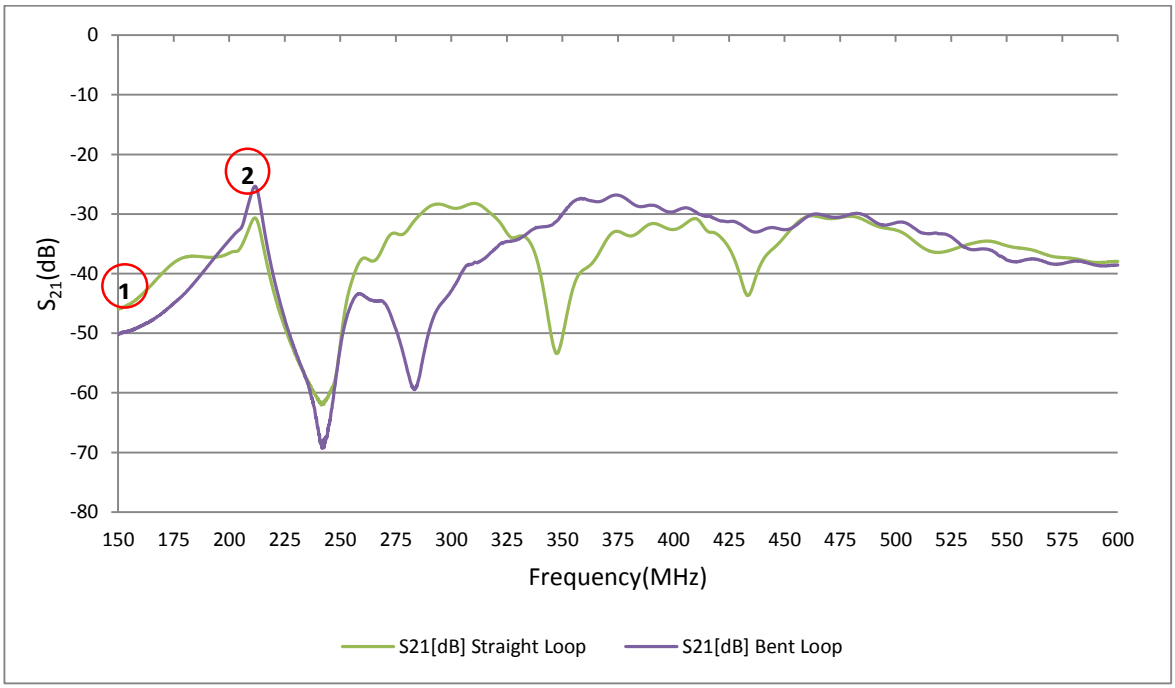

Figure 41: Cut-off frequency in the water pipe

The transmission starts above the pipe theoretical cut-off frequency determined

earlier in chapter 2. Furthermore, the two markers (1) and (2) show the transmission around 168MHz through 200MHz and dropping to the ambient noise level within the pipe below -50dB before restarting at above 250MHz as the frequency increases. These 'OFF' zones can be explained by the presence of different propagation modes that exist in the water pipe acting as a circular waveguide.

The antenna that will be used for the prototype is a loop for its low radiation resistance and its high sensitivity to the magnetic field H of the electromagnetic waves.

3.3 Laboratory facility

After using the 720mm cast iron section to determine the minimum frequency that would be used for the sensor, a test rig was built in the laboratory and it was used for all subsequent experiments.

The test rig is a 12 metre long, horizontal run comprising various sections, as shown in Figure 42.

A 5m long Ø118mm cast iron section was cut into at 2.5m for leak simulation, and a Ø118mm cross section was used to simulate T junctions while it is also used for antenna radiation tests in the pipe.

A 1.5m Ø118mm PVC section was included for the asset management experiments while a 5.5m Ø170mm pipe section was also connected for both asset management and leak detection experiments.

The insertion of any test equipment into the pipe was through an access hatch, which connects the Ø118mm section to the Ø170mm section.

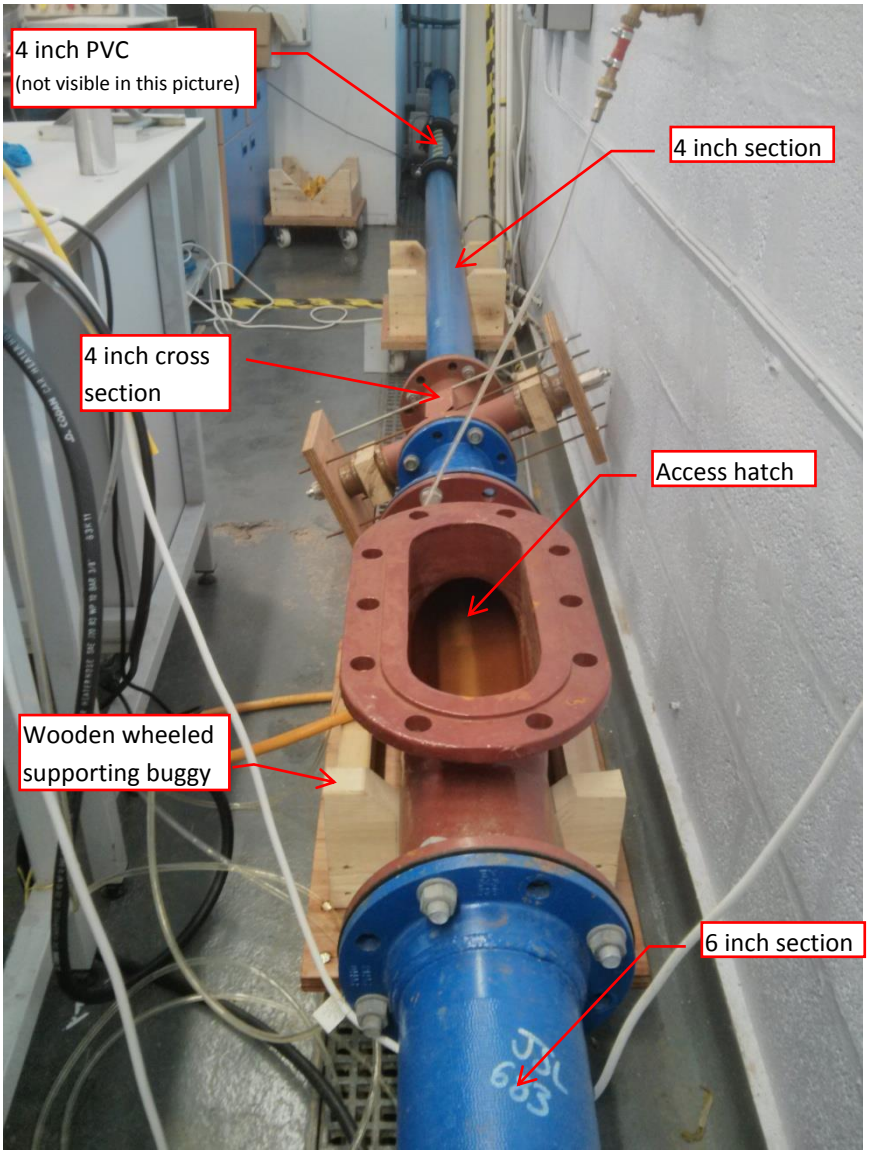

Figure 42: Laboratory test rig

To facilitate the insertion and removal of pipe sections into the rig, all the sections were mounted on wooden wheeled buggies, which also kept the rig level along its whole length.

3.4 Signal Attenuation

In wave propagation, the signal attenuates as the distance of propagation increases. This attenuation is dependent on the frequency and medium of propagation.

The wave attenuation in the propagation medium is the reciprocal of the skin depth δ

which is the distance that the wave will travel before its power is reduced to 36.8% [46]. It is expressed by equation (36):

$$\delta = \frac{1}{\alpha} = \frac{1}{\omega\sqrt{\mu\varepsilon}\left\{\frac{1}{2}\left[\sqrt{1+(\frac{\sigma}{\omega\varepsilon})^2}-1\right]\right\}^{1/2}} m \qquad (36)\ [46]$$

α the attenuation constant

σ the medium conductivity

This test was carried out using the 5m Ø118mm pipe filled with water, shown in Figure 43, with an antenna attached on a flange at its end which then was connected to the VNA port 1. Another antenna was connected to port 2 and pulled away at fixed distances to measure the transmission coefficient S21 for comparison at various frequencies.

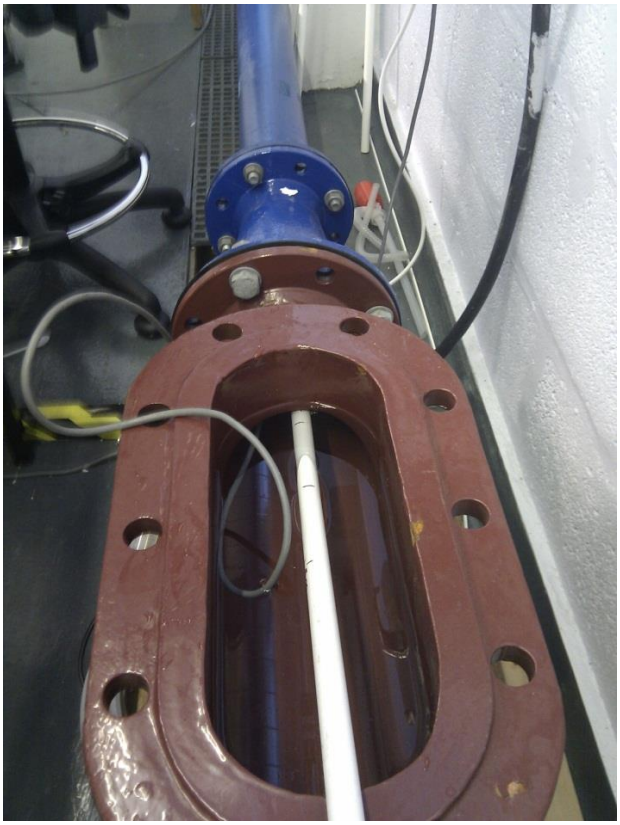

Figure 43: Sensor pushed inside the test pipe

Considering 187.51MHz, the cut-off frequency in the pipe derived earlier in water,

the attenuation was tested using a loop antenna in the range of 100MHz to 1GHz to cover both the TE and TM dominant modes. The results of the test are plotted in Figure 44.

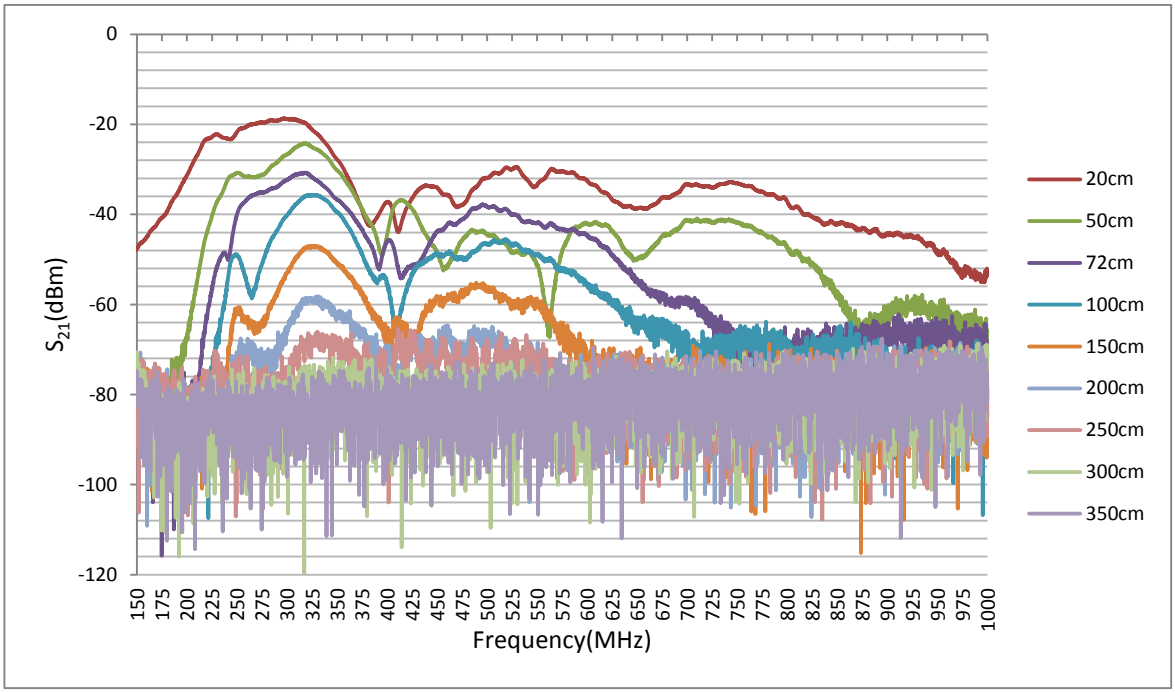

Figure 44: Attenuation with a loop antenna

As expected, it can be observed that the attenuation increases at high frequency in water and the waves propagation starts above the cut-off frequency.

For example, the loop antenna, at 250MHz, the attenuation is 21.7dBm at 20cm rising to 72dBm as the distance increases to 200cm and 83dBm at 350cm. Meanwhile, at high frequency, the amplitude starts as low as -33dBm at 20cm and dropping to -93dBm within the ambient noise level of the VNA.

With attenuation of the wave at the set frequency range determined, the size of the antenna was reviewed following an amendment to the sensor design dimensions by the stakeholders. This allowed the maximum diameter to be 60mm and meant that a larger loop could be considered.

3.5 Antenna sizing

In a water distribution network, access valves like the one shown in Figure 45 at the United Utilities Worthington test site are placed strategically along the network to allow system maintenance. These have a limited diameter from which the sensor is expected to be inserted using a launching system. This launching system, which will be designed by a partner company, will allow the insertion of the sensor without disrupting the water to the customer in the section under inspection.

However, the length of the sensor is still set to 100mm maximum in relation to the tight insertion angle usable in existing access valves.

Figure 45: Access valve in the Worthington UU test site

The implication of this change was that the diameter of the loop antenna could be increased if necessary, thus affecting the resonance frequency of the antenna. To determine the resonance frequency of the loop antenna, equation (37) is used:

$$f = \frac{c}{\lambda} \qquad (37)$$

with $\boldsymbol{\lambda = \pi \times d}$ (38)

With this sizing flexibility, different types of antennas shown in Figure 39 were tested in the rig built in the lab - Figure 42. However, only the results of four loops were included in this document as a loop antenna type was chosen for the sensor. With the new constraints, tests were carried out in the laboratory using the 12m long rig. In addition to measuring the coefficient of reflection of the antennas, each loop antenna was tested against its 90° bent version to determine the best orientation. Each section of the rig had corresponding marks taped along the PVC pushing rod. The antenna was pushed at distances corresponding to a section. The acronyms BL and SL represent bent loop and straight loop respectively. Branching in the network is simulated by the insertion of a Ø118mm cast iron cross section referenced on all the graphs as Cross.

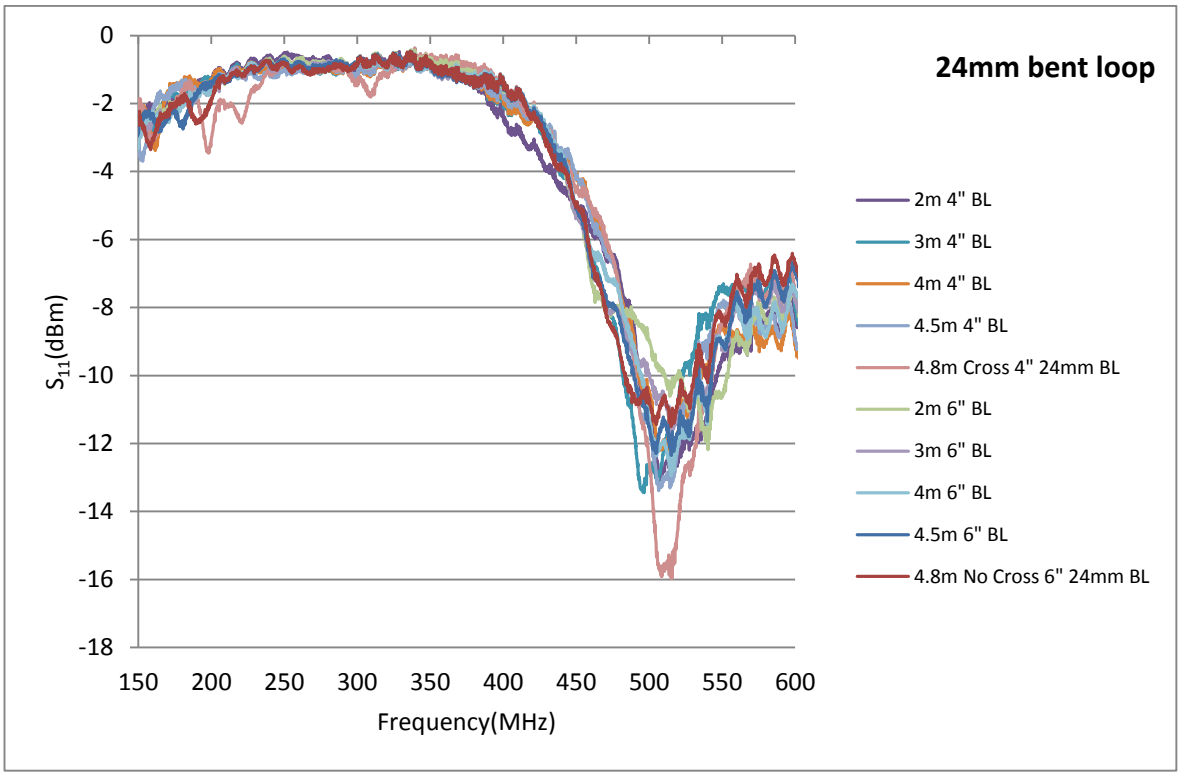

Figure 46: Test with 24mm bent loop

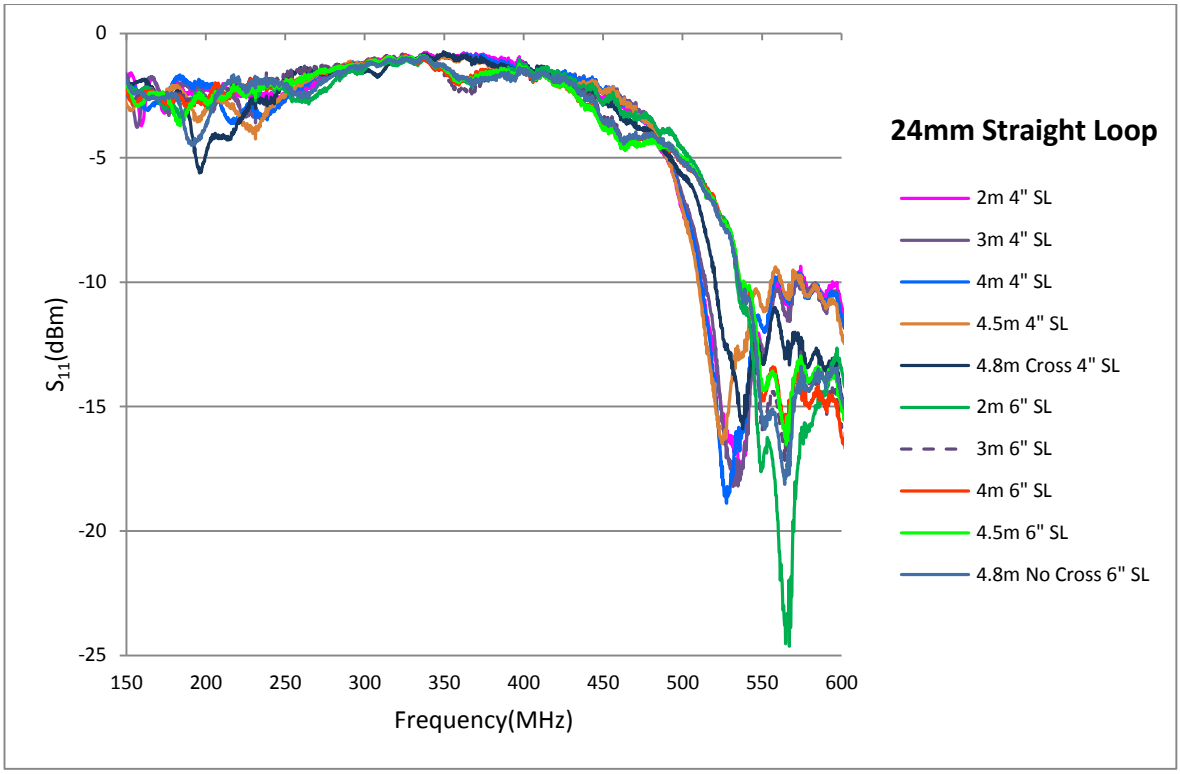

Figure 47: Test with 24mm straight loop

Both the 24mm straight and bent loops resonated in the 500MHz region in the pipe filled with water, and it was decided to design one for lower frequency so to reduce the attenuation. Thus, a bigger loop was designed in order to shift the resonance in a lower frequency region. The diameter of the antenna was increased to 39mm corresponding to a resonant frequency in air of 2.45GHz, which reduces to around 272MHz in water. The range of the frequency of interest in water was set to between 50MHz to 600MHz. This range was chosen because it covered the cut-off frequency in water required for the Ø118mm and Ø170mm pipe which is 187.51MHz and 124MHz respectively.

The resizing of the antenna improved the signal coefficient reflection response in the region of 170MHz to 350MHz from -5dBm to -7dBm.

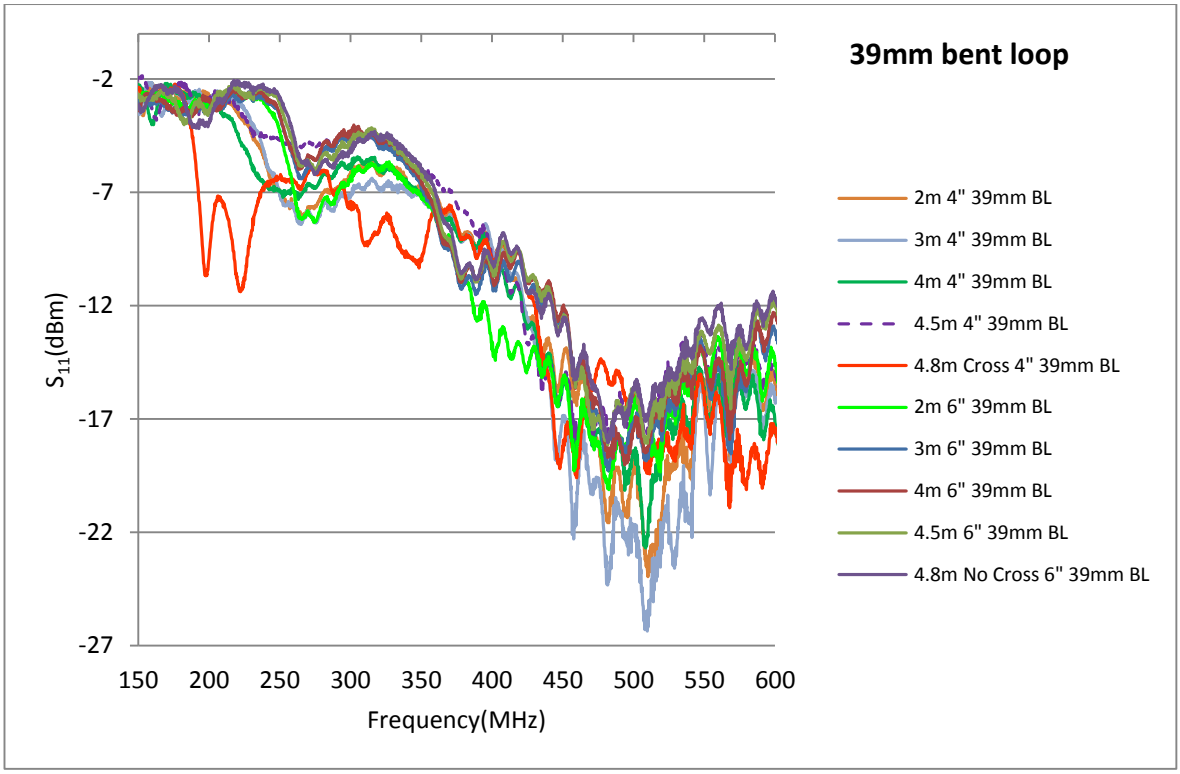

Figure 48: Test with 39mm bent loop

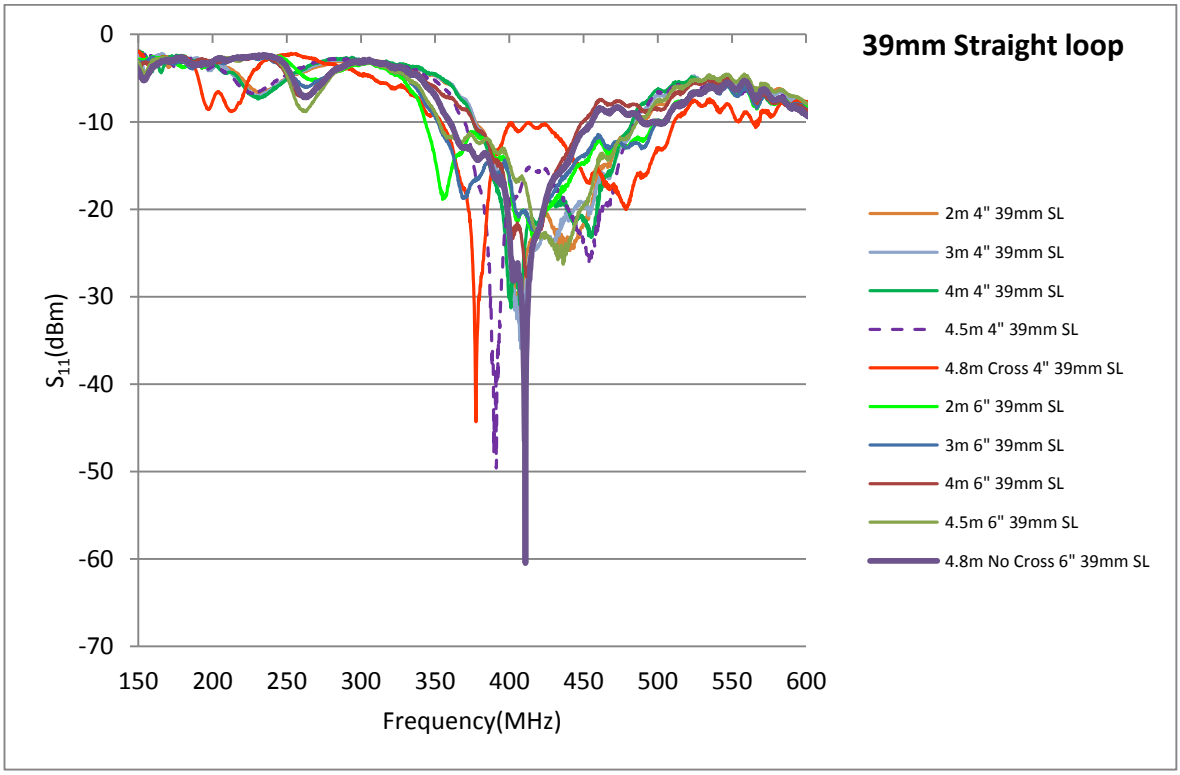

Figure 49: Test with 39mm bent loop

Experiments with the 39mm loops showed a shift in the resonance peaks and a clearer difference between the frequency responses.

The 39mm standard straight loop (39mm SL) antenna showed the best characteristics for leak detection and asset management in the water distribution pipes with distinct frequency responses for each pipe section and condition in the rig. The coefficient of reflection and the frequency response bandwidth were shown to be acceptable as the power level range from -5dBm to -50dBm, in the frequency range of 200MHz to 600MHz, was well within the capability of the VNA.

3.6 Antennas radiation pattern

In this section, the radiation of the antenna was investigated. The antennas were tested in both the pipe filled with water and in an open water tank. The radiation pattern is “a mathematical function or a graphical representation of the radiation properties of the antenna as a function of space coordinates. In most cases, the radiation pattern is determined in the far-field region and is represented as a function of directional coordinates...” [54]. This was done to show how the electromagnetic waves radiated in the pipe compared to open water. Radiation, which interacts with the full circumference of the internal wall of the water distribution pipe is desired.

When the antenna dimension is significantly smaller than the wavelength, the following near field and far fields conditions apply:

For the near field:

$$\frac{\lambda}{2\pi} < r < 3\lambda \quad (39)\ [44]$$

For the far field:

$$r > 3\lambda \quad (40)\ [44]$$

r is the distance from the antenna

With the loop antennas used for these measurements in the Ø118mm pipe, the radiation field was in the near field region as r was less than the maximum 52mm internal diameter for the Ø118mm and less than the maximum 152mm internal diameter for the Ø170mm pipe.

With the wavelength of the 39mm loop using equations (39) [44] and (40) [44], the distance of the antenna at 3λ from the receivers or the walls of the pipes, were 226.1mm and 367.5mm respectively.

In the pipe, this distance is greater than the maximum radius available of the pipe. Therefore, the radiation pattern to be measured was within the near field region.

To carry out this test, 3 antennas were used for the setup as shown in Figure 50.

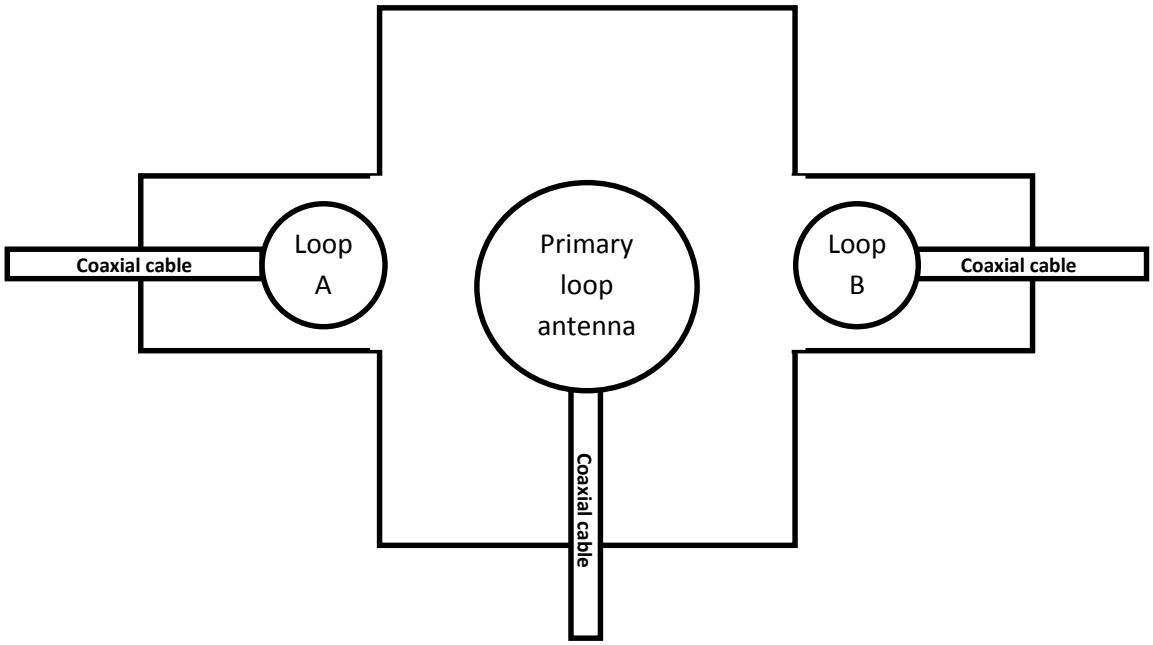

Figure 50: Antennas setup diagram in the Ø118mm cross section

Using 'Loop A' and 'Loop B' to receive the power transmitted from the 'Primary loop antenna' will show if the sensor is able to cover the full circumference of the pipe. The advantage of reading from two symmetrical positions (Loop A and Loop B) was that the rod was only turned 36 times instead of the 72 times required to complete

the 360^{o}.

This was setup for the experiment shown in Figure 51.

In the pipe setup, a primary antenna was connected to a signal generator – R&S SMB-B103[57] through a 360 degree dial plate. The primary antenna was turned in 5 degree steps to a full circle. Two identical secondary antennas A and B were positioned symmetrically on both side of the primary antenna and connected to a spectrum analyzer – HAMEG HMS-3G [58] - to read the power level of the signal radiated as shown in Figure 51.

With this distance of $226.1mm$, $\mathrm{r} < 3\lambda$ and the plotted radiation pattern is in the near field region.

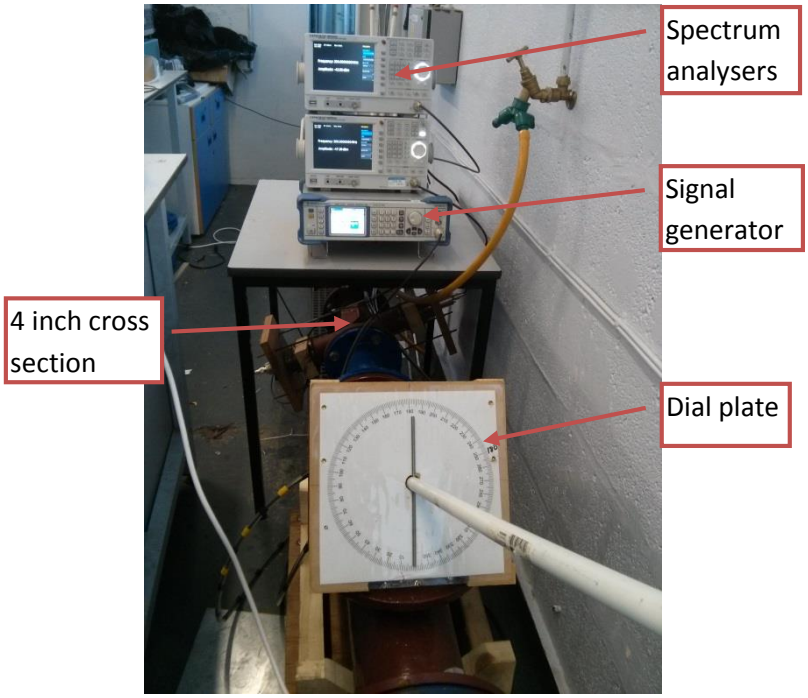

Figure 51: In pipe radiation pattern setup

The readings taken were then plotted to show the radiation pattern within the pipe.

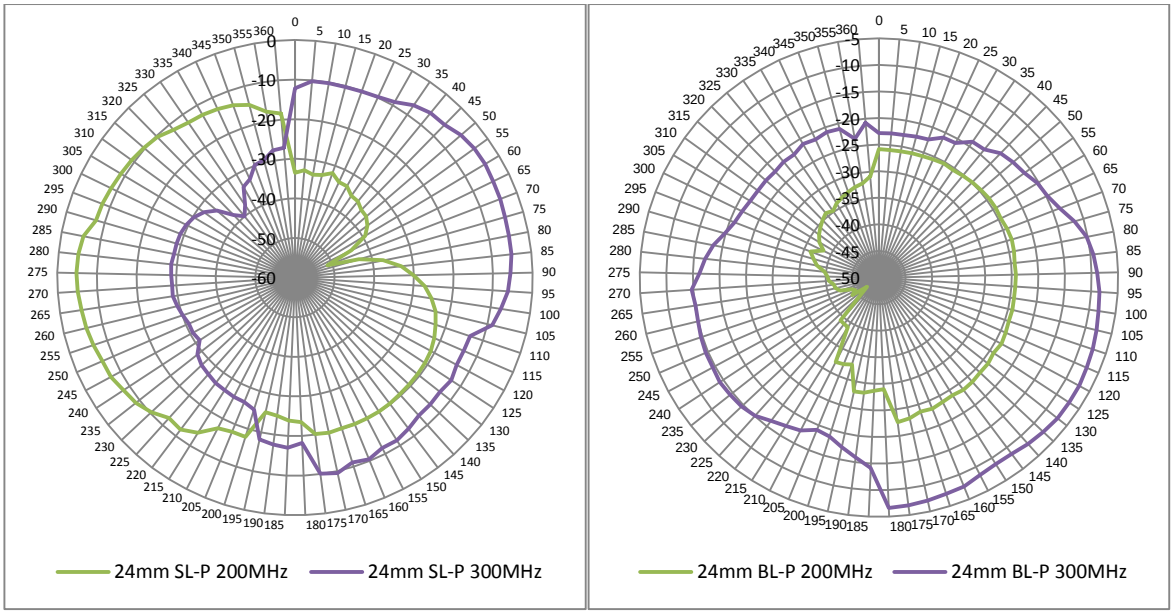

Figure 52: Radiation pattern of 24mm loop in the Ø118mm water pipe

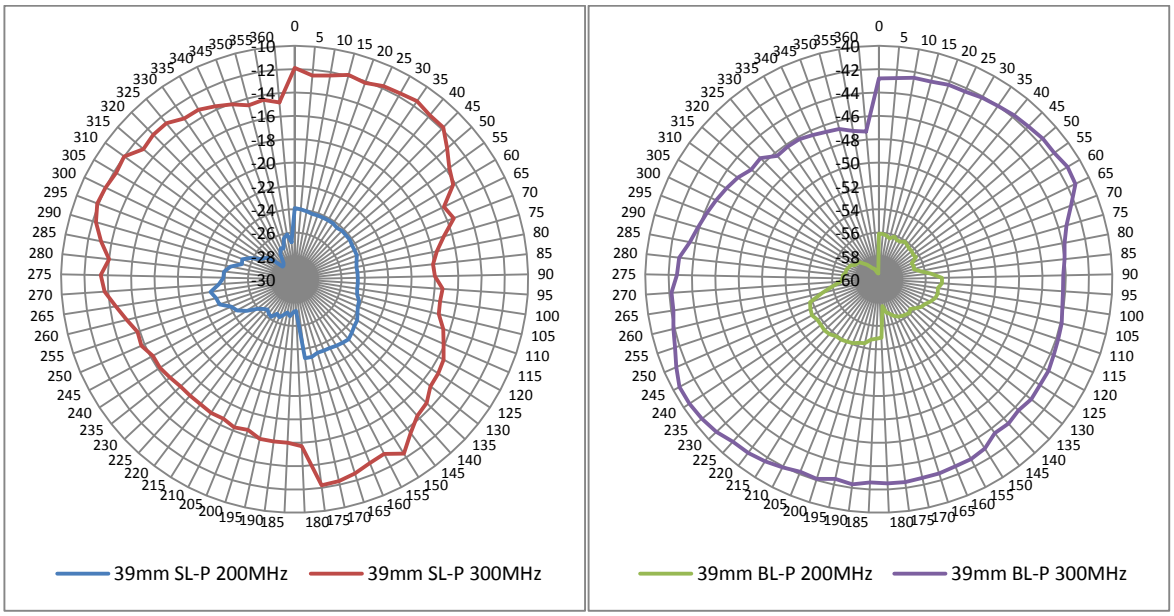

Figure 53: Radiation pattern of 39mm loop in the Ø118mm water pipe

The results for the pipe filled with water showed that all the loops displayed a nearly omni-directional radiation pattern at 300MHz. Using these antenna for the sensor at a range including this frequency would therefore ensure the full coverage of the circumference of the pipe internal wall.

Because the sensor also needs to be used in bigger pipes, a second experiment to

determine the behaviour of the antenna was also carried out in an unbounded environment to simulate the increase of pipe diameter. The amount of water surrounding the antenna was large enough that any waves reflected from the boundary are absorbed.

This experiment was setup as in the diagram in Figure 54 in a plastic tank filled with fresh water. The Tx antenna was maintained under water by a concrete block attached to the transmitting antenna casing made to keep the connector watertight.

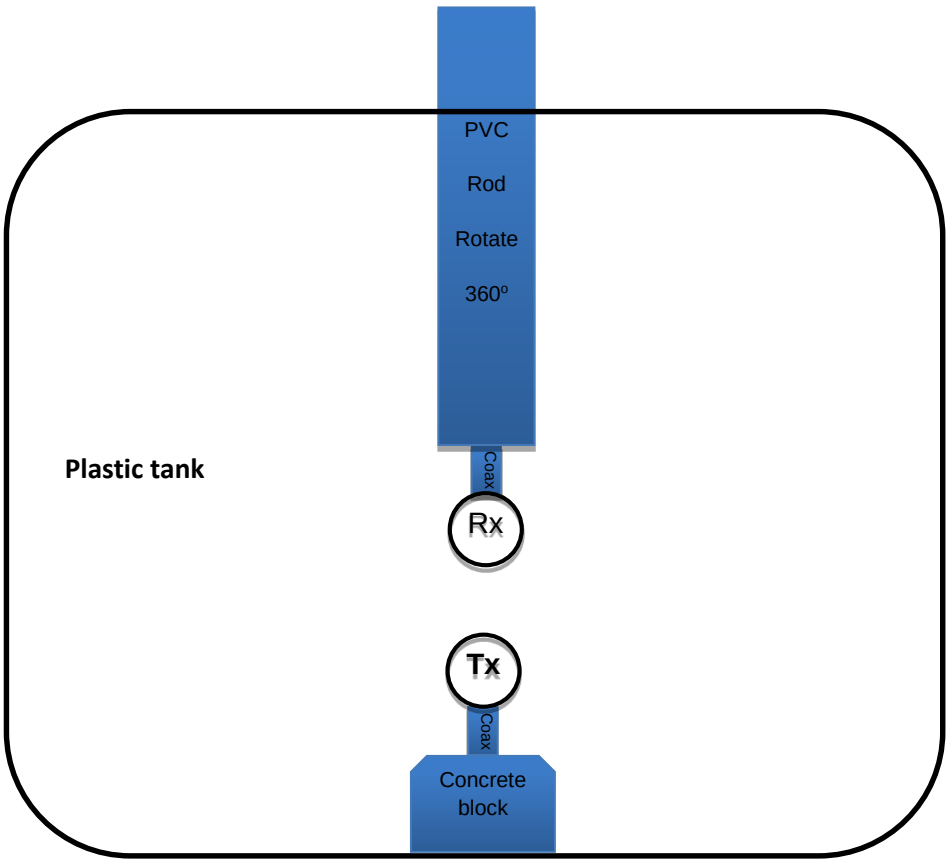

Figure 54: Setup diagram in the tank

The transmitter loop antenna Tx was connected to the same signal generator – R&S SMB-B103 while the antenna under test Rx was connected to the spectrum analyzer – HAMEG HMS-3G as the previous setup and 72 measurements were taken at 5º steps.

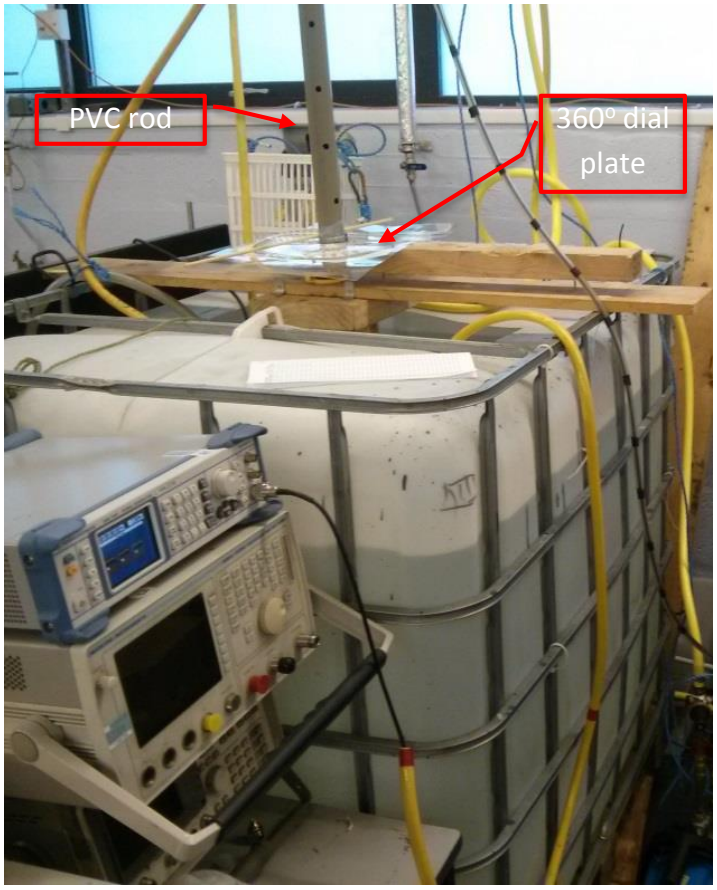

Figure 55: Tank radiation pattern setup

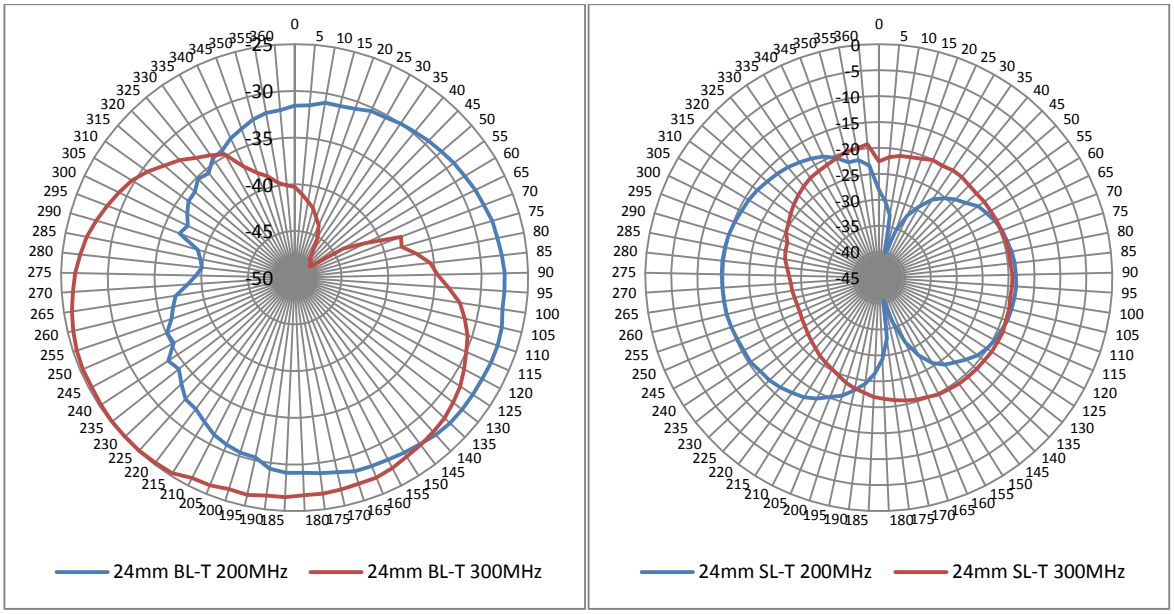

Figure 56: Radiation pattern of 24mm loop in the Ø118mm water tank

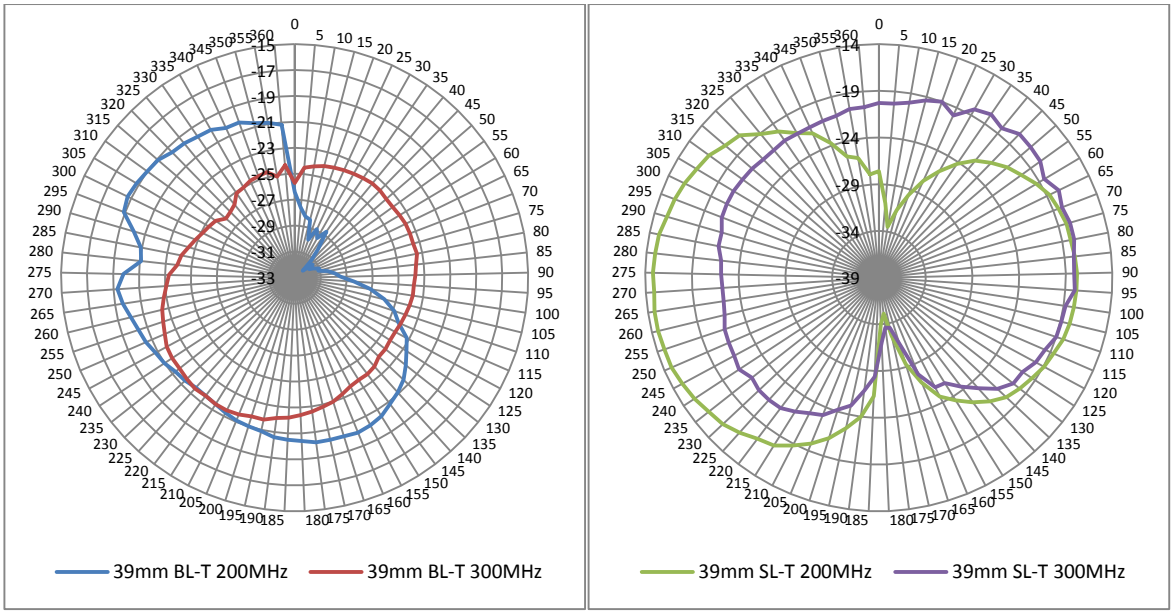

Figure 57: Radiation pattern of the 39mm loop in the Ø118mm water tank

As in the pipe, the radiation plots taken from the tank experiment are nearly omni-directional at 300MHz.

However, for both straight loops (SL), the radiation pattern at 200MHz matches the pattern of a typical loop antenna.

This observation confirmed the frequency range to be used for the sensor; which would be above the cut-off frequency in the pipe filled with water to 600MHz as a maximum.

3.7 Casing effect

The sensor needed to be waterproof if to protect the antenna and electronic components. However, enclosing the antenna within a medium will affect the antenna performance to some extent.

A nylon [59] casing was machined as shown in Figure 58, to determine whether this effect would be significant.

A transmission (S21) test was conducted in the Ø118 water filled pipe with and

without the nylon casing.

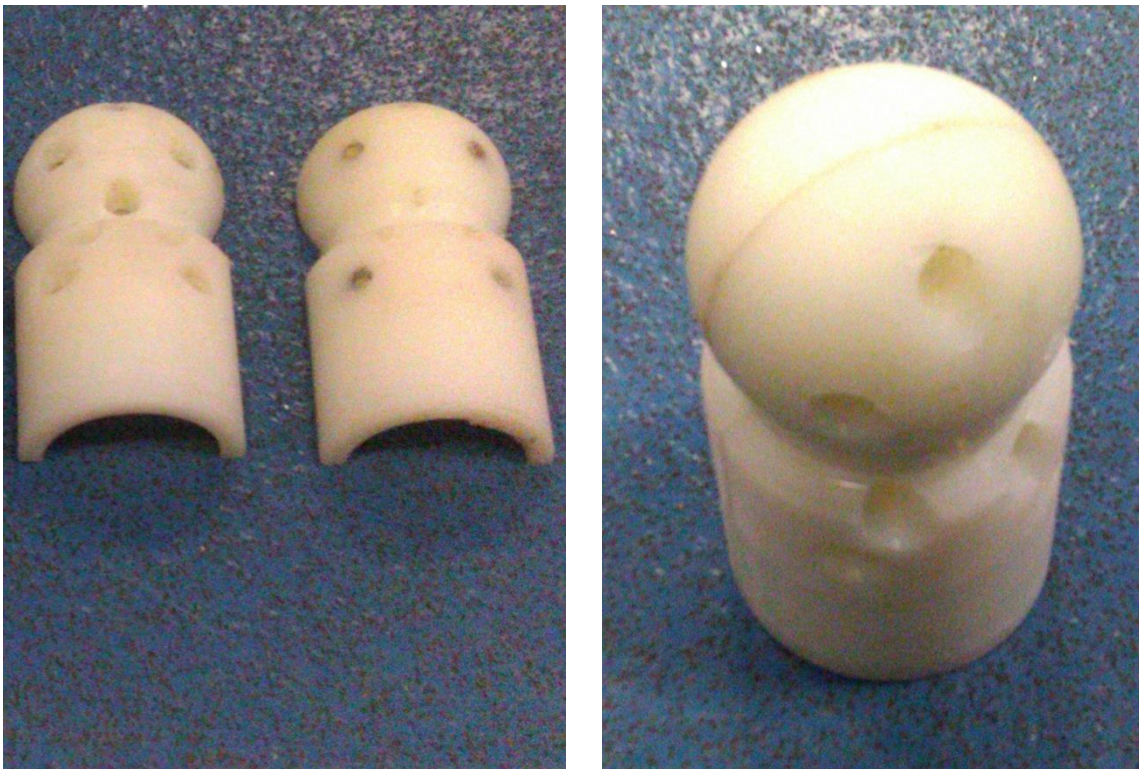

Figure 58: Nylon casing

This nylon casing housed the 39mm straight loop antenna. The two parts were bonded together around the Ø1.6mm wire forming the antenna.

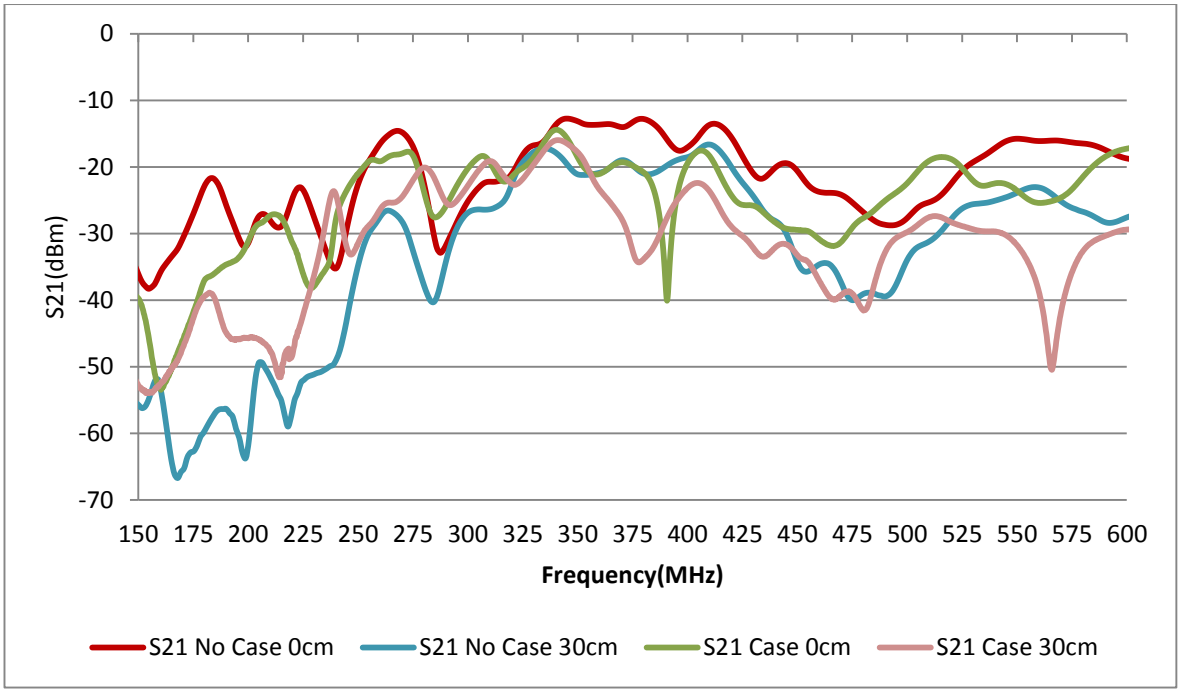

Figure 59: Test with no casing in water

Results of this test showed that the transmission S21 between the transmitter and the receiver has attenuation less than 5dBm for transmission within most of the frequency range but over 5dBm from 350MHz when at 30cm distances and rising to 20dBm at 560MHz. The frequency range of the sensor will be set below 1GHz to minimise the attenuation while starting above the cut-frequency of the pipe.

3.8 Summary

While the three selected antenna types performed well in air, only the monopole and the loop antenna showed an acceptable return loss in water. The loop antenna was selected because of its physical strength and ease of integration into the circular sensor casing. The signal attenuation test showed that the potential range of the sensor is up to 1.5m at 300MHz. The radiation pattern test in the pipe and the tank confirmed that the loop antenna covers the circumference of the pipe, reaching cracks developing into the shell. This distance between the sensor and the wall is

within the near field region of the antenna, so if the pipe size significantly increases, the diameter of the antenna may also need to be increased in order to detect leaks.

Chapter 4: Leak detection and asset management

This chapter explores the use of electromagnetic waves to detect simulated leaks using nylon rings and detecting pipe materials and diameters to simulate asset management. The loop antenna will be connected to a VNA and measurements taken and compared.

4.1 Leak detection experiments

Experimentation was required to test if the designed loop antenna is able to identify a leak in a water distribution pipe.

The laboratory experiment setup shown in Figure 60, is a 1230 mm long pipeline filled with fresh water made with two Ø118mm cast iron sections of individual length of 720mm and 510mm and using a 50mm PVC pipe to keep the sensor centred. It is expected that if a leak is present, the spectrum frequency and or amplitude should vary with the magnitude of the leak.

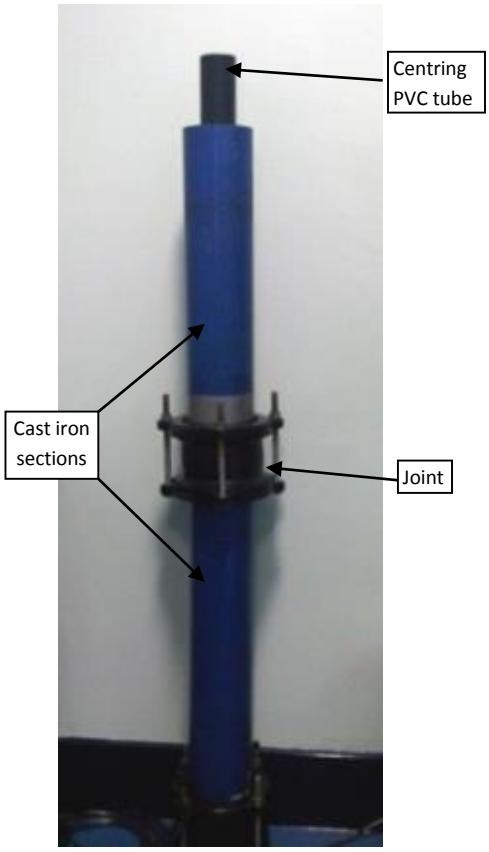

Figure 60: Lab experiment setup pipe filled with water

In order to simulate leaks, three nylon rings of different thickness shown in Figure 61 were used between the two cast iron pipe sections. The thickness of the rings were 3mm, 5mm and 10mm respectively. When no ring is used between the two cast iron sections, the gap used to simulate the leak is less than 1mm.

Figure 61: Three nylon ring thickness used

A 28mm straight loop antenna prototype was used to take measurements of the frequency response of all the simulated leaks for comparison from 150MHz to 600MHz. This frequency range was selected based on the cut frequency of the pipe determined in chapter 2 and the signal attenuation level determined in chapter 3. The antenna was connected through a coaxial cable to the Rhode & Schwarz ZVL-3GHz VNA and lowered to the coupled section through the centring PVC pipe. Measurements were then taken with all 3 rings inserted in turn and as well as without any ring to simulate the 1mm leak.

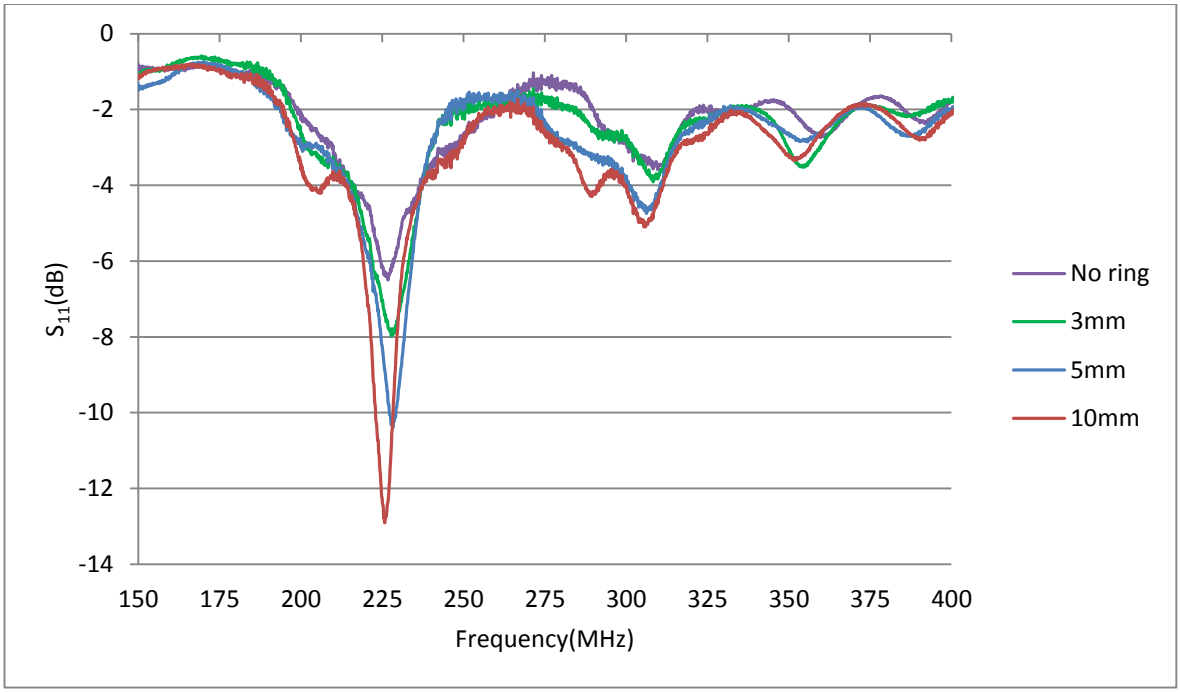

Figure 62: The S_{11} measurement with the loop antenna

The result plotted in Figure 62 showed a different frequency response for each simulated leak, varying between 200MHz to 310MHz. However, the most significant response is in the range of 209MHz and 240MHz.

After the setup experiment with these short pipe sections, tow leaks were simulated in the 12m horizontal rig by partially sawing through the metallic shell of both the 5 metre Ø118mm section and the Ø170mm section at the 2.5m mark on each shown in Figure 63 and Figure 64.

Figure 63: Crack to simulate leak

Figure 64: Leakage from the Ø118mm pipe

After experimenting with multiple antenna types and sizes, the 39mm straight loop, Figure 65, was retained as it showed consistent results, which could be used to determine whether the sensor was close to the leak.

To make the connection water proof the antenna and the coaxial cable were glued

in a 50mL polypropylene centrifuge tube and wrapped with parafilm as shown in Figure 65.

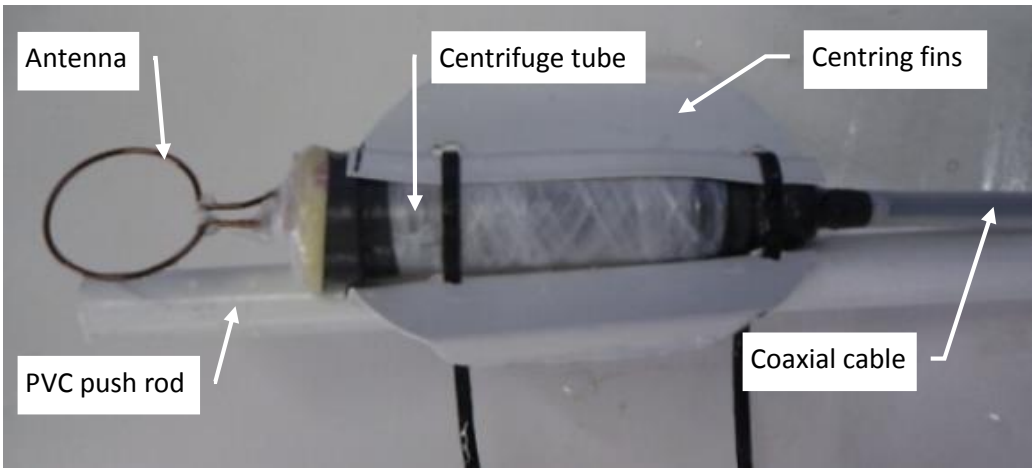

Figure 65: Loop antenna with fins and coaxial cable on the push PVC rod

This loop antenna assembly was then pushed inside the rig filled with water - Figure 66. The loop antenna was connected to the Rhode & Schwarz ZVL-3GHz VNA with the coaxial cable insulated from the water using a clear plastic tube. Measurements were then taken at fixed distances along the Ø118mm pipe.

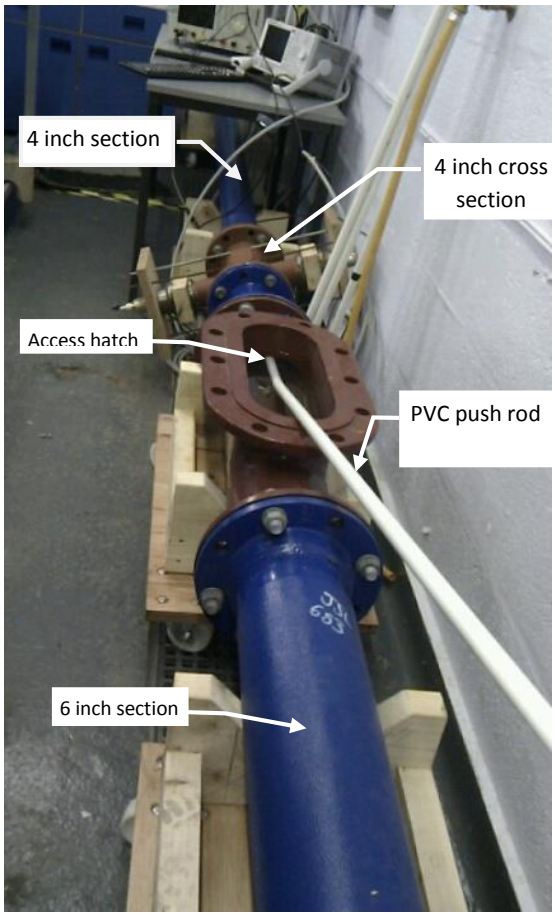

Figure 66: Test rig in the lab – 12m long

The frequency response from the measurements showed a distinct spectrum for the leak and no leak condition in Figure 67.

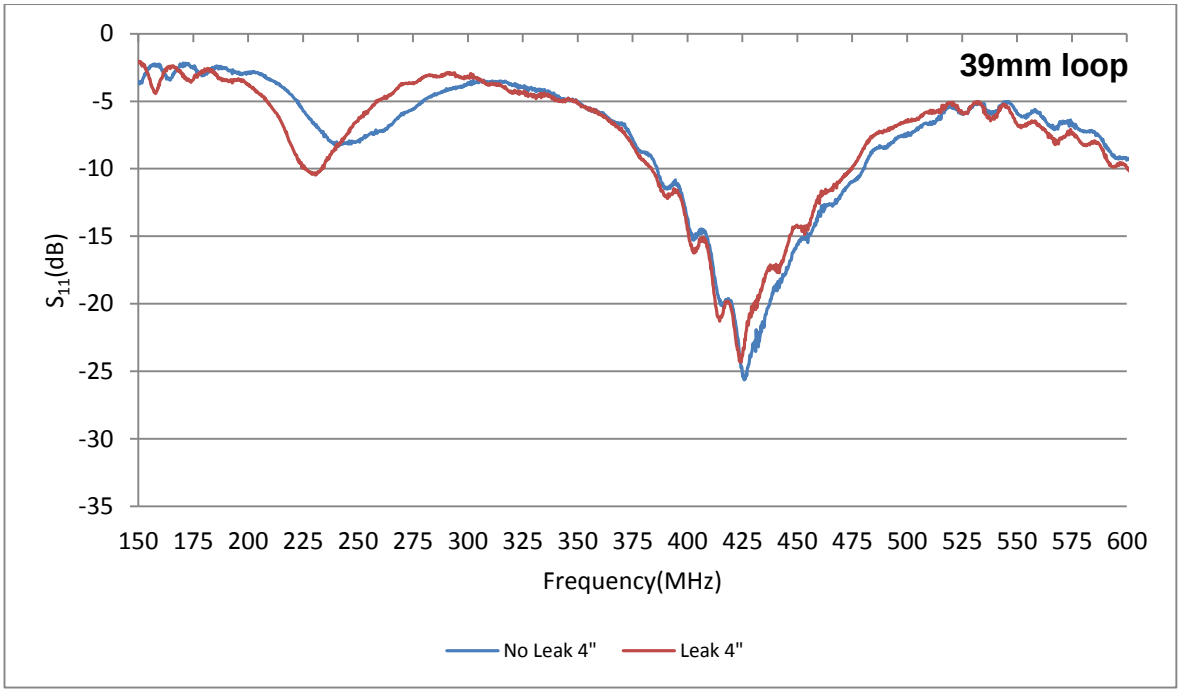

Figure 67: Leak detection on the Ø118mm pipe

Using the PVC rod, the sensor was then pushed inside the Ø170mm which also was sawn to simulate the leak.

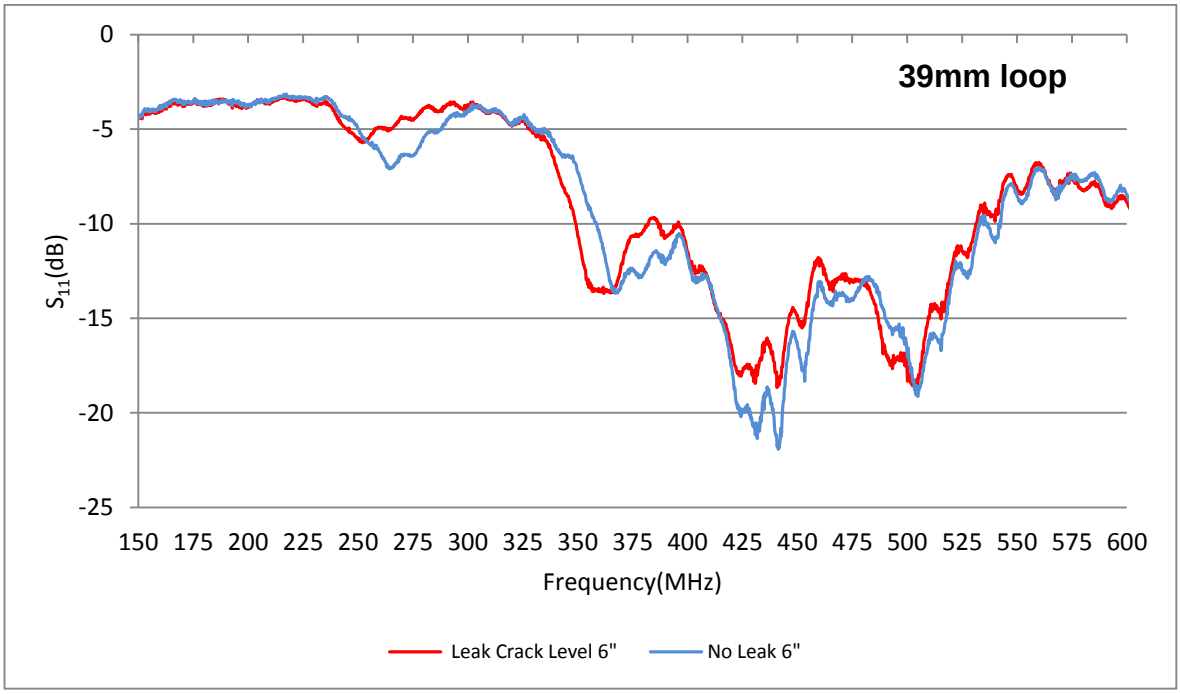

Figure 68: Leak detection on the Ø170mm pipe

Again distinct spectrum were observed for the 2 conditions of leak and no leak when

the sensor is away from the crack by 80cm.

A further test was completed to demonstrate that what sensor was measuring was in fact the disturbance of the electromagnetic field due to the insertion of a discontinuity (crack) into the pipe metallic shell. The areas around the cuts into both pipes were sanded to remove the surface paint and then aluminium tape AT502-50 – TAPE [60] was used to restore the conductive continuity of the pipe.

Figure 69: Non-conductive paint removed

Measurements were taken and compared with previous test on from both pipes.

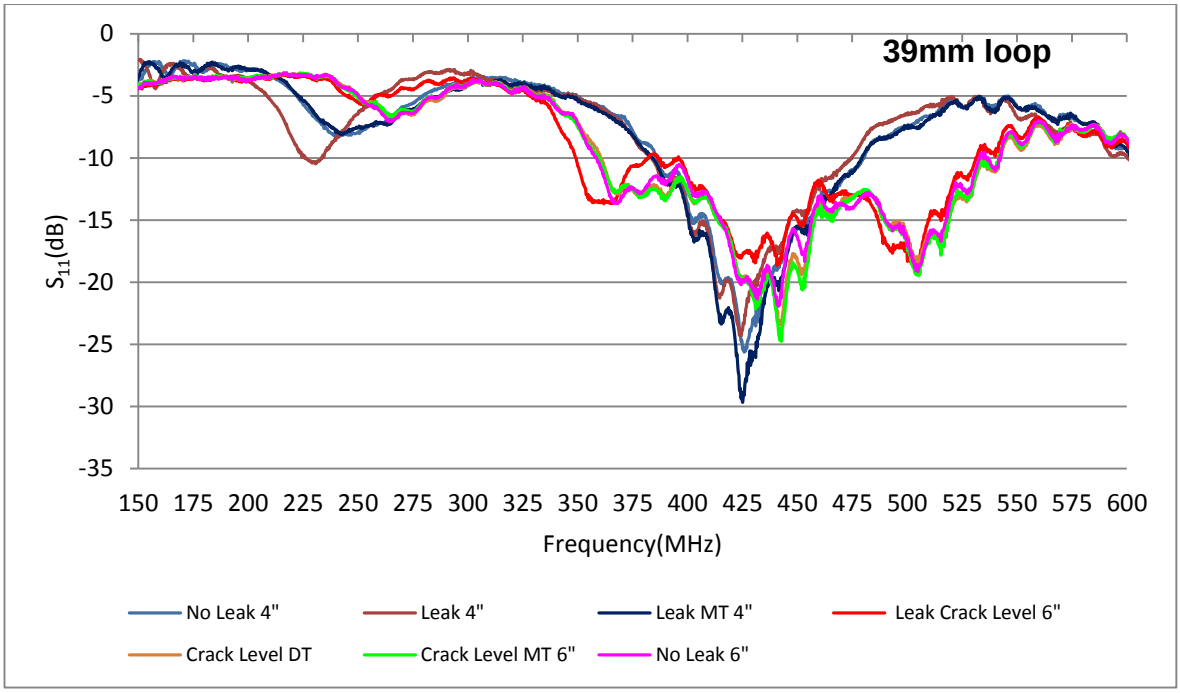

Figure 70: Pipe shell integrity restoration

As the frequency responses for 'No Leak 4' and 'Leak MT 4', and 'No Leak 6' and 'Crack Level MT 6' respectively overlap in Figure 70, a high correlation of 0.987 and 0.992 is calculated. This high correlation is because of the metallic tape (MT) used to restore the continuity of the metallic shell with the electrical field thus the integrity of the pipe was no longer compromised.

Meanwhile, with duct tape (DT) used on the Ø170mm section, the spectrum was still consistent with a leak.

Both pipes conditions corresponding spectrums are showing significant peaks within 190MHz and 393MHz region.

This experiment proved that leaks on the standard Ø118mm and Ø170mm water distribution mains can be detected using electromagnetic waves. In the next section, it will be shown that electromagnetic waves can be used for asset management for the water industry. The experiments and results will be discussed.

4.2 Asset Management

It is believed that water wastage due to leaks in the distribution network can be significantly reduced with better asset management because of the numerous unaccounted connections and ageing pipes encountered on the network.

Asset management of buried utility services has been overlooked for years. In the UK, it is estimated that there are 335,000 km of pipe network managed by the water companies [61]. However, after trunk mains, there are still considerable portions of the network that the water companies are unaware of and that are not shown in their records [8] because these were laid at a time when the need of an accurate location did not seem to be a priority. Today, this results in financial loss, poor service management and longer down times in the event of failure.

With 40% of pipes over 100 years old in areas such as London [62], ageing water network repairs often involve the introduction of sections of different materials. The ability to reflect these changes in surveys will improve decision making for repair or replacement planning. Figure 71 summarises the effects of poor asset management.

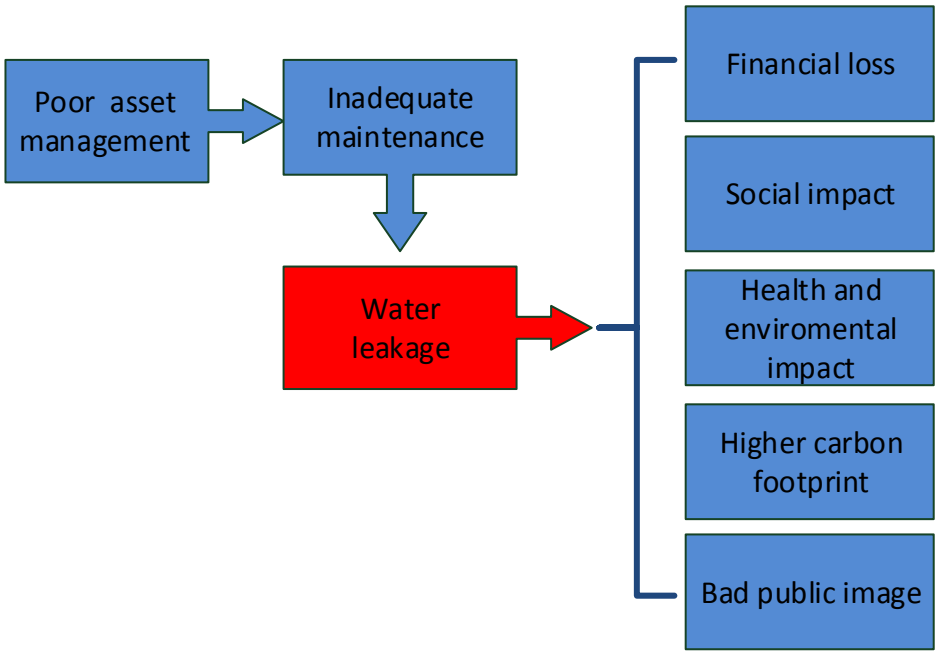

Figure 71: Effect of poor asset management [8] [14] [16]

To reflect the insertion of a section made from a different material, a Ø118mm PVC pipe section measuring 420mm in length was introduced. The new setup with the PVC section inserted between two cast iron sections, shown in Figure 72, was used to investigate asset management with electromagnetic waves.

In chapter 2, it was shown that a water pipe can be considered as a waveguide and that electromagnetic waves can propagate along it provided the frequency of operation is above the cut-off for that particular mode.

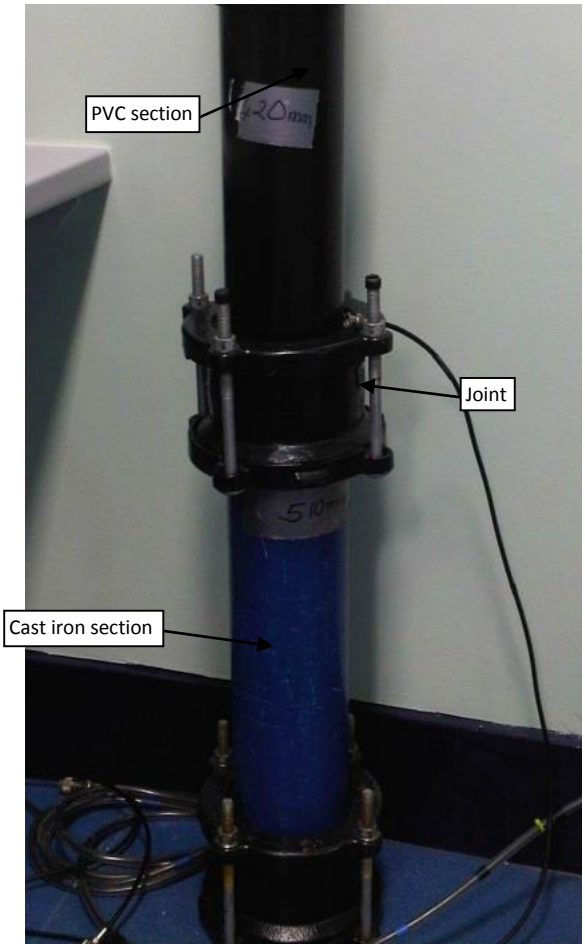

Figure 72: Asset management experiment setup with the PVC section

This test setup had a total pipe section length of 1650mm. The 28mm loop antenna was connected to the vector network analyser - Rhode & Schwarz ZVL-3GHz through a coaxial cable and pushed down the pipe. The bottom of the pipe was closed using a nylon block to prevent the water from escaping.

Measurements were taken at 225mm, which is inside the first cast iron section; at 510mm where the cast iron meets the PVC pipe; in the middle of the PVC section at around 720mm; at 935mm, the second junction between the PVC and the bottom cast iron, and finally at 1295mm half way down the lower cast iron section. No nylon rings that were used to simulate the leaks were inserted as this experiment was to investigate asset management.

Table 9: Results summary

Pipe section	**Resonant peak**	**Notes**
PVC section	170MHz	Length 420mm
Upper cast iron section	227MHz	Length 720mm
Lower cast iron section	213MHz	Length 510mm
Joint top	224MHz	Junction of the cast iron with the PVC section.
Joint bottom	204MHz	Junction of the PVC with the cast iron section.

In addition to amplitude difference in the cast iron sections, there was a 14MHz frequency shift observed while the two junctions showed a 20MHz difference.

The PVC section was clearly identifiable through this frequency shift in Figure 73.

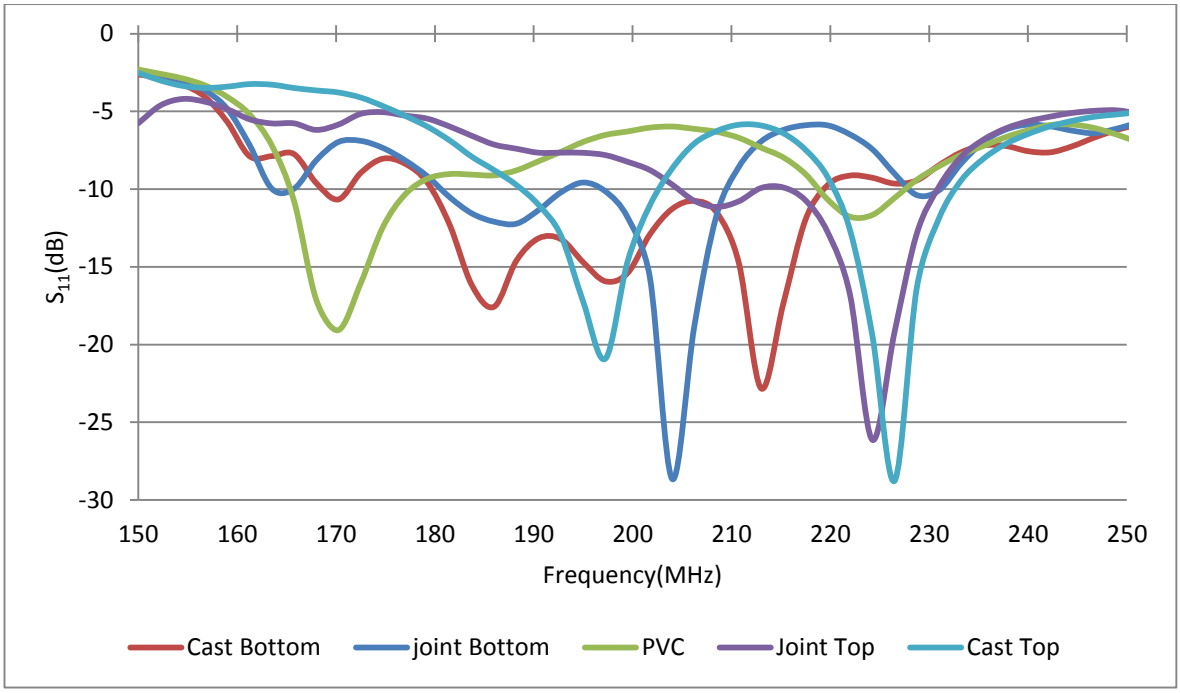

Figure 73: Pipe section distinction with EM waves

This test was repeated using the new 39mm loop size on the 12 metre rig that had a Ø118mm 2.5m cast iron pipe with a cross section and a Ø170mm cast iron pipe section. However, the Ø118mm cast iron pipe section was cut into two pieces of 2.5m to insert the Ø118mm 1.5m PVC pipe section.

Measurements taken from the vector network analyser - Rhode & Schwarz ZVL-3GHz showed specific frequency response for all three sections for the Ø118mm pipe and the Ø118mm cross section as well as for the PVC section shown in Figure 74.

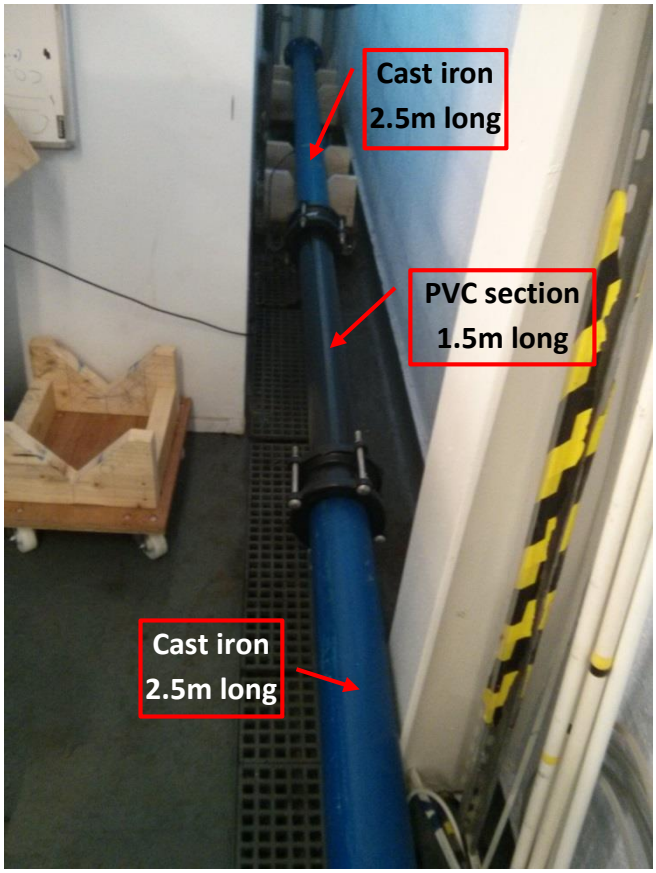

Figure 74: Ø118mm section cast iron with PVC inserted

In Figure 75, the combined results show each section and pipe state has a distinct frequency response. Moreover, the PVC section has return loss above -10dBm because the electromagnetic waves escape from the pipe walls giving a lower return loss compared to the cast iron pipe.

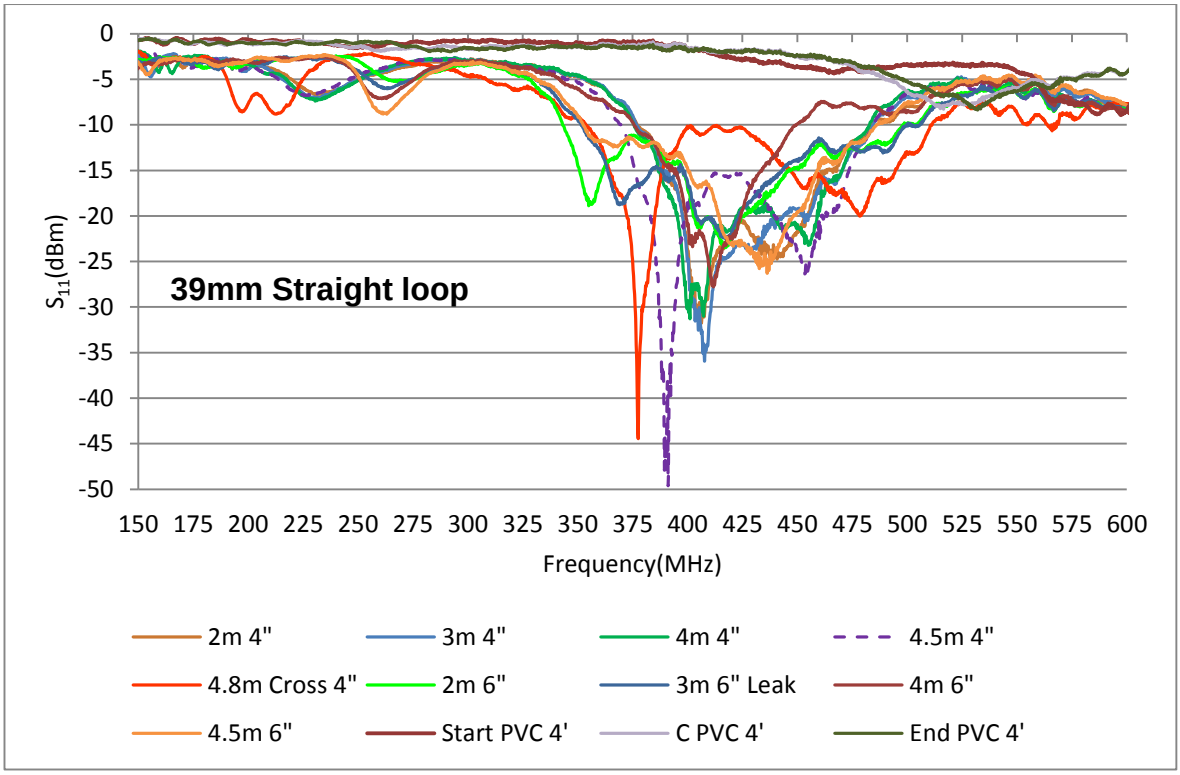

Figure 75: Combined frequency responses

After these successful experiments which proved that electromagnetic waves could be used to improve leak detection and asset management, field tests were organised in Worthington, United Utilities reservoir and training site, on 19th, 20th, 21st and 24th of March 2014.

However, the original sensor with the 39mm loop was not used due to the lack of a suitable access hydrant. The sensor head with its 60mm diameter could not be inserted in any of the hydrants, so a 45mm sensor head diameter with a 25mm antenna was constructed as shown in Figure 76.

Figure 76: 45mm test sensor head

The test was carried out on a buried Ø118mm section with no prior information about the pipe type.

The sensor was connected to the Rhode & Schwarz ZVL-3GHz VNA and inserted through the access point as shown in Figure 77, and moved in 1m increment along the pipe, using a carbon fibre reinforced glass rod.

The sensor was then inserted from the opposite end and the experiment repeated.

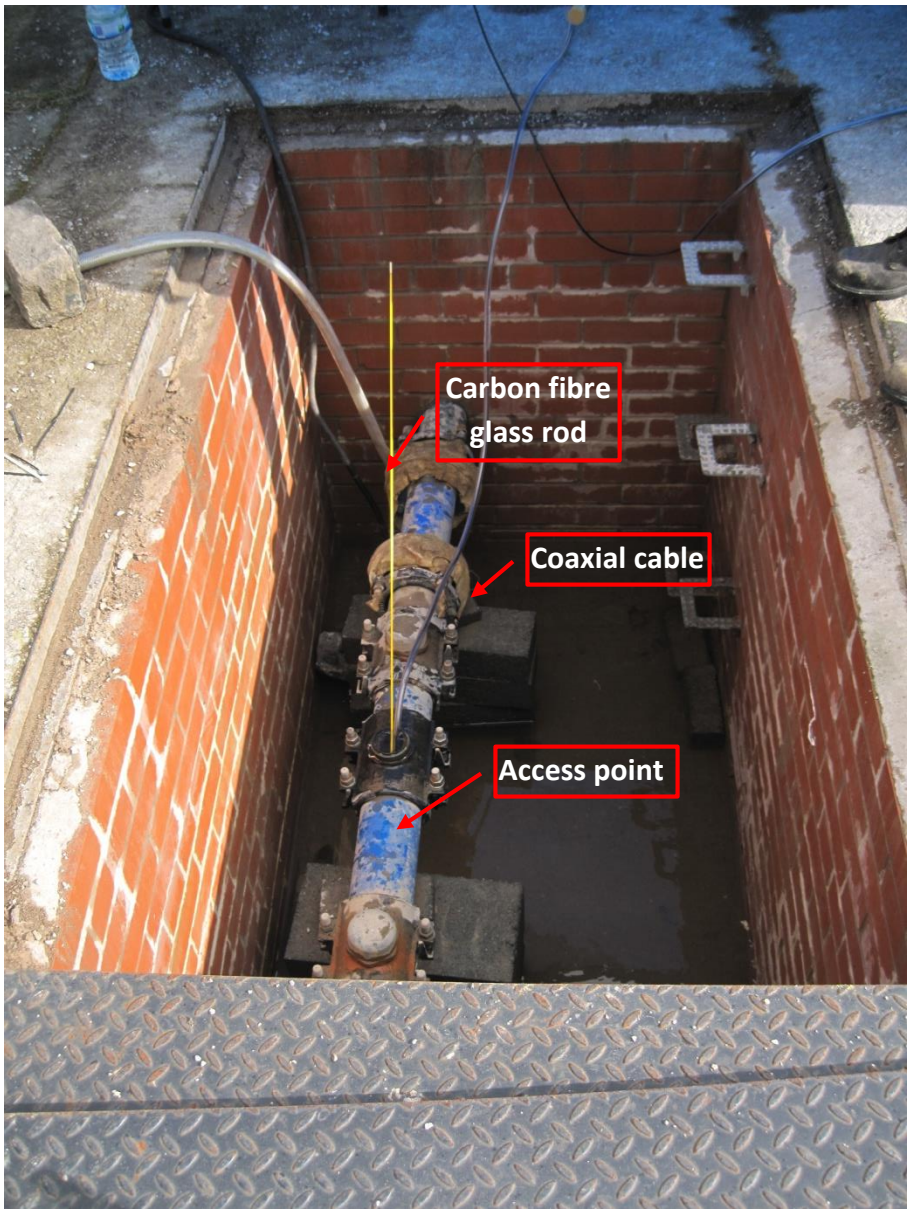

Figure 77: 2 inch access point

The frequency responses are shown in Figure 78 and Figure 79.

Used for training, the test site has a stop valve end isolating it from the distribution network. The flanged end is used to drain the this isolated section as necessary without impacting consumers connected to the public network, upstream.

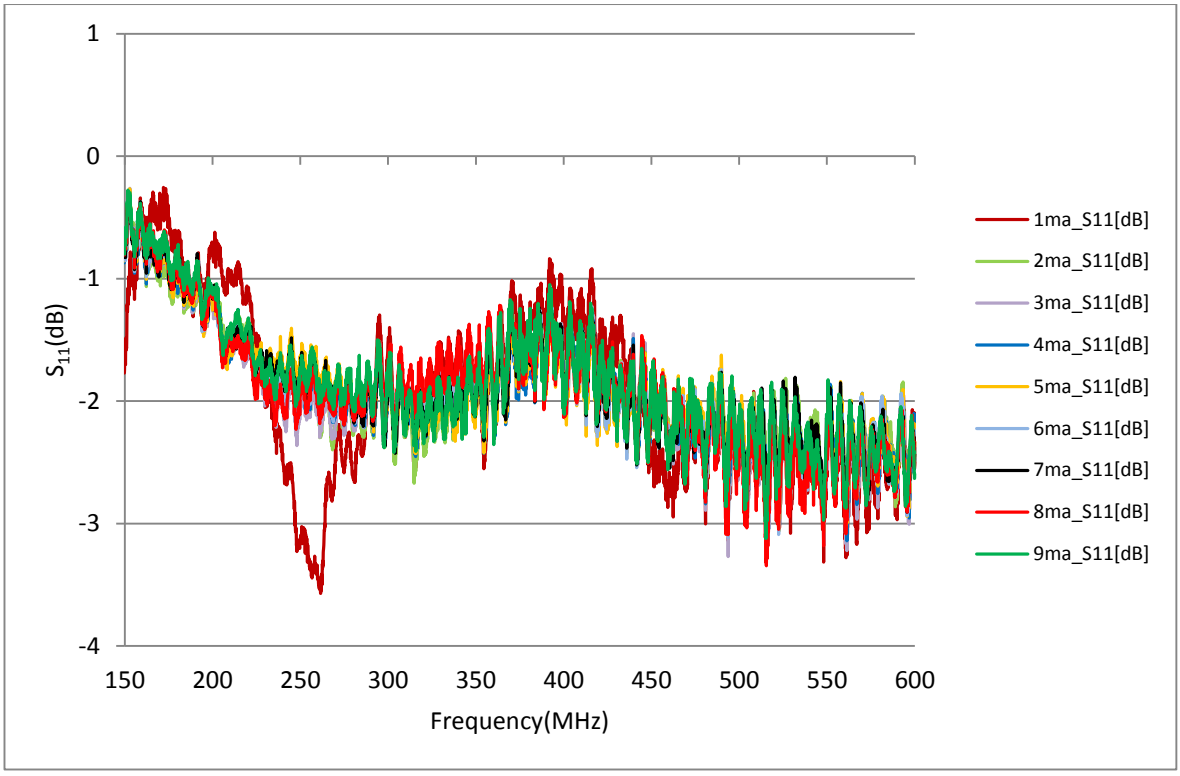

Figure 78: Stop valve end (underground)

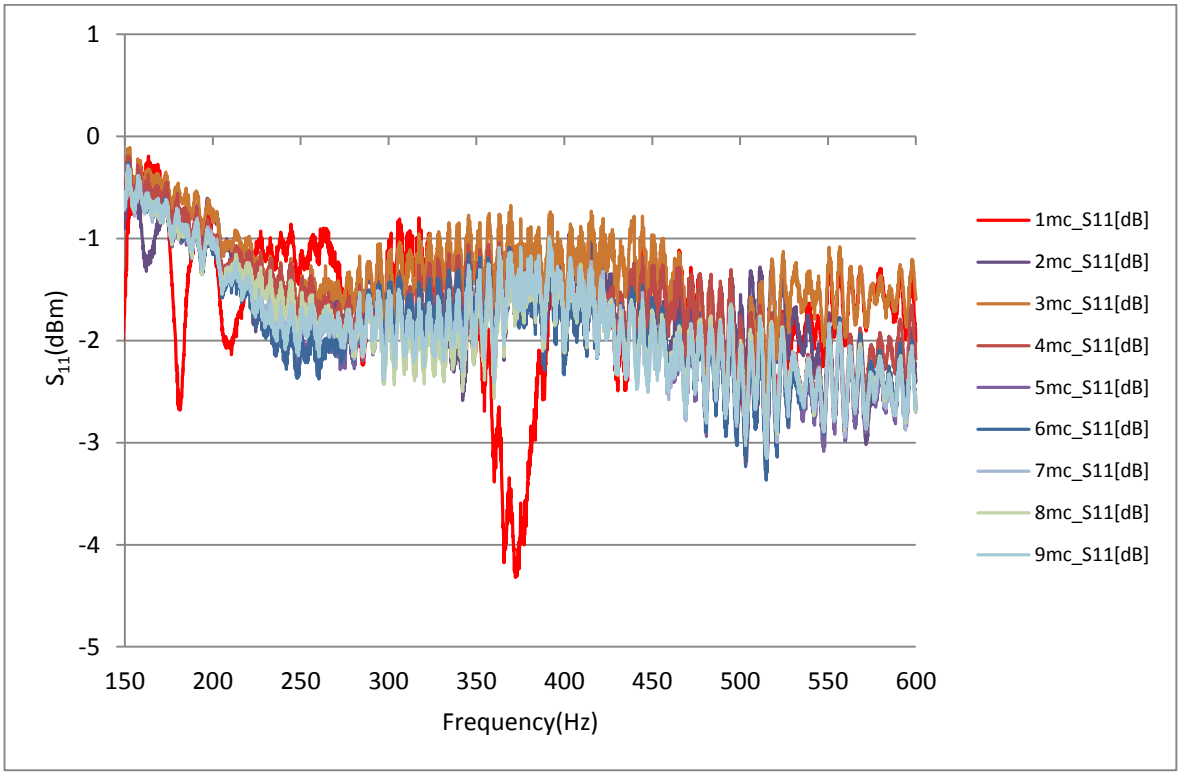

Figure 79: Flanged end

Both buried sections sides spectrum responses were highly correlated except near the access point area (1m to 2m) as shown in Table 10.

Table 10: Correlation table

Signals	Correlation
1ma and 1mc	0.86156
2ma and 2mc	0.89838
3ma and 3mc	0.91877
4ma and 4mc	0.92296
5ma and 5mc	0.92801
6ma and 6mc	0.94566
7ma and 7mc	0.96661
8ma and 8mc	0.95008
9ma and 9mc	0.98118

The lower correlation around this region is due to the difference in length of the pipe sections on each side of the used access point shown in Figure 80.

Figure 80: Sections around the access point used

Results from the measurements taken from the test setup in the laboratory using the same sensor showed that the pipe buried underground was unlikely to be of any of the type from the sections available in the lab test rig setup.

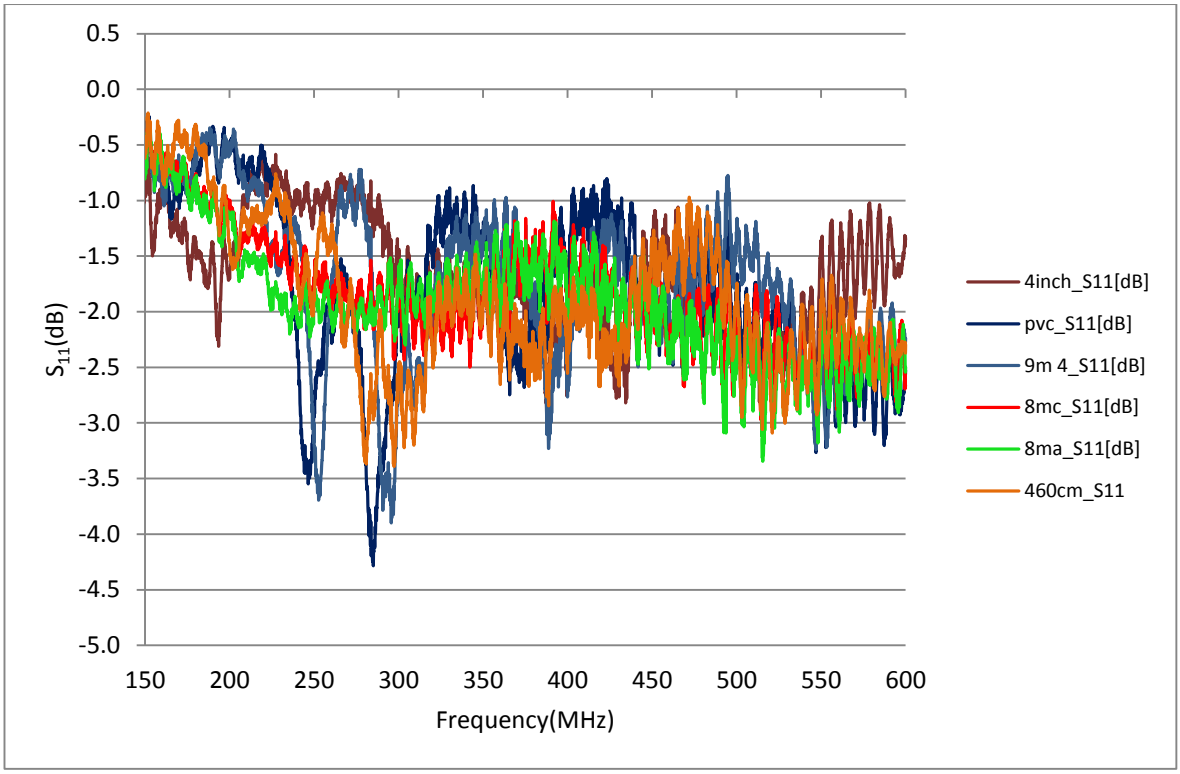

Figure 81: Lab rig results compared to field test

The resulting signatures from the underground pipe shown in Figure 81 (red and green), are different from signatures for sections available in the lab.

These results showed that both ends are likely to be made of the same material and that the diameters of the pipes are the same. It is believed that these unknown buried sections are PE100 Ø118mm due to the low return loss, which need to be confirmed with further tests.

4.3 Summary

In this chapter, it has been proven that electromagnetic waves can be used to detect leaks and identify various pipe materials and diameters for asset management by identifying unique frequency responses. These signatures were measured above the cut-frequency determined in chapter 2. The leak simulation using different nylon rings has shown that the frequency response of the leak in the form of amplitude

variation has a magnitude which corresponds to the thickness of the ring. While in the asset management experiment, tests showed that each pipe type and diameter also has a unique frequency response. The next chapter describes the proposed electromagnetic wave sensor system including the applied data analysis and the graphical user interface.

Chapter 5: Data capture interface system

The success of the electromagnetic sensor system needs to be consolidated by a robust data analysis method. Samples stored in the database representing the signature of a given pipe condition and or type will be recalled and compared with the current reading in real time. This technique will be used for the automation of the detection and the result will be displayed on a graphical user interface. The aim of the system is to allow its operation by network maintenance engineers, with minimal additional training.

5.1 Graphical user interface GUI

The graphical user interface was designed using the visual programming software, LabVIEW version 13.0f2 [63]. This software from National Instruments is a development platform widely used in the control and measurement systems with graphical user interface, it also has dedicated drivers to interface with third party equipment such as the Rhode & Schwarz ZVL series making it very attractive for prototyping.

The user interface included three status lights to display when the sensor is in air, in a bucket or the water distribution pipe section both filled with fresh water.

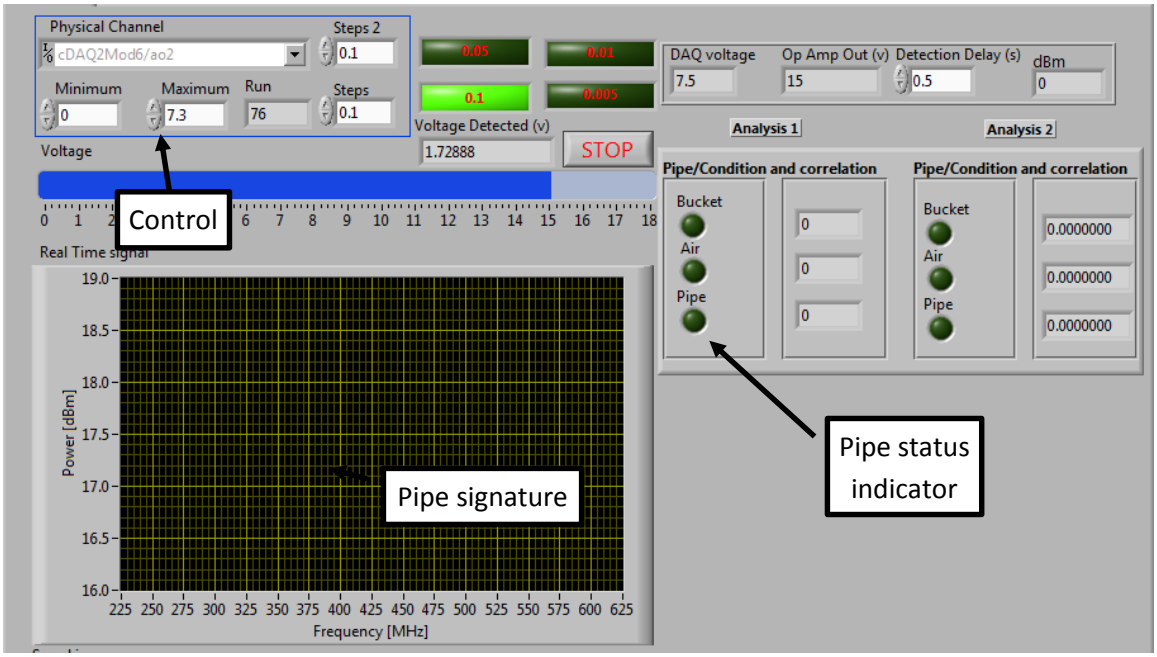

Figure 82: Graphical User Interface - GUI

The prototype success will reside in the ease of interpretation of the measurements by displaying the results using a traffic light method.

The colour red will be used for inconclusive results while the green will be used when the confidence of the data analysis fits within a set threshold.

The GUI will show the current frequency spectrum resulting from the section under test as the data is being acquired with the option to discard or save the final data as a new sample file if no fit is found.

5.2 Database

The various pipe signatures were added to a system database, in the comma separated values (csv) format - Figure 83.

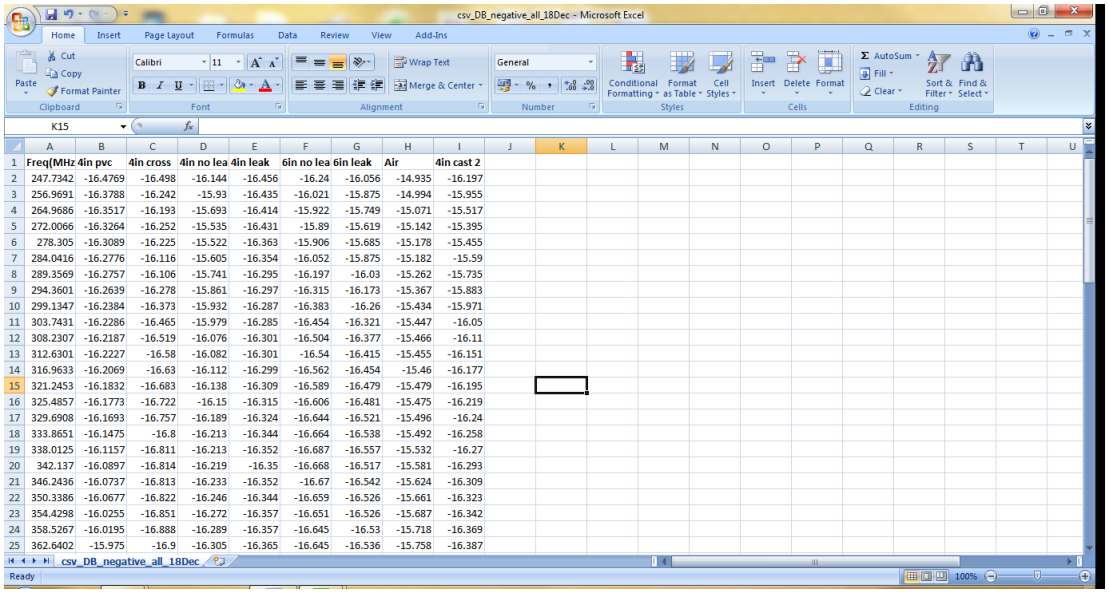

Freq(MHz	4in pvc	4in cross	4in no lea	4in leak	6in no lea	6in leak	Air	4in cast 2
247.7342	-16.4769	-16.498	-16.144	-16.456	-16.24	-16.056	-14.935	-16.197
256.9691	-16.3788	-16.242	-15.93	-16.435	-16.021	-15.875	-14.994	-15.955
264.9686	-16.3517	-16.193	-15.693	-16.414	-15.922	-15.749	-15.071	-15.517
272.0066	-16.3264	-16.252	-15.535	-16.431	-15.89	-15.619	-15.142	-15.395
278.305	-16.3089	-16.225	-15.522	-16.363	-15.906	-15.685	-15.178	-15.455
284.0416	-16.2776	-16.116	-15.605	-16.354	-16.052	-15.875	-15.182	-15.59
289.3569	-16.2757	-16.106	-15.741	-16.295	-16.197	-16.03	-15.262	-15.735
294.3601	-16.2639	-16.278	-15.861	-16.297	-16.315	-16.173	-15.367	-15.883
299.1347	-16.2384	-16.373	-15.932	-16.287	-16.383	-16.26	-15.434	-15.971
303.7431	-16.2286	-16.465	-15.979	-16.285	-16.454	-16.321	-15.447	-16.05
308.2307	-16.2187	-16.519	-16.076	-16.301	-16.504	-16.377	-15.466	-16.11
312.6301	-16.2227	-16.58	-16.082	-16.301	-16.54	-16.415	-15.455	-16.151
316.9633	-16.2069	-16.63	-16.112	-16.299	-16.562	-16.454	-15.46	-16.177
321.2453	-16.1832	-16.683	-16.138	-16.309	-16.589	-16.479	-15.479	-16.195
325.4857	-16.1773	-16.722	-16.15	-16.315	-16.606	-16.481	-15.475	-16.219
329.6908	-16.1693	-16.757	-16.189	-16.324	-16.644	-16.521	-15.496	-16.24
333.8651	-16.1475	-16.8	-16.213	-16.344	-16.664	-16.538	-15.492	-16.258
338.0125	-16.1157	-16.811	-16.213	-16.352	-16.687	-16.557	-15.532	-16.27
342.137	-16.0897	-16.814	-16.219	-16.35	-16.668	-16.517	-15.581	-16.293
346.2436	-16.0737	-16.813	-16.233	-16.352	-16.67	-16.542	-15.624	-16.309
350.3386	-16.0677	-16.822	-16.246	-16.344	-16.659	-16.526	-15.661	-16.323
354.4298	-16.0255	-16.851	-16.272	-16.357	-16.651	-16.526	-15.687	-16.342
358.5267	-16.0195	-16.888	-16.289	-16.357	-16.645	-16.53	-15.718	-16.369
362.6402	-15.975	-16.9	-16.305	-16.365	-16.645	-16.536	-15.758	-16.387

Figure 83: Signature samples in the CSV file

In the database, each sample has a unique frequency response based on the condition of the pipe structure – leak, no leak, PVC, Ø118mm or Ø170mm. These frequency responses can be compared to any other recorded spectrum in the frequency range using appropriate data analysis.

5.3 Data analysis

Each data sample stored in the CSV file will be compared to the real-time sample using cross correlation method to compare frequency and amplitude of the signals. Ideally, two complementary data analysis types will be applied in comparing the measured data with the stored data to strengthen the degree of confidence into the returned results displayed to the operator.

The primary data analysis method used is the Pearson cross-correlation technique between the current sample and each stored sample. This technique determines how tight the relationship between two signals is.

The Pearson correlation coefficient function is expressed as:

$$r = \frac{\sum x_i y_i - (\sum x_i y_i)/n}{\sqrt{\sum {x_i}^2 - (\sum x_i)^2/n}\sqrt{\sum {y_i}^2 - (\sum y_i)^2/n}} \qquad (41)\ [64]$$

n measurements of x_i and y_i

i = 1 to n

x_i and y_i the sample data

Using equation (41) to compare two samples will return a value between -1 a perfect negative correlation and 1 a perfect positive correlation.

To improve the degree of confidence, a secondary data analysis method was implemented to compare the amplitude of the signals.

$$d = \sum_{i=n}^{n} ||x_i| - |y_i|| \qquad (42)$$

n measurements of x_i and y_i

i = 1 to n

This method sums the results of the absolute value of subtracted individual data points representing the amplitudes of the real-time sample with the stored sample. The total sum of subtraction results are then evaluated to determine which has the lower value thus corresponding to the best match.

If each of the data analysis method returns the same result, then it can be considered highly likely to be the correct pipe type or condition, and the green light is shown. Otherwise the result is inconclusive due to the mismatch and the red light shown. If no match is found, the data can be stored for future use in the once the attributes are known.

The process of the data acquisition and analysis is illustrated by the flow diagram in Figure 84.

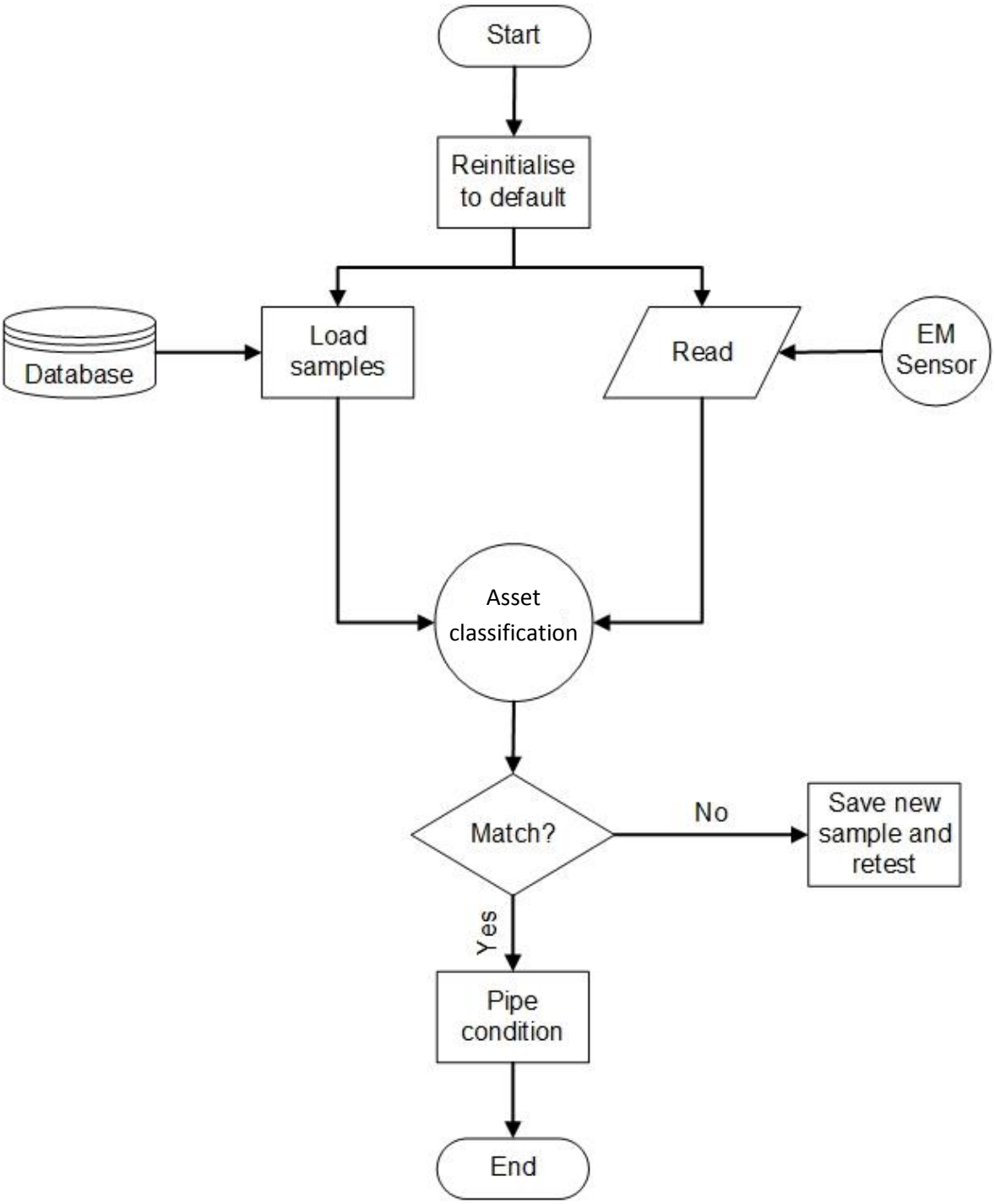

Figure 84: Data acquisition and processing

5.4 Sensor

A standalone sensor has to partially replicate the Rhode & Schwarz ZVL vector network analyser used in the initial experiments.

The sensor has to be able to generate a signal within the frequency range determined above the cut-off frequency of the Ø170mm pipe at 124MHz and up to 600MHz with a power level of 0dBm to 5dBm and be able to detect any reflected power from the antenna above the noise floor of -50dBm.

For this purpose, the sensor system is designed based on the block diagram in Figure 85 with the interconnected components.

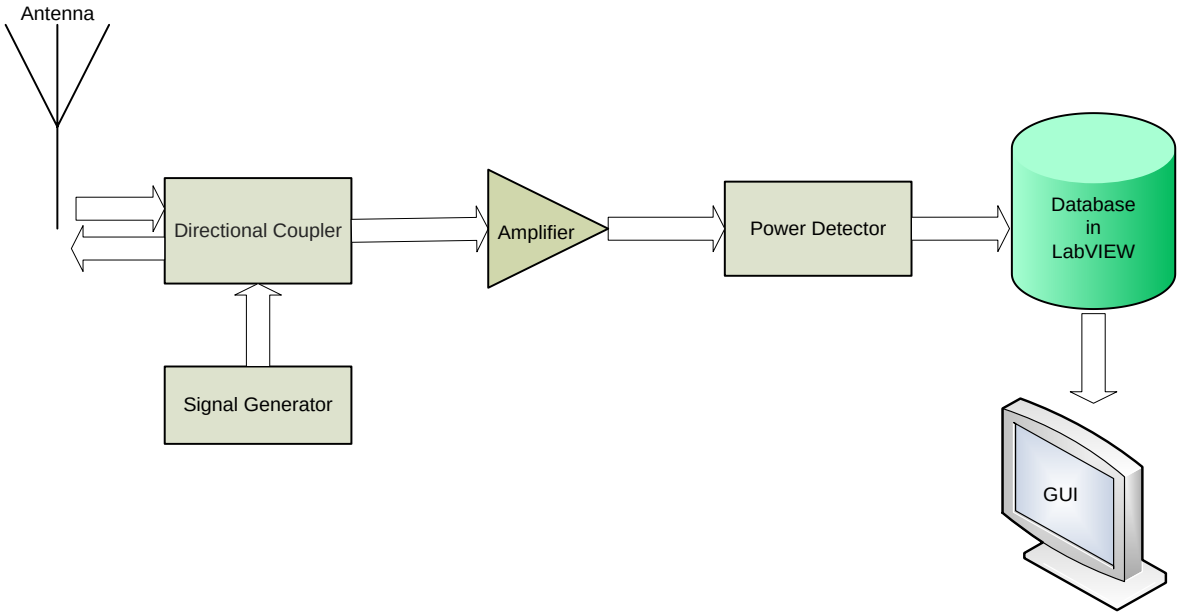

Figure 85: Sensor block diagram

Each component was chosen with the characteristics to match the sensor requirement. The sensor was designed in a modular form to facilitate troubleshooting and upgrades. These specifications of the modules are as follows:

- The signal generator: a sweep frequency 247MHz-600MHz will be generated to feed the antenna.
- The antenna: will be capable of resonating within generated frequency range.
- The directional coupler: will be able to sample the power reflected from the

antenna at it coupled port with low insertion loss on the mainline and below the ambient noise level observed with VNA at -50dBm.

- The amplifier: this component will be optional and only added to the circuit if the received signal is too close to the noise level.
- The power detector: will be an RF detector range that can operate in the frequency sweep range and detect power as low as -50dBm.
- The database: will store sample files in the comma separated values (csv) format. These samples are a combination of frequency and amplitude responses of pipe types and conditions.
- The graphical user interface: will use coloured light indicators to display test results to the operator.

5.5 Summary

A graphical user interface was developed using LabVIEW with the results of measurements captured from the VNA and displayed in a traffic light system. These results are obtained by comparing the stored signatures with the measured frequency response using two separate data correlation methods. If the measured sweep frequency does not match any stored frequency response in the database, the result is stored for post processing or discarded. To develop the electromagnetic sensor system, modules were identified based on their function and operating frequency to form a block diagram. In the next chapter, the prototype of the sensor system electronic circuit will be designed and evaluated using the existing 12m test rig in the lab.

Chapter 6: Prototype design

The final prototype size must be small enough to freely fit inside a Ø118mm standard pipe. It should be noted that in order to protect the sensor from water damage, it will be housed in a casing not exceeding the 100mm by 60mm dimensions set to allow its insertion into the pipe through existing hydrants and meeting the IP68 rating for prolonged submersion in water.

6.1 Electronic circuit design

To design the electronic circuit version on a printed circuit board (PCB), off shelf components were acquired and used to test the concept and operation of the sensor. A prototype of the sensor was assembled on the bench and connected to a computer.

Different configurations were tested - Figure 86 and Figure 87 - using the spectrum analyzer to monitor the frequency generated by the voltage controlled oscillators POS-400+[3] and ZX95-535-S+[4] and a voltmeter to measure the output voltage from a ZX47-60-S+[5] power detector.

[3] Plug in voltage controlled oscillator by Mini-Circuits (www.minicircuits.com)
[4] Coaxial voltage controlled oscillator by Mini-Circuits (www.minicircuits.com)
[5] Coaxial power detector by Mini-Circuits (www.minicircuits.com)

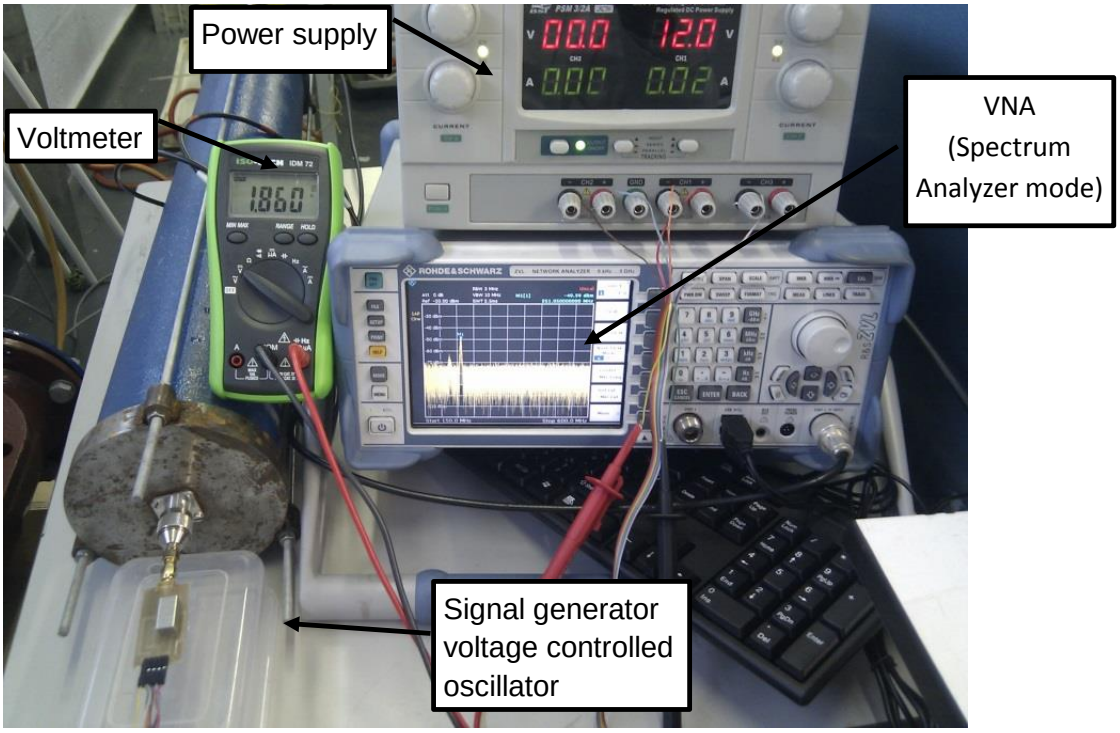

Figure 86: POS-400+ VCO evaluation

In Figure 87, the different components were interconnected and tested to observe the generated frequency and amplitude as well as the reflected signal through the directional coupler and power detector.

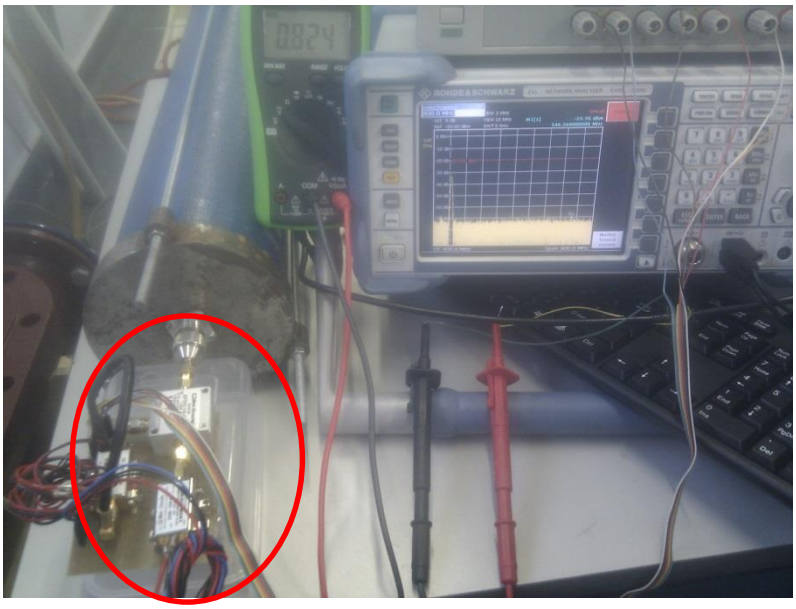

Figure 87: ZX95-535-S+ VCO evaluation

Following the evaluation, the components listed below were chosen and used for the bench test shown in Figure 88:

- The antenna: the size of the antenna can be changed according to the requirement, provided that the resonant frequency is kept within the limit imposed by the electronic components and the water distribution pipe cut-off frequency but no more than 45mm diameter due to the imposed sensor size dimensions.
- The signal generator: this module was built around the ROS-625-219+[6], a voltage controlled oscillator which generated frequencies from 247.5MHz to 618.2MHz using up to 14.6 volts for tuning to the desired frequency.
- The directional coupler: the ZFDC-10-5-S+[7], a directional coupler with a wideband frequency 1MHz to 2000MHz capable of coupling to 10dB.
- The amplifier: this is made with the ZFL-500LN+[8] low noise 24dB amplifier. The use of an amplifier is to boost the reflected signal before detection.
- The power detector: the MAX2015[9] logarithmic detector with up to 3GHz frequency range. It can detect down to -75dBm well below the ambient noise level measured inside the pipe at around -50dBm.
- The control automation and data processing: this part of the system is built using LabVIEW, running on a host computer. The data acquisition hardware is the CompactDAQ NI cDAQ-9172[10] through which the tuning voltage is supplied to the voltage controlled oscillator and the reflected power read as

[6] Surface mount voltage oscillator by Mini-Circuits (www.minicircuits.com)
[7] Coaxial directional coupler by Mini-Circuits (www.minicircuits.com)
[8] Coaxial low noise amplifier by Mini-Circuits (www.minicircuits.com)
[9] Logarithmic power detector by Maxim (www.maximintegrated.com)
[10] Data acquisition system by National Instruments (www.ni.com)

voltage from the power detector.

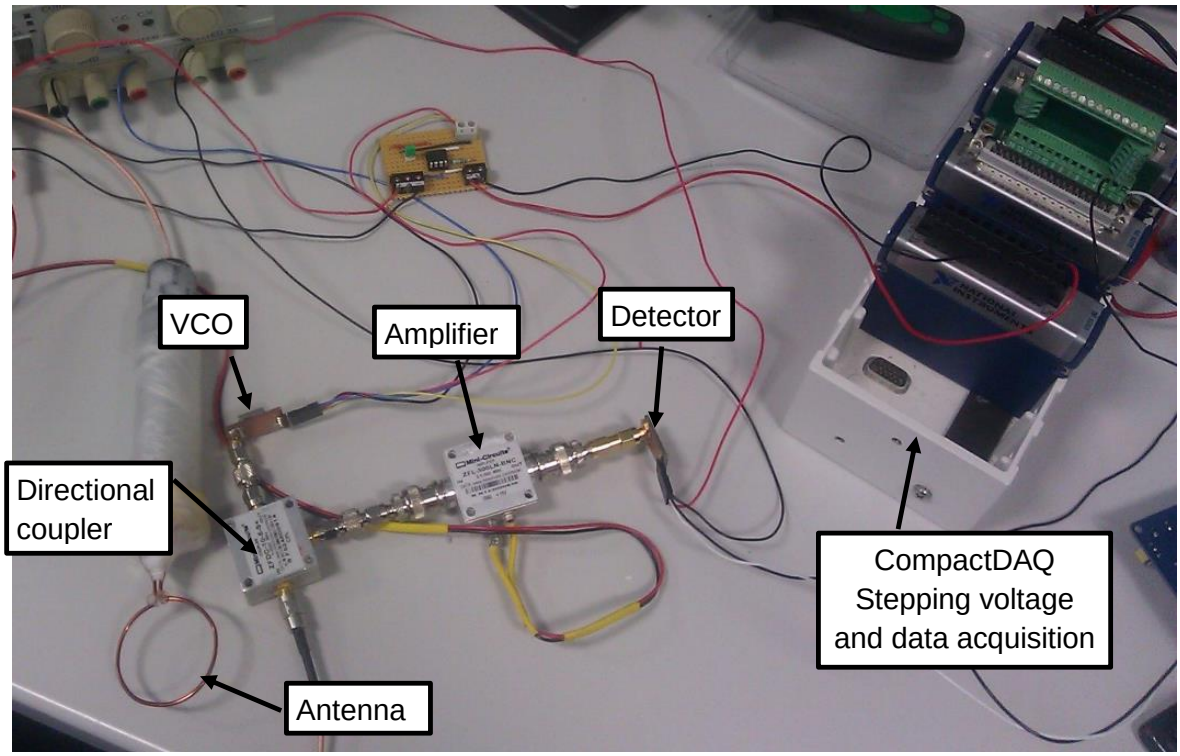

Figure 88: Electronic concept test

After the electronic concept test, surface mount components (SMD) were chosen to be used instead. However, the ZFDC-10-5-S+ directional coupler was changed for the DBTC-7-152LX+[11] which has a smaller frequency range of 10MHz to 1500MHz and a 3dB better coupling factor.

[11] Surface mount directional coupler by Mini-Circuits (www.minicircuits.com)

Figure 89: Modular SMD components

These components mounted, on modular PCBs, were assembled as shown in Figure 89 to allow testing of the modules separately or together in Figure 90.

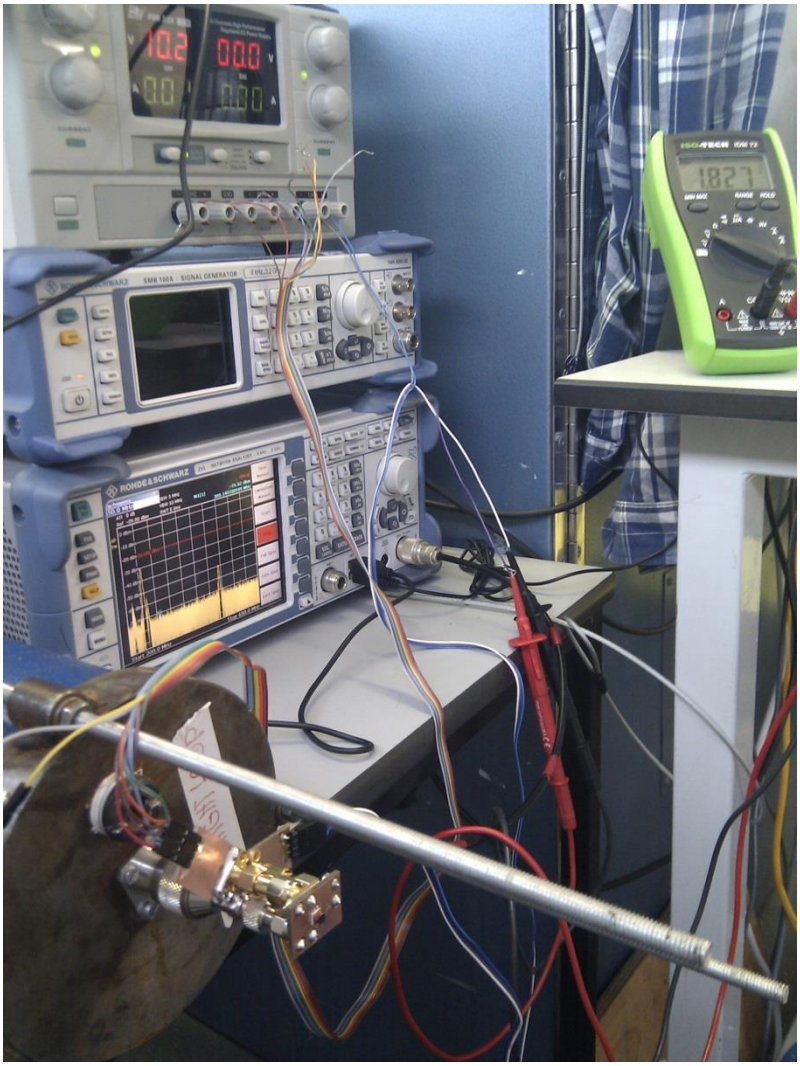

Figure 90: SMD modules evaluation

With the modules operating separately and together as intended, a schematic was drawn with all the components wired on a single circuit board. The board was generated from the circuit diagram (Figure 91 and Figure 92) using the CAD software EAGLE (Easily Applicable Graphical Layout Editor) [65] version 6.5.0.

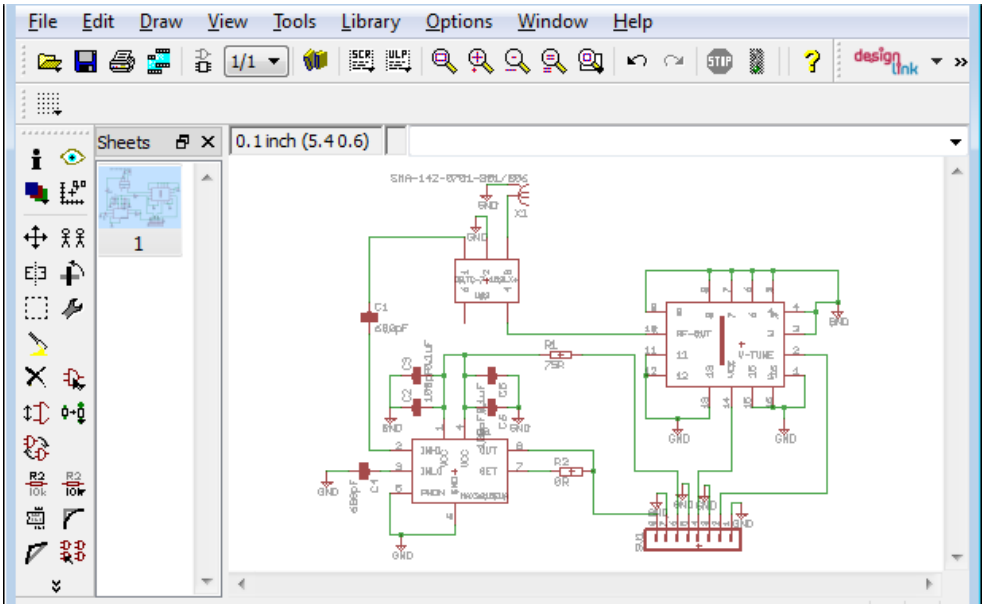

Figure 91: Circuit schematic

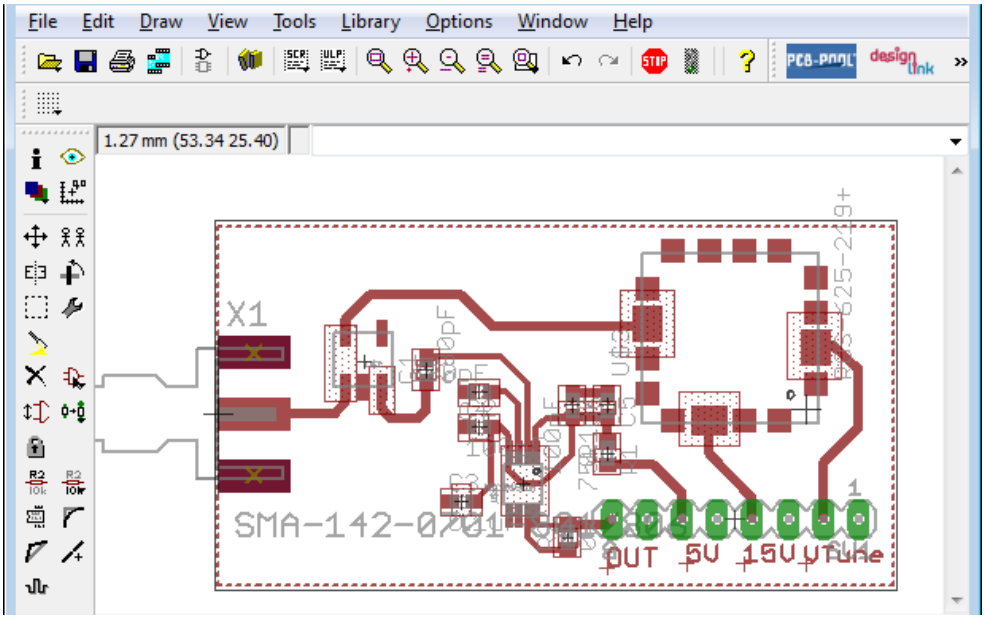

Figure 92: Circuit board layout

The EAGLE file was then exported to a vector based file format compatible with the PCB milling machine and routed in the lab.

The resulting board, shown in Figure 93, was checked using an electronic magnifier to ensure correct connectivity, as per the schematic and board layout files, before being populated using solder paste and heated on a hot plate to up 280^{o}C.

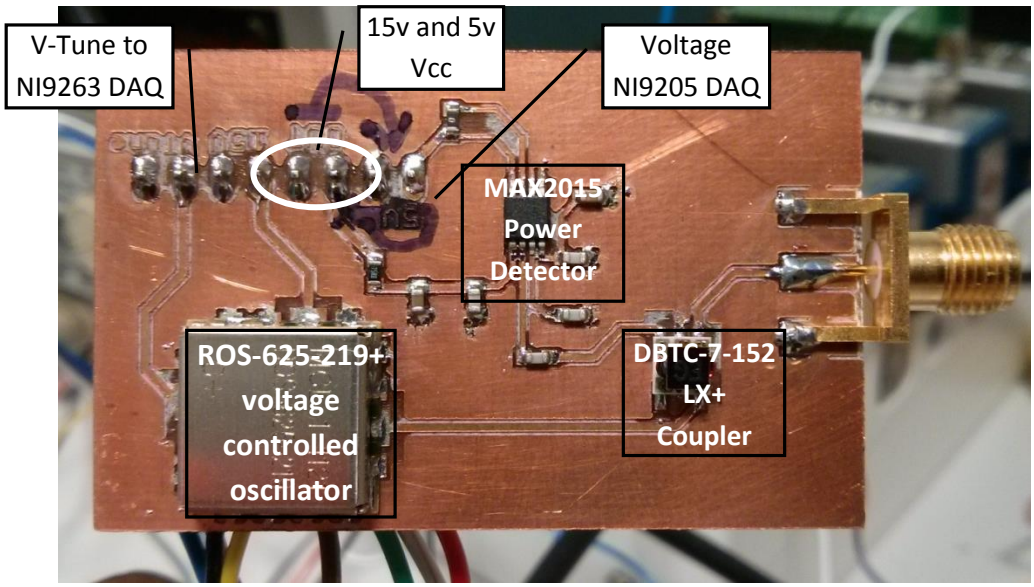

Figure 93: Sensor circuit prototype v2.0

6.2 Prototype test

In order to assess the designed sensor, measurements were taken while being operated through LabVIEW connected to the CompactDAQ.

The printed circuit board prototype in Figure 93 was connected to the 39mm loop antenna. A voltage of up to 14.6V was applied to the VCO in 0.2V increments controlled through the analogue output NI9263[12] module in order to generate the signal in the frequency range of 247.5MHz to 617.1MHz. Meanwhile, the power detector MAX2015 output pins were connected to the analog input NI9205[13]module to record the reflected signal as an output voltage.

Multiple readings were taken in a bucket filled with water (Test1, Test 2 and Test 3), in air (Test 4, Test 5 and Test 6) and then the antenna was covered by hand (Hand) and plotted in the graph in Figure 94.

[12] Analog output module by National Instruments (www.ni.com)
[13] Analog input module by National Instruments (www.ni.com)

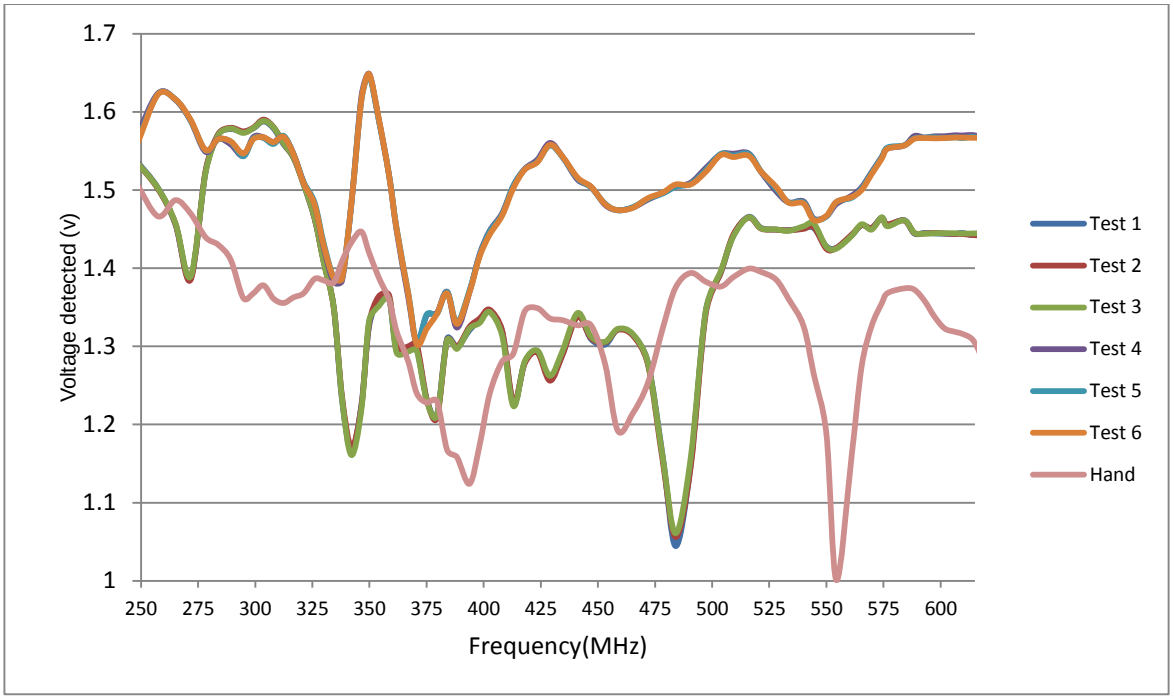

Figure 94: Sensor circuit prototype reading with the 39mm loop antenna

Plotting all the readings showed that frequency responses within these three conditions were highly correlated at over 0.99.

The power detected by the MAX2015 was 4dBm which may require the use of the amplifier module at the directional coupler output in the event of considerable noise in the water main pipe.

The sensor operated correctly with the available VCO frequency range - 247.5MHz to 617.1MHz. However, repeated measurements showed that the output frequency from the ROS-625-219+ voltage controlled oscillator varied by as much as 4.1MHz. This was due to noise in the tuning voltage.

6.3 DAC and Microcontroller

To solve this problem, a digital-to-analog converter (DAC) was introduced in the circuit, generating the tuning voltage for the VCO as shown on the circuit board in

Figure 95 using the integrated circuit MAX5312[14] which is a 12-bit serial voltage output, configured as a unipolar 10V output with a 5V reference voltage. It has a 4 bit control word and 12 bit DAC data.

The data output function is expressed as [66]:

$V_{out} = LSB_{UNI} + CODE$ (43)

Where $LSB_{UNI} = \frac{2 \times V_{ref}}{2^{12}}$ (44)

V_{out} the output voltage

LSB_{UNI} the unipolar Least Significant Bit step size

V_{ref} the reference voltage

$CODE$ the decimal equivalent of the binary 12 bit dac data

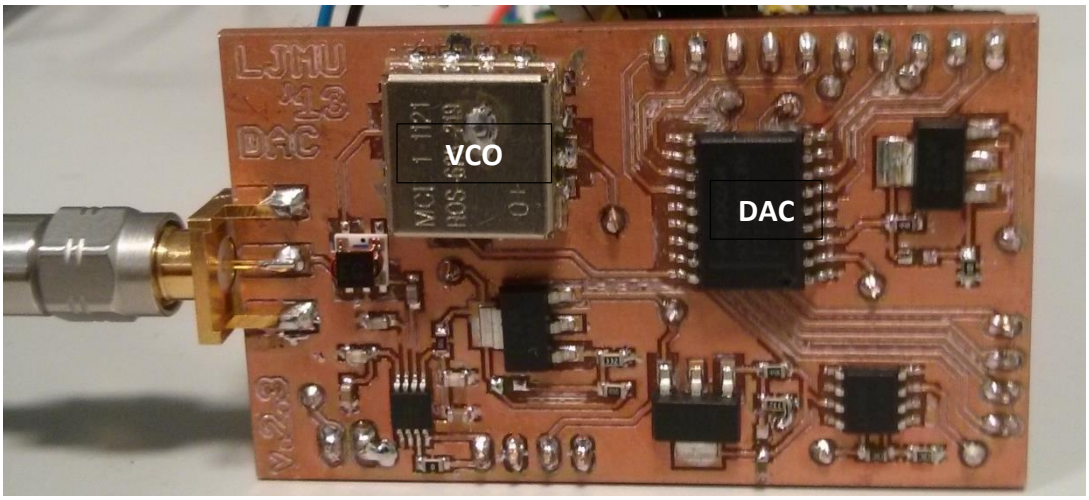

Figure 95: Sensor circuit v2.3 with DAC

As the maximum output of the DAC is 10V, a voltage doubling unit was inserted using the operational amplifier CA3140 [15] to attain the maximum required 14.6v tuning voltage to generate the highest frequency from the VCO. The full schematic and board design are attached in *Appendix 1: VCO with DAC sensor schematic*.

[14] Digital-to-analog converter by Maxim (www.maximintegrated.com)
[15] Operation amplifier by Intersil (www.intersil.com)

Having improved the stability of the sensor, the CompactDAQ was dropped for a faster controller able to connect the sensor directly to computer hosting the GUI. This required serial or parallel connectivity to the computer. However, the serial connectivity was a natural choice as it requires fewer wires and moreover, most modern computers have no parallel port available.

To control the DAC and the data input/output to the host computer of the GUI, the Arduino open-source prototyping electronic hardware and software was used based on the ATmega328[16] microcontroller chip. This widely available module can be configured to provide all of the serial digital inputs to the DAC and analogue inputs for the power detector. The connection to LabVIEW is achieved using the transmit pin (TX) and the receive pin (RX) of the serial port.

Figure 96: Arduino mini [67]

The choice of the Arduino Pro Mini breadboard (in Figure 96) is motivated by its availability, flexibility, speed and ease of programming.

The integration of the DAC and microcontroller in the sensor system block diagram is shown in Figure 97.

[16] Microcontroller by Atmel (www.atmel.com)

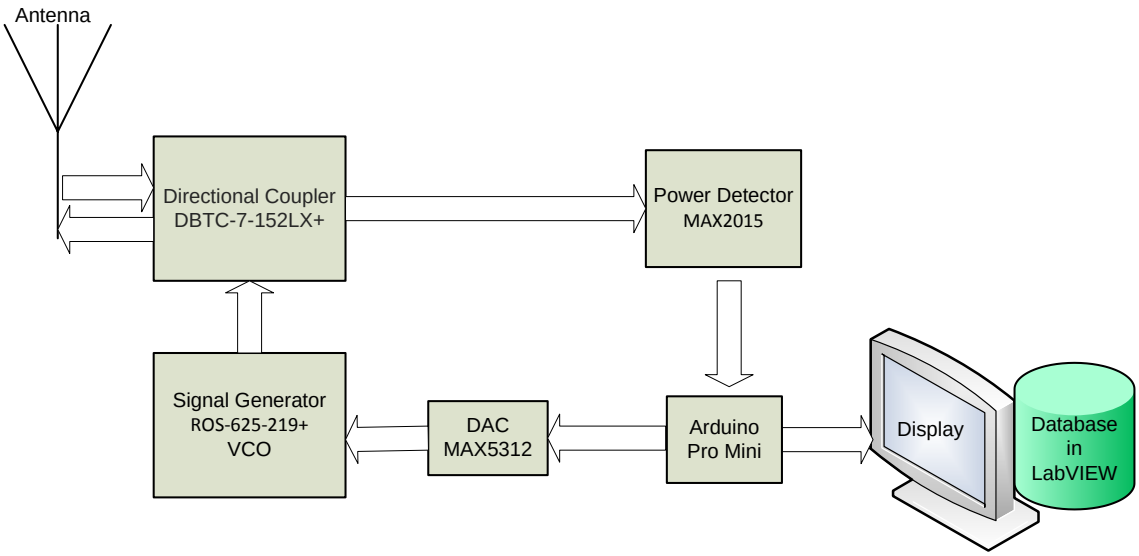

Figure 97: Block diagram with Arduino and DAC

Figure 98 shows the redesigned prototype with the Arduino Pro Mini microcontroller attached underneath for control.

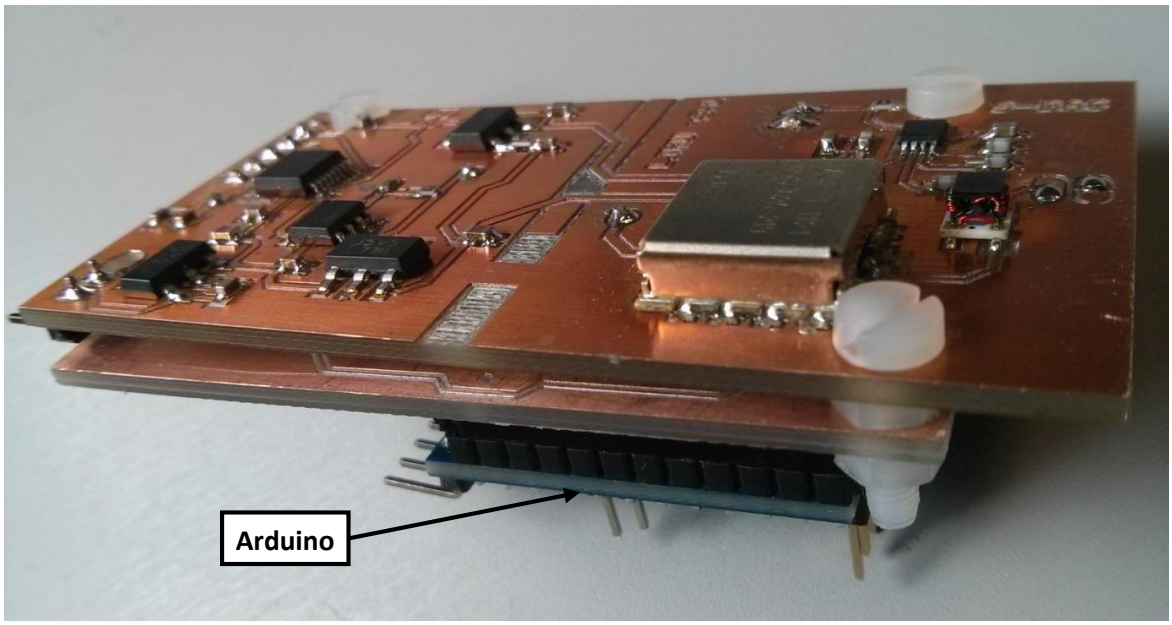

Figure 98: Arduino and DAC added

To control the sensor, the Arduino microcontroller needed to be programmed to generate the required bits for stepping the output voltage from the MAX5312 DAC chip using its C like programming language shown in the sketch in Figure 99.

The use of the MAX5312 allowed a resolution of up to 12 bits for the voltage thus the generated frequency from the VCO becomes very accurate with negligible fluctuations due to the voltage fluctuation.

To have control over the execution of the programme when running, special characters (> and #) are used as triggers for the interrupts and also to read the analogue pin A0 which was the input for data from the power detector, and was then transferred to LabVIEW.

Figure 99: Arduino sketch

The sketch is preloaded into the Arduino mini and LabVIEW connecting to it through the serial port shown in Figure 100 in the block diagram at 115200 baud rate. The

full Arduino code and LabVIEW block diagram are attached in the Appendix 2 and Appendix 3.

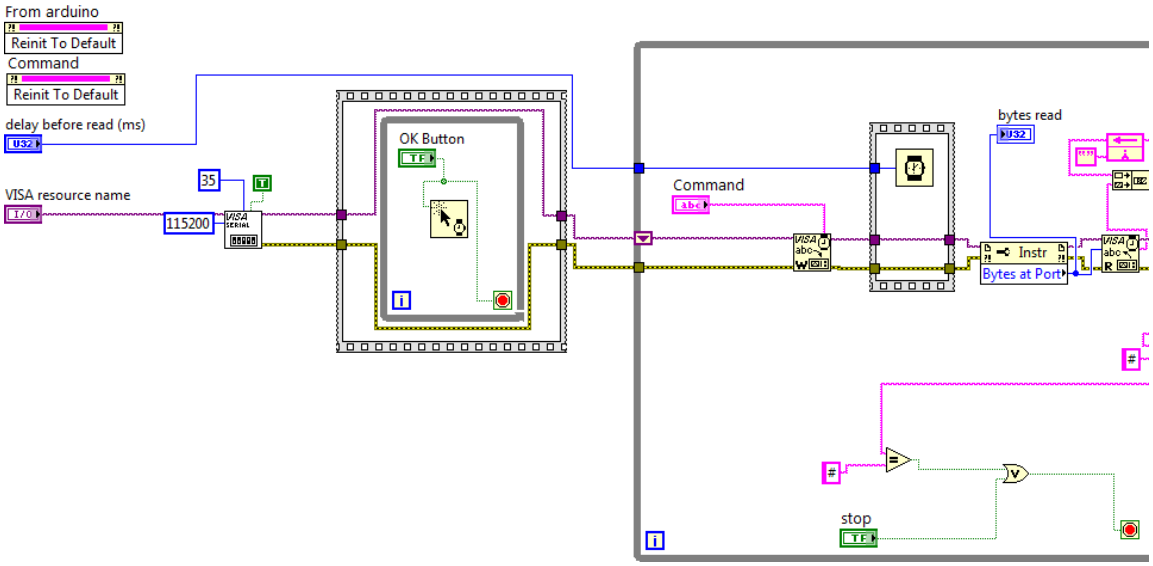

Figure 100: LabVIEW serial connection

The evaluation of the generated signal using the sensor with the DAC through the microcontroller showed high repeatability with the frequency sweep range without noticeable variation of either the frequency or the amplitude using the ZVL-3 VNA [48] set in the spectrum mode connected to LabVIEW in Figure 101 to record the frequency sweep.

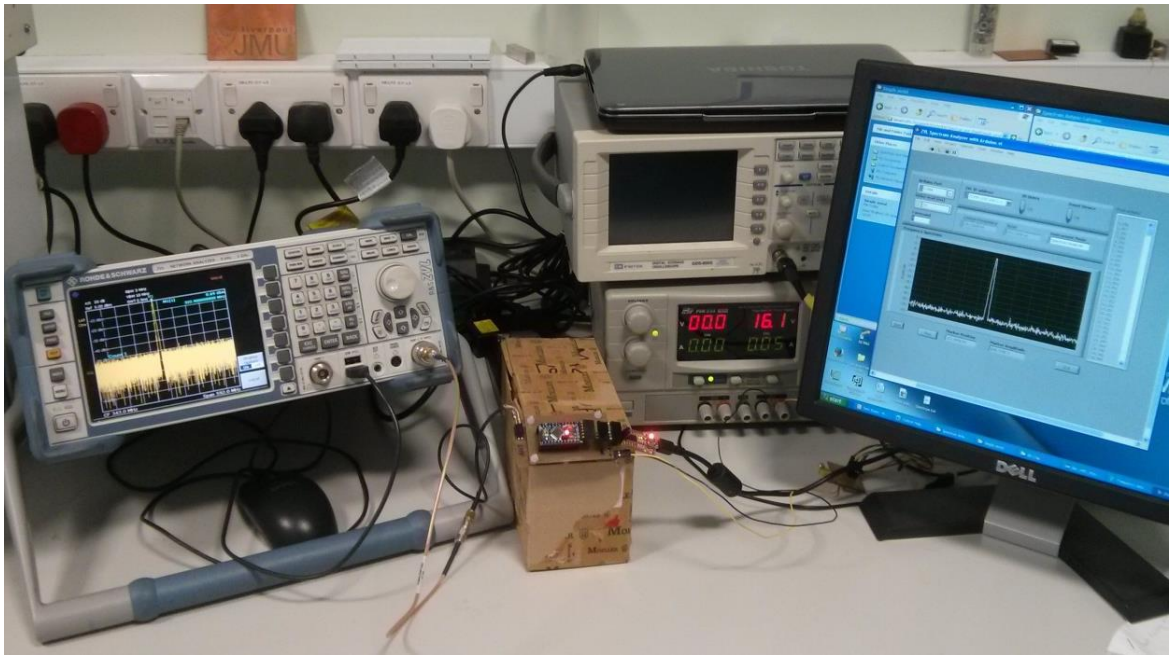

Figure 101: Sensor evaluation

Regarding the amplitude, the plotted data showed attenuation of the signal as the frequency increased. However, this variation is in the range of 3dBm to -2dBm at 5 and 10 milliseconds interval between readings in Figure 102, slightly less than 5dB.

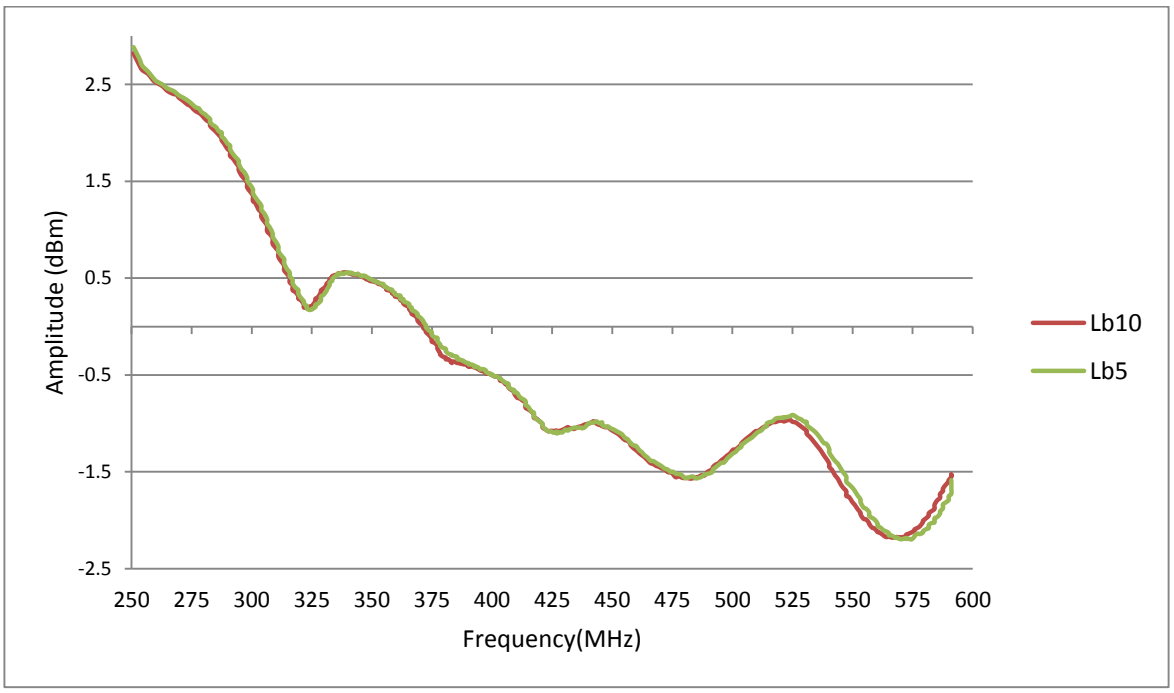

Figure 102: Amplitude variation

Furthermore, loop antennas - 39mm loop and 28mm loop – were alternatively used with delay set at 5 (5D) and 10 (10D) milliseconds through LabVIEW. The reading from the power detector output showed different frequency responses for the antennas in air and when covered with by a hand in

Figure 103:.

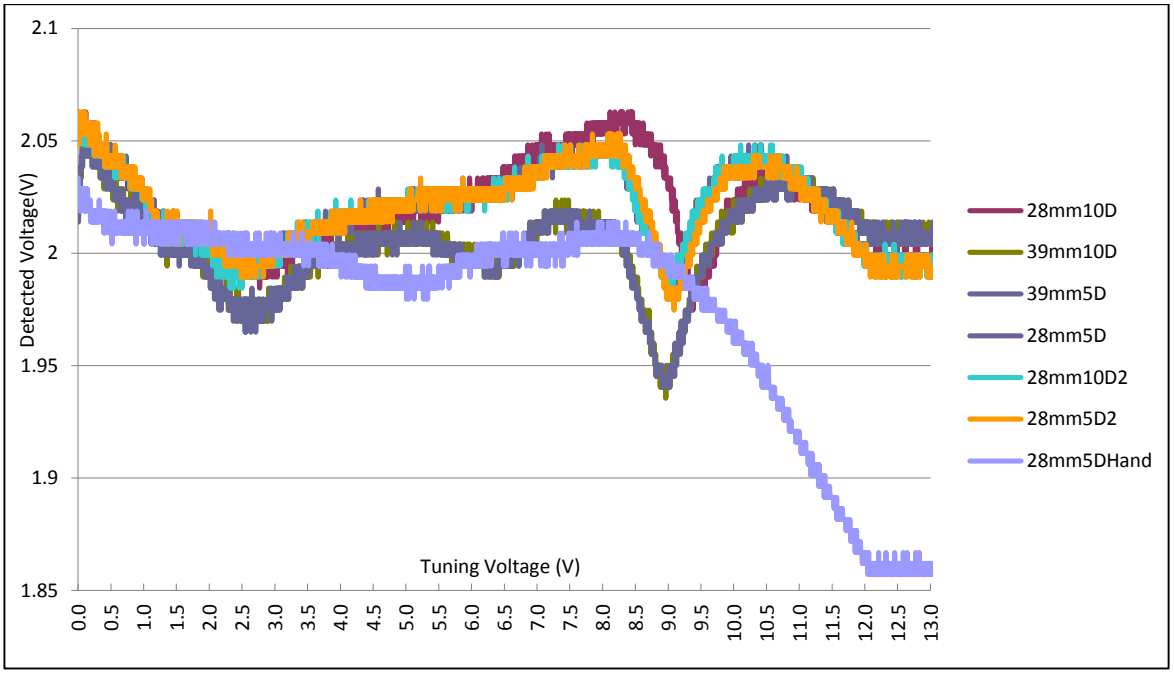

Figure 103: Sensor system connected to antenna

6.4 Sensor Range

The aim of this electromagnetic magnetic sensor is to improve fault or asset localisation, saving water companies money and public image damage due to dry digs. In order to know the distance within which to investigate following the use of the sensor in the field, it was important to estimate its range of detection inside the pipeline.

For this test, only a power detector module was used with an independent (external) signal generator – R&S SMB-B103 [57].

This sensor contained a MAX2015 power detector chip module connected to a

24mm 90^{o} bent loop antenna as shown in Figure 104 through an SMA connector.

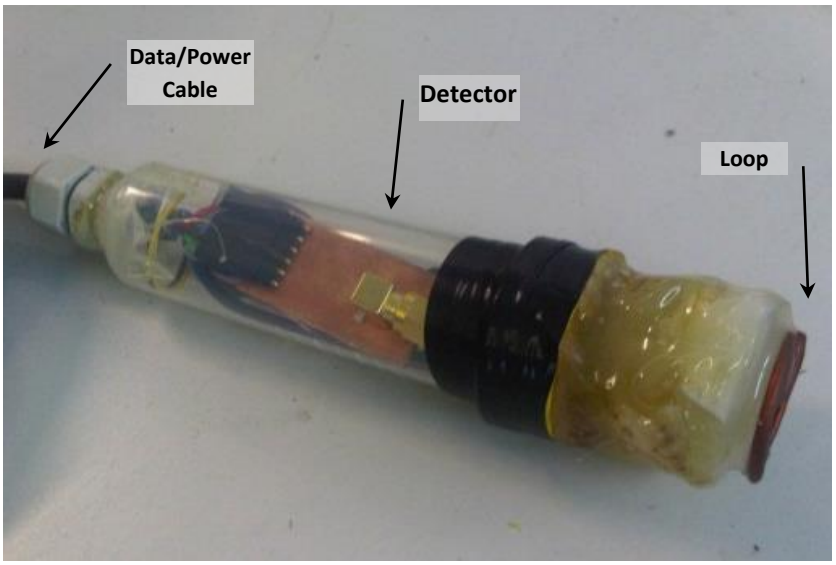

Figure 104: Electromagnetic sensor in the protective tube

This sensor was connected to LabVIEW through a NI9205, a 32-Channel, ±200 mV to ±10 V, 16-Bit analogue input to read and record the voltage detected by the MAX2015 power detector.

The sensor was powered with a 5V DC power supply. A second antenna positioned at the other end of the pipe mounted on a PVC flange, was connected to the SMB-B103 - signal generator with a variable frequency range and the power set at 0dBm. The sensor was then pushed inside the pipe - Figure 105 - to the desired distance using the Data/Power cable attached to a PVC rod. Both the fixed loop at the end flange and the sensor inside the pipe were centred within the water pipe using fins.

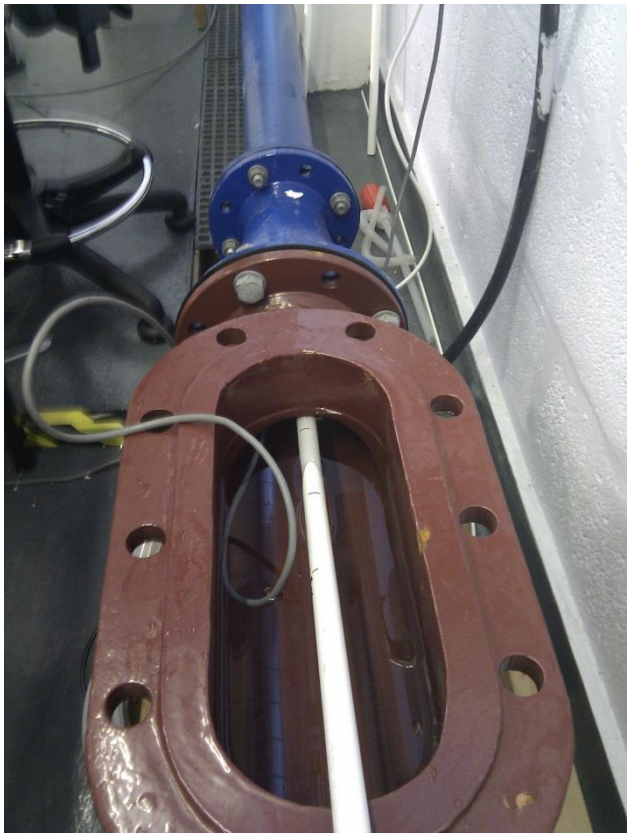

Figure 105: Sensor pushed inside the test pipe

The results at 0dBm showed that the frequency with the largest transmission was 300MHz while 250MHz was shown to give the worst performance as observed from Figure 106 through to Figure 108. The sensor range was determined to be no more than 1.5m at 300MHz in Figure 108; however, at 1m distance, the signal was well above the ambient noise as shown in Figure 106.

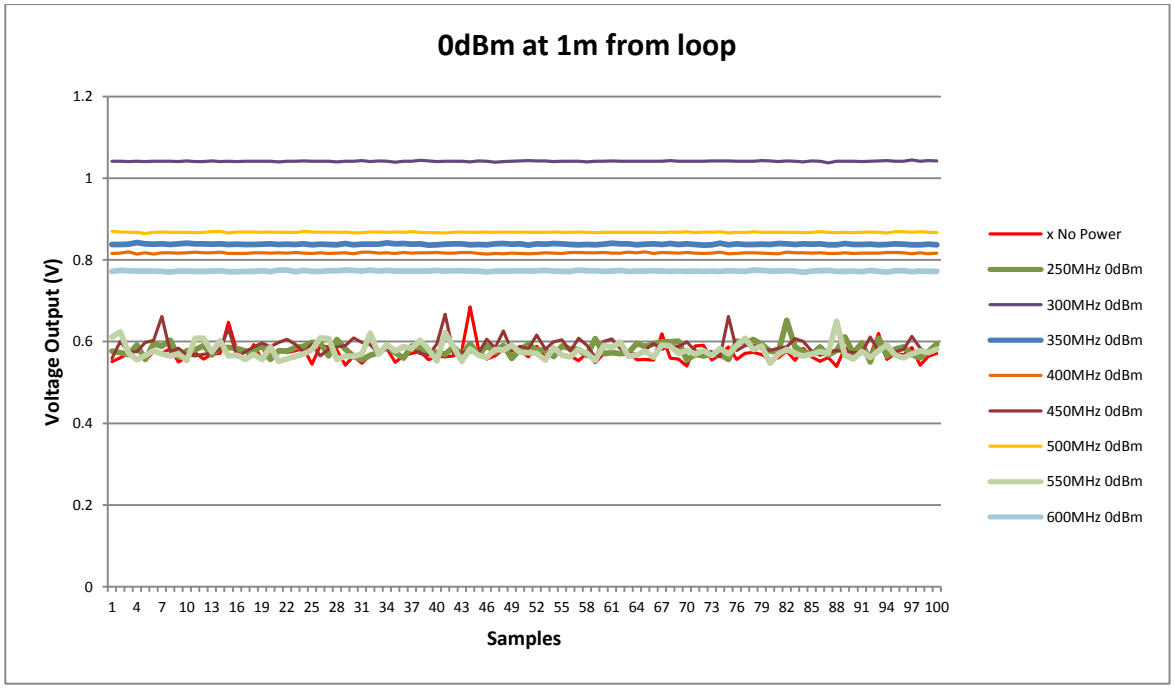

Figure 106: Sensor position 1m

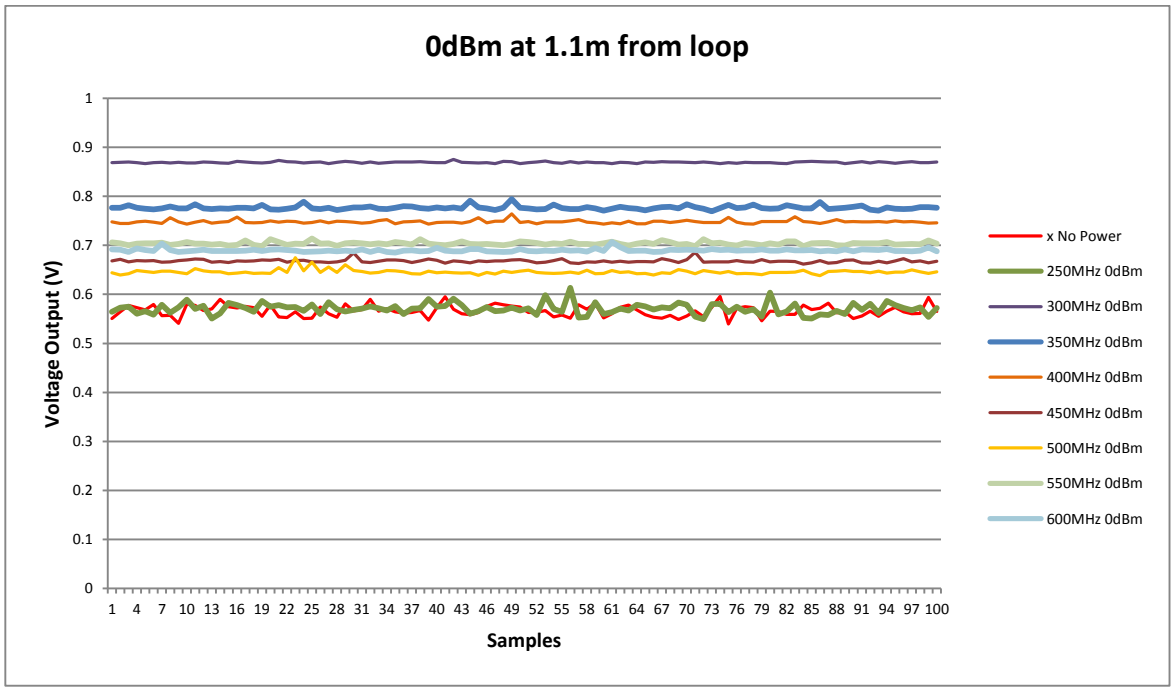

Figure 107: Sensor position 1.1m

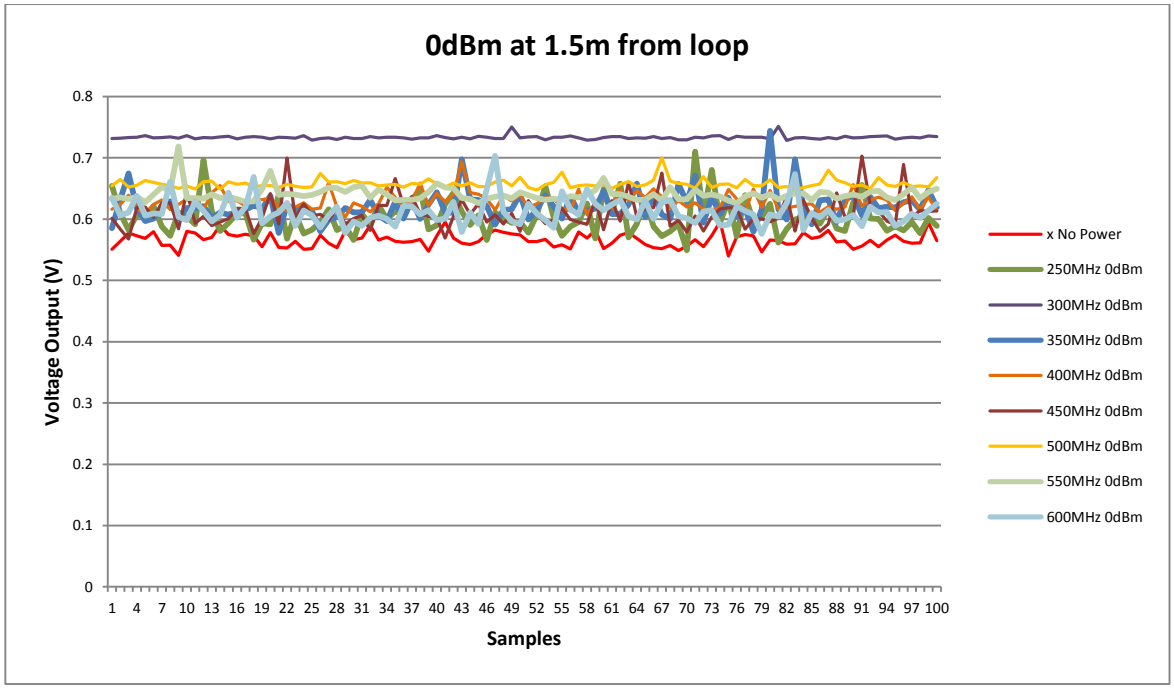

Figure 108: Sensor position 1.5m

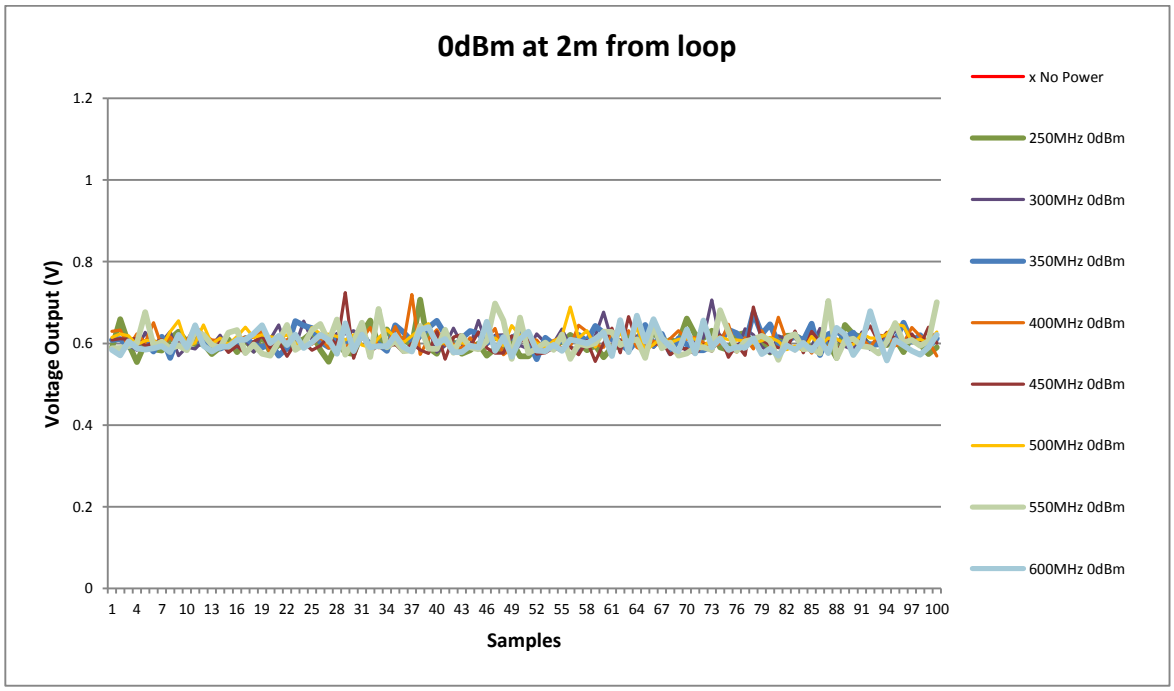

Figure 109: Sensor position 2m

Furthermore, at 1m distance from the fix antenna, the best operation frequency was confirmed to be 300MHz with the smallest attenuation. While at 2m distance, the signal could not be dissociated from the ambient noise level inside pipe at any

frequency as shown in Figure 109.

6.5 Sensor casing

To deploy the sensor inside the water distribution pipe, the electronic circuit needs to be protected against dust ingress and continuous submersion in water, therefore the casing must meet the IP68 rating, the degree of protection provided by enclosures of the British BS EN 60529:1992 standard. Also, the antenna needs to be protected against physical damage caused by collisions with the pipe walls.

To protect the electronic circuit board and the antenna without affecting the electromagnetic waves, a Polyvinyl chloride (PVC) casing was designed using the CAD software SolidWorks [68]. The casing dimensions were provided by the project stakeholders from the water industry. This latest front casing design was dictated by the antenna type used, while its overall dimensions remained unchanged.

For a 90^{o} bent loop, the casing for the straight loop antenna (Figure 58) was no longer convenient, therefore a new casing was designed and is shown in Figure 110 with the integration of two bent loop antennas sizes and a centre hole to accommodate a camera as the sensor is improved in the future.

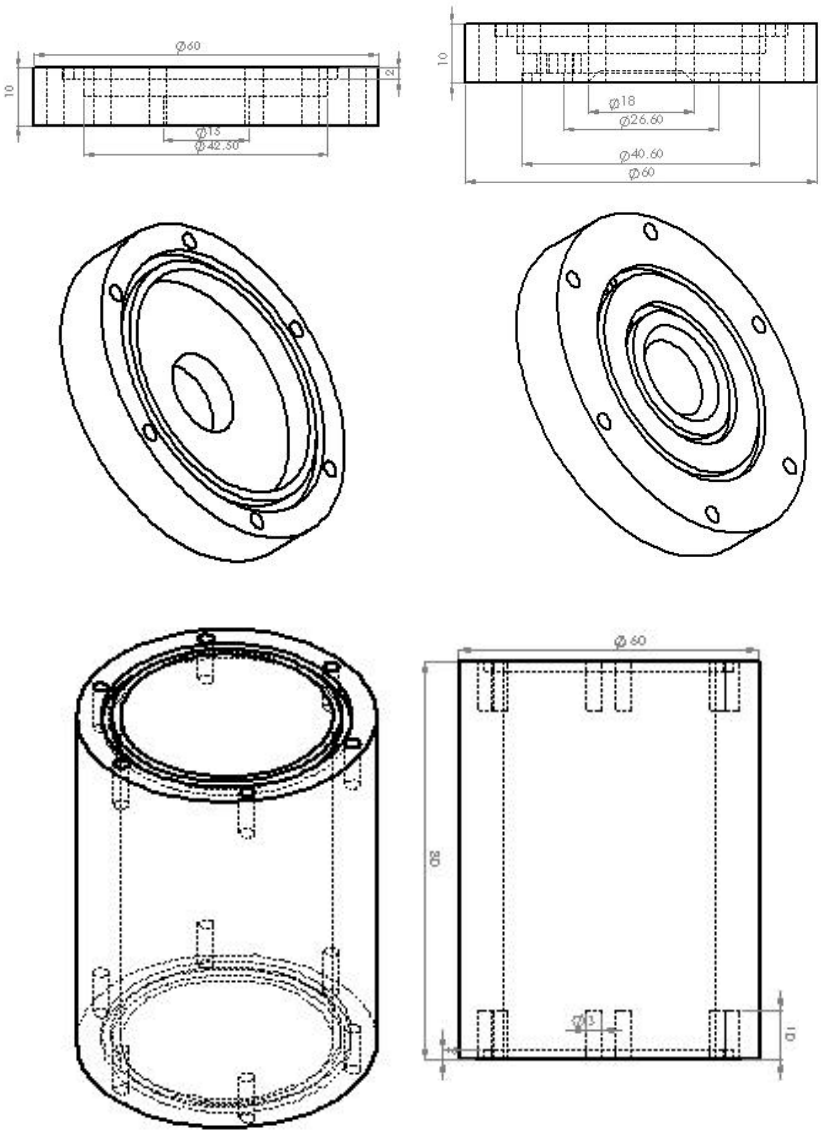

Figure 110: Sensor casing drawings (dimensions in mm)

The casing was then machined in a grey polyvinyl chloride rod [69] shown in the assembly in Figure 111.

Figure 111: Sensor PVC casing assembly

The use of PVC was motivated by the Water Regulations Advisory Scheme (WRAS) safety requirement to prevent waste, misuse and most importantly contamination of public drinking water. According to the WRAS material guidance [70], non-metallic materials should not introduce a change in odour or flavour, change the colour or cause turbidity, increase microbial growth or leach metal or substances harmful to human consumption into the water.

Any component that has to come into contact with drinking water whereby contaminants may be introduced into the public potable water network has to be WRAS approved. However, in general no approval for metallic materials is

considered unless the supplier has a satisfactory method of assessing the effect of the metallic product on the water quality.

Thus only already WRAS approved materials are to be used for the sensor case to allow its use in the field where test site are connected to the public water network as opposed to an independent self-contained loop.

The bill of material of the sensor is included in Appendix 4.

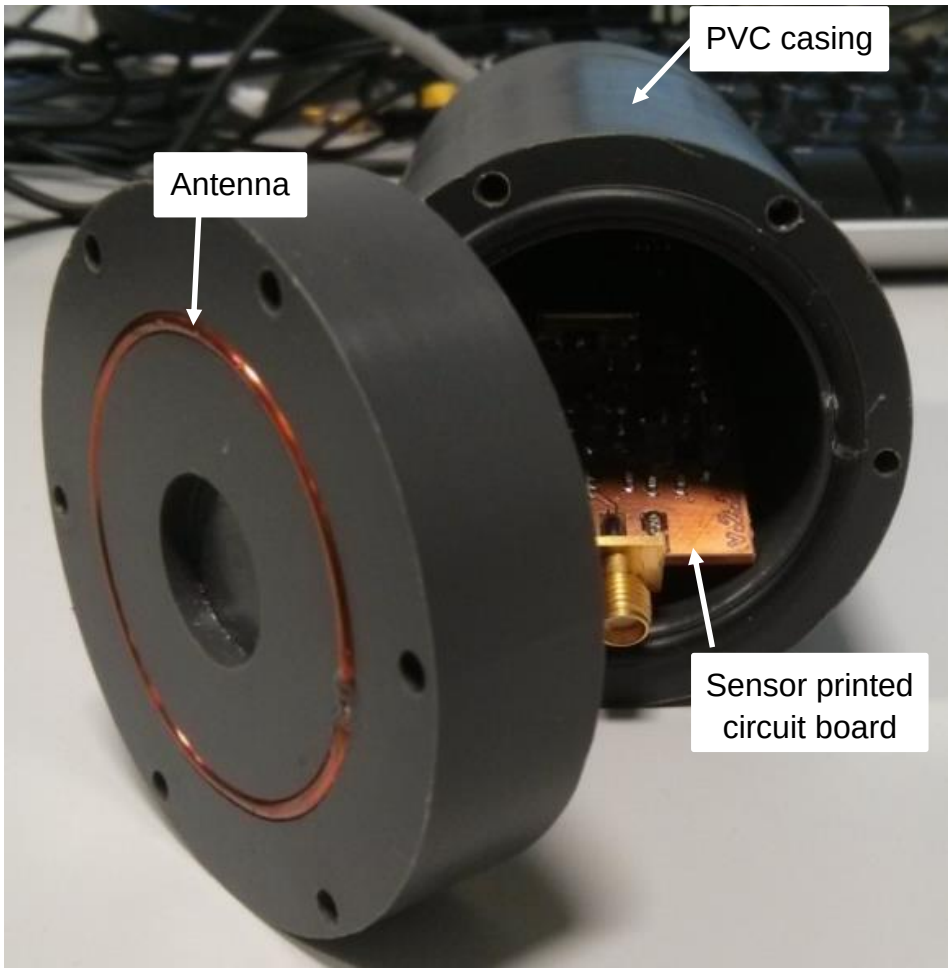

Figure 112: Sensor assembled

When the sensor was fully assembled, no water ingress was observed due to the O-rings on each cap and WRAS approved jointing compound.

6.6 Sensor system setup and operation

The earlier sensor prototype was controlled through an external data acquisition

interface the CompactDAQ NI cDAQ-9172 [71] prior to the introduction of the MAX5312 DAC and Arduino microcontroller as shown in Figure 113.

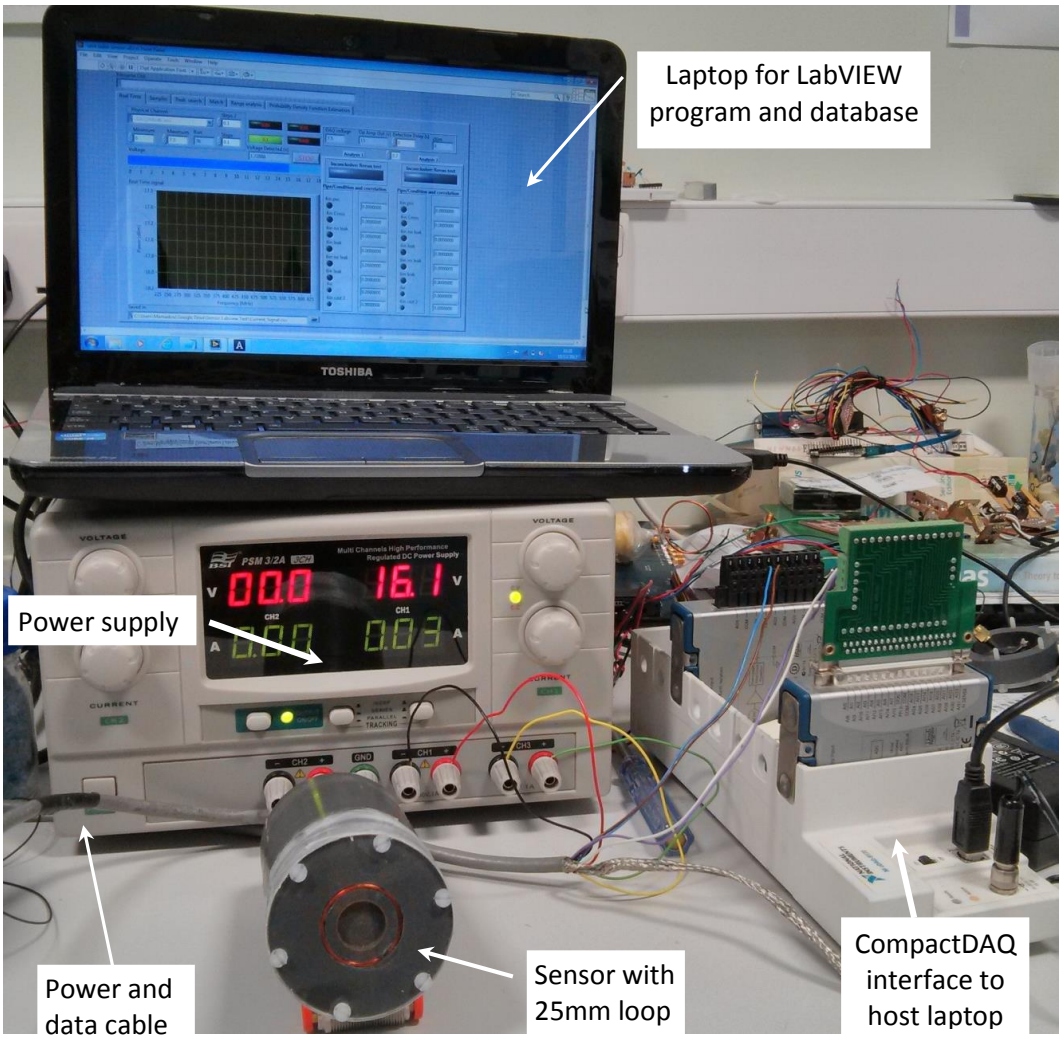

Figure 113: Sensor prototype with NI cDAQ-9172

The sensor was connected to the computer using the external data acquisition CompactDAQ NI cDAQ-9172 with a NI9263, which is a 4-Channel, ±10V, 16-bit analogue voltage output module used to generate the stepped voltage for the ROS-625-219+ VCO frequency generation and the NI9205, a 32-Channel, ±200 mV to ±10V, 16-bit analogue input to read the voltage detected by the MAX2015 power detector.

This setup was bulky and slow. Furthermore, the tuning of the VCO was at a step

of 0.2V, with less than 100 resolution points along the full voltage range.

After the integration of the MAX5312 serial DAC and the Arduino mini pro, the full system setup was much more compact as shown in Figure 114 using our project partner JD7 chassis design.

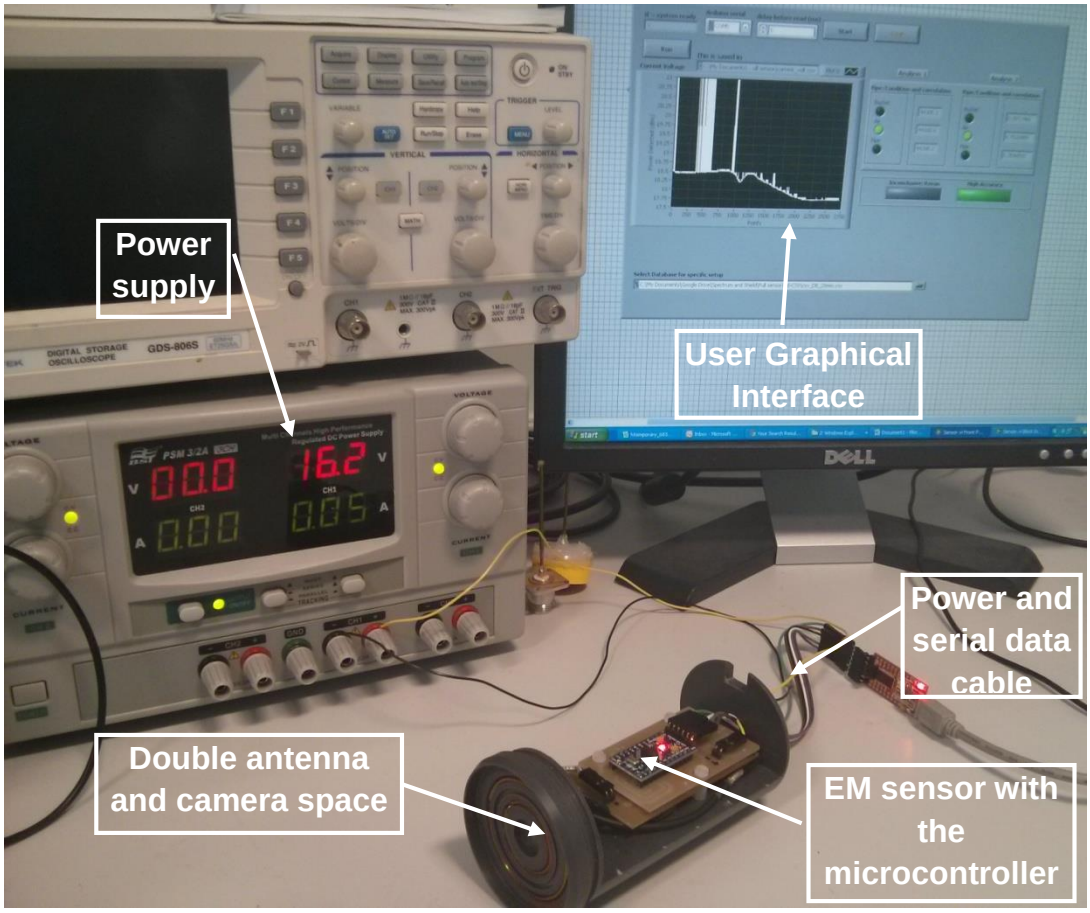

Figure 114: Integrated sensor prototype system setup

The system still required a host computer for the operator and a 16 volts power supply (100mA) as the sensor required 87mA when in operation. A 6 core stranded cable was used for the transmit/receive wire to the microcontroller as well as supplying power to the sensor.

The sensor was connected to the computer using serial communication to LabVIEW at a rate of 115200 baud. With the tuning voltage up to 15 volts, the VCO could

generate a sweep frequency between 247.9MHz and 618MHz. The integration of the DAC and the microcontroller greatly improved the tuning resolution to thousands of points with good signal stability both in frequency and amplitude and the speed of operation was less than 5 seconds for a full sweep of 2710 points.

The operation of the sensor was straightforward as the objective was to allow inexperienced network maintenance engineers to be able to use the system with minimal training.

When the sensor is inserted into the pipe under test, measurements were taken at regular interval that can be tracked as the length of the data cable is known. The current test measures the reflected power that is detected through the logarithmic MAX2015 power detector. This detector provides output voltage proportional to the input power. Due the small variation range, the detected signal is converted into decibels using equation (45) :

$$\boldsymbol{V(dB) = 20log\left(\frac{V(V)}{1V}\right)} \qquad (45)\ [44]$$

The current data sample acquired by the sensor is compared against each stored signature in the database in real-time applying the two data analysis methods implemented in LabVIEW.

The sensor was tested on the 12m rig in the lab with different pipe sections connected. The sensor was inserted into the water pipe filled with water and positioned using a set of Ø20mm PVC round conduit marked along its length according to the rig pipe section.

Tests carried out using the 25mm and 39mm bent loop antenna alternatively with the sensor showed distinct frequency responses. Different pipe sections showed corresponding match from samples stored in the database and shown from Figure

115 to Figure 118 with the 25mm loop to the left and 39mm loop to the right.

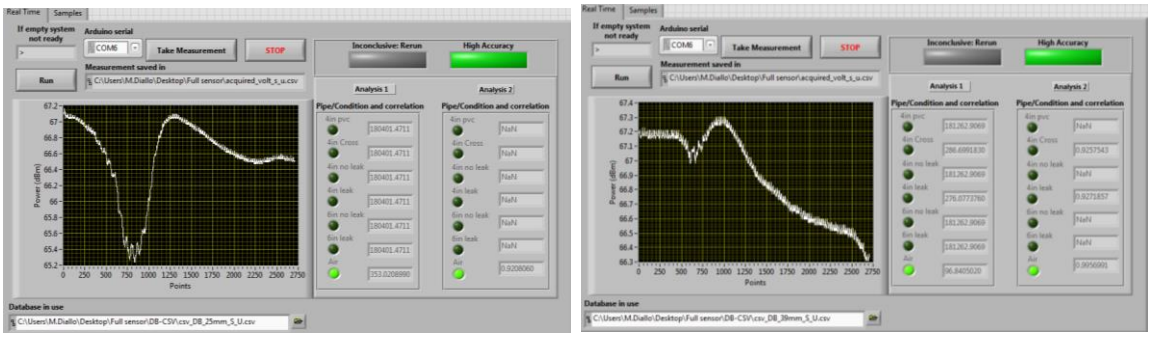

Figure 115: Sensor in air

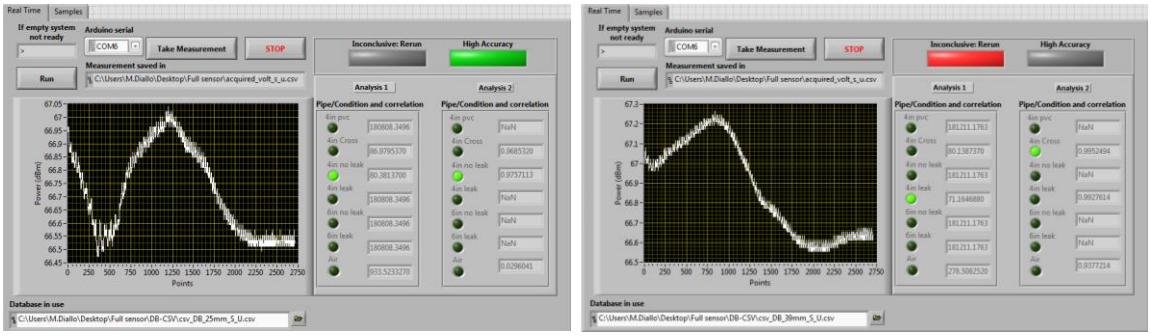

Figure 116: 4 inch no leak

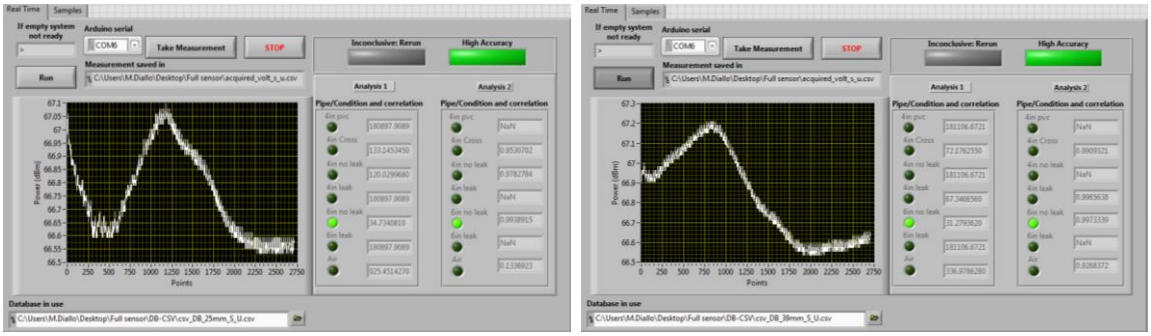

Figure 117: Cast iron 6 inch no leak

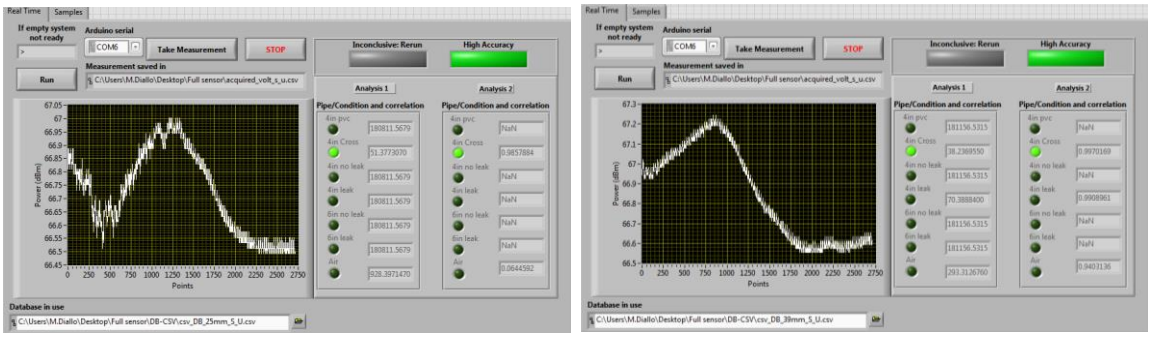

Figure 118: Cast iron 4 inch cross section

The test results above positively identifies the pipe type and or condition as stored in the database. This sensor with the integrated DAC and evaluation has shown remarkable performance. However, a closer look to the correlation values shows a very small margin between one pipe type or condition detected to the next different pipe between as low as 0.003 to 0.015. This tiny different between the results means the slightest change on the signal will impact the results as the accuracy of the sensor decreases.

To verify the accuracy of the electromagnetic sensor and to validate the results from the test, a camera was integrated, allowing visual verification of the results returned on the display.

This visual inspection module should operate without interfering with the electromagnetic wave sensor.

Figure 119: Sensor head with camera and LEDs lights

To investigate this potential impact, an off the shelf camera - HUE HD [72] in Figure 119 - was used to determine the interference level over the signal generated by the electromagnetic sensor. This USB camera was mounted in a replica sensor case use for the prototype. A 5m USB cable ran from the camera to the computer and a 5m coaxial cable connected the integrated loop antenna to the Rhode & Schwarz ZVL-3GHz VNA.

The concern was that when the 12 light emitting diodes (LED) ring is turned On - Figure 120 - to improve visibility in the water pipe, this might interfere with the frequency response from the electromagnetic sensor.

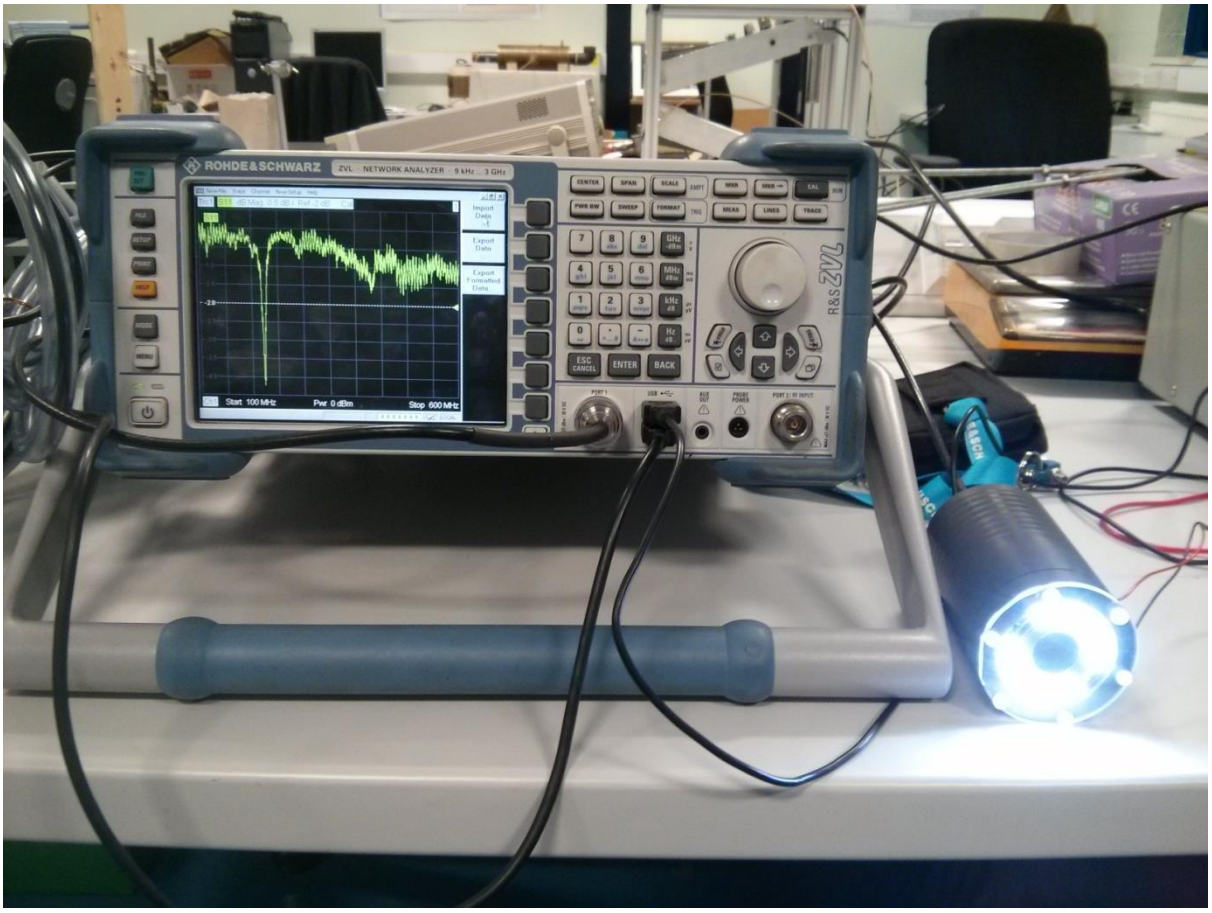

Figure 120: LEDs lights ring

This is because, LEDs on or off may change the electromagnetic signal frequency response.

The effect of the LEDs was tested both in air and in water using the sensor head in Figure 119. The sensor was pushed inside the rig filled with water and then measurements were taken with and without the LEDs on for comparison using the setup shown in Figure 121.

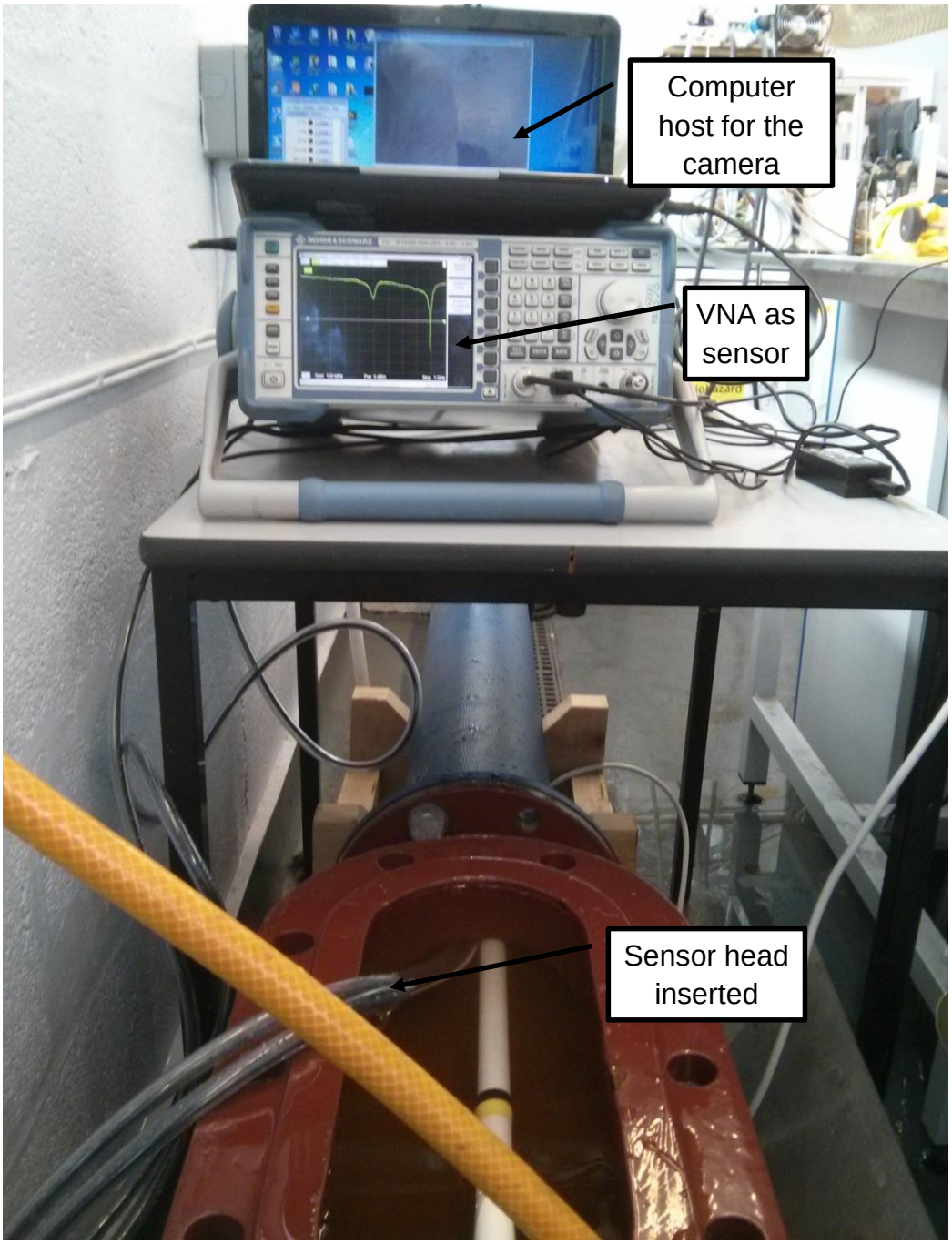

Figure 121: Test setup in the lab

The first test consisted of checking the LEDs effect on the frequency response in air. Both traces of the frequency response with and without the LEDs On were plotted and compared Figure 122. The results showed little effect from the LEDs operation.

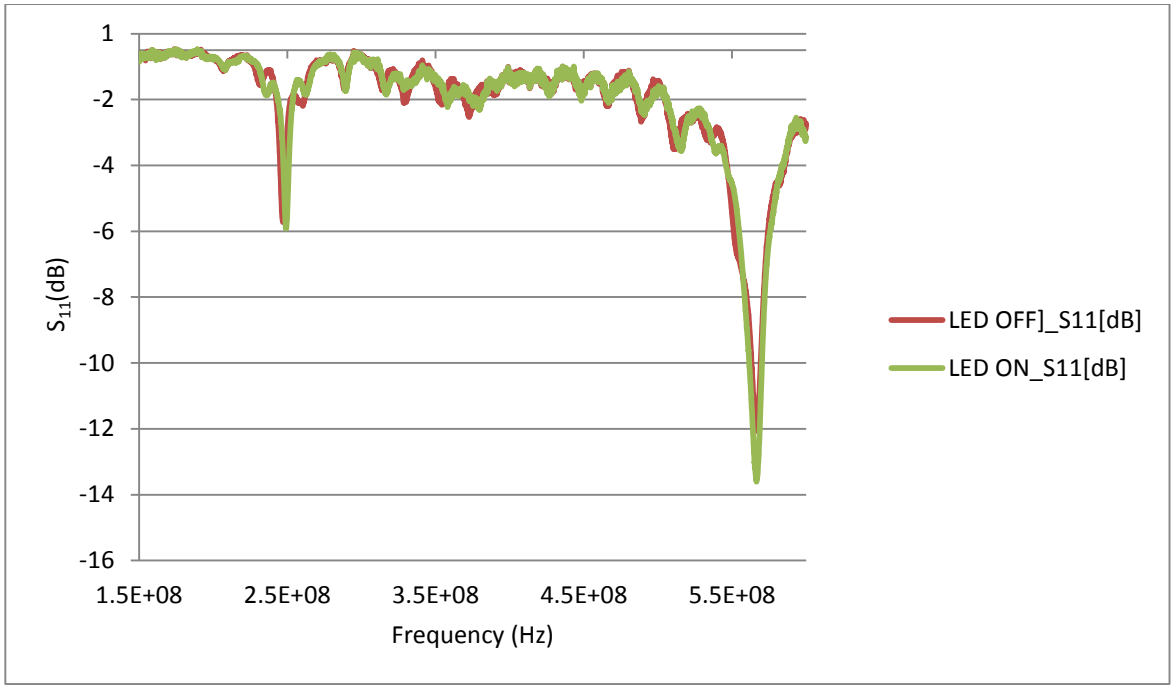

Figure 122: LEDs test in air

The next test was carried inside the pipe filled with water which, however showed very slight shift on the frequency and amplitude as observed in Figure 123.

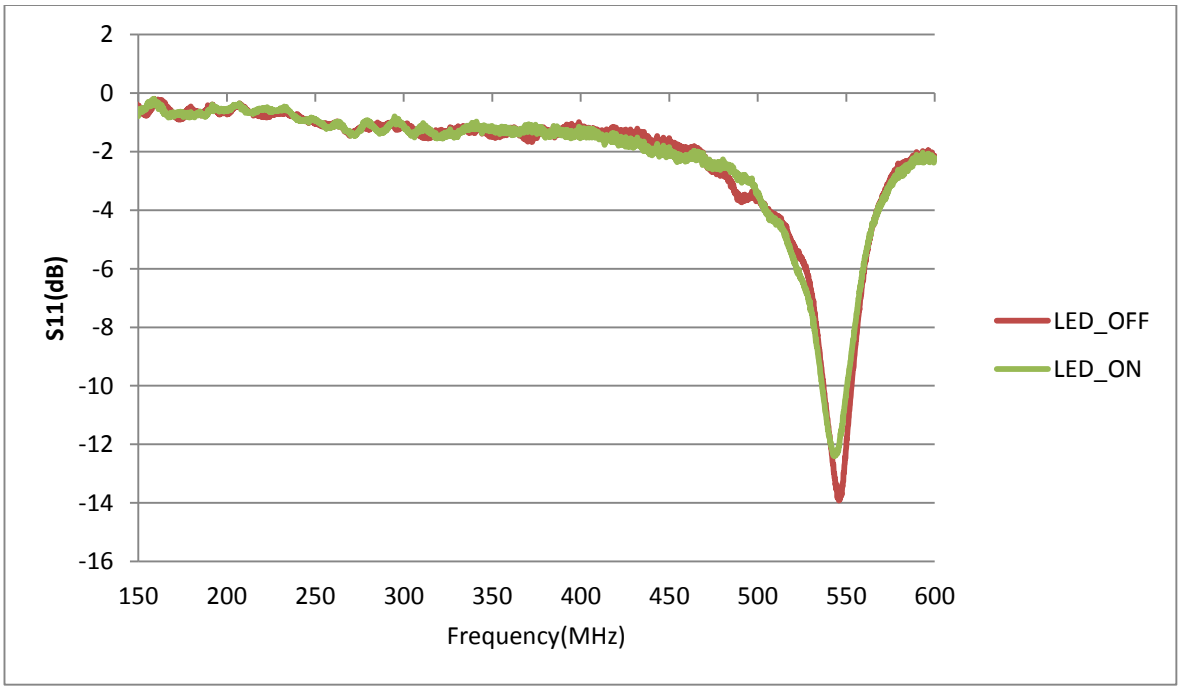

Figure 123: LEDs test in water

The results showed that using the LEDs did not significantly affect the signature.

While carrying out this testing, a pocket of air was discovered inside the top part of the test rig in the lab. This discovery was made thanks to the use of the camera.

In a real situation, the operator would visually confirm that no air pockets such as the one shown in Figure 124 are present using the camera which will affect the frequency response thus changing the signature due the difference in dielectric properties. Air pockets are not expected in water pipes under pressure unless there is a severe pressure issue due to a failure in the network therefore this visual inspection module is expected to be used primarily for confirming pipe type or status when the electromagnetic sensor results are inconclusive.

Figure 124: (a) Air pocket in non-inclined and (b) inclined pipe

To minimise the air pocket, one end of the rig was lifted enough to reduce the air pocket in the water filled pipe as shown in Figure 124.

Below are some snap shots taken using the camera to confirm the internal condition of the pipe.

Figure 125: Reducer to 4inch cross section

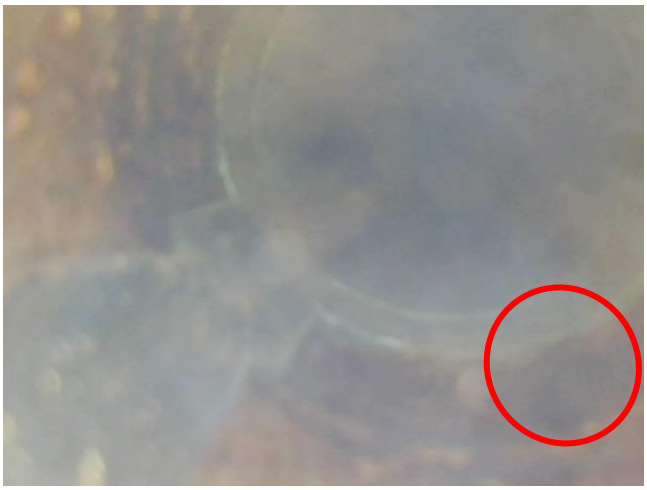

Figure 126: Cross section to 4inch cast iron.

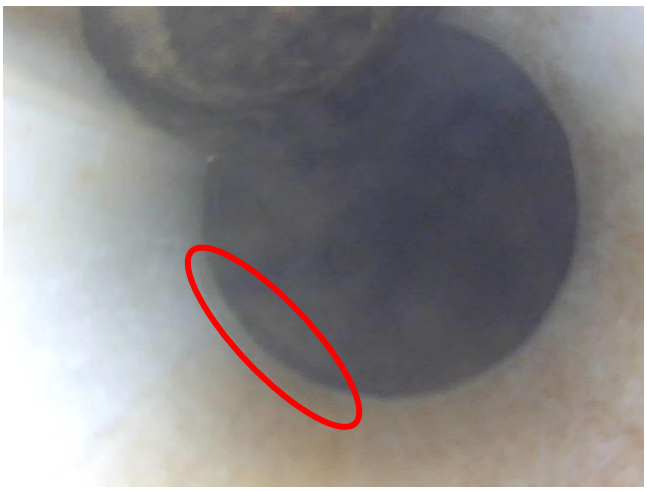

Figure 127: Cast iron to PVC.

The integration of the camera had shown the potential of considerably improving the asset management side of the sensor capability by increasing it detection rate. However, more work is needed in order to truly integrate the camera module with the electromagnetic sensor by implementing an image processing algorithm to compare snapshots with saved samples alongside the frequency response analysis.

6.7 Summary

An incremental design method was used to develop the sensor system prototype using off-the-shelf components before progressing to surface mount components on a single printed circuit board to fit into the designed waterproof casing in line with agreed dimensions. A graphical user interface with a traffic light system was designed to minimise the training requirement for the users, saving the water companies time and money. This integrated sensor prototype was then tested in the lab using a rig with various pipe sections and conditions. Results showed that the electromagnetic wave sensor prototype can be used for leak detection and asset management as it conclusively detected the pipe condition and diameter of the Ø118mm and Ø170mm pipes section on test rig in the lab.

Chapter 7: Conclusion

The overall aim of this research was to develop a non-destructive sensor for leak detection and asset management for the water industry.

The novelty of this work has been its focus on the water distribution network as an asset that include leaks and pipe infrastructure of different materials and diameters. This has led to the development of a novel method of detection using an electromagnetic sensor capable of detecting pipes materials, diameters and conditions to improve leak detection and asset management in the water industry without extensive digs and modifications to the existing access valves for system deployment. Furthermore, this sensor can potentially be used in the gas industry by modifying the frequency of operation to match gas filled cylindrical metal structures.

The development of the sensor was constrained by the requirements set by the project partners regarding its size and the material coming into contact with drinking water, as well as cost saving through ease of operation by field engineers. The size constraint dictated the use of the 90^{o} bent loop antenna which allowed the overall sensor size to be kept within 100mmx60mm as set by the industrial partners.

To achieve the aim of the research, some objectives were set such as reviewing currently used leak detection techniques, investigating electromagnetic wave propagation in the standard ductile iron cement lined water pipe, designing a suitable antenna for the sensor, developing the sensor system and a prototype and finally evaluating the performance of the electromagnetic wave sensor prototype.

- The current techniques used in the water industry and ongoing research to improve leak detection and locate buried assets, were reviewed and this highlighted their limitations due to environmental interference and poor

knowledge of pipe location. These techniques also focus mainly on detecting leaks when they are reported without considering the state of the infrastructure and missing or unrecorded branches all together. Regulatory and public pressure has been pushing the water industry to reduce the water wastage thus the need for a novel system.

- The propagation of electromagnetic waves were investigated and it has been shown that the standard ductile iron cement lined water distribution pipes act like cylindrical waveguides and as such electromagnetic waves above a certain cut-off frequency propagate along the pipe in a number of modes. This cut-off frequency was found to be 187.69MHz for the Ø118mm pipe and this frequency would also be suitable for larger pipe diameters.
- Three common antennas were tested for use with the sensor: monopole, patch and loop. Experiments using these antennas proved that the frequency response varies with the diameter and condition of the pipe thereby enabling the use of electromagnetic waves for leak detection and asset management.
- The loop antenna was shown to be better suited for the intended application because of better return loss and physical robustness allowing it to withstand knocks and tolerate the aqueous environment inside the water distribution pipe. The 90^{o} bent loop antenna version proved to be more suitable to be integrated to the PVC casing due the size constraints imposed by the project's industrial partners. These results led to the development and design of a sensor prototype based on the scattering wave theory for a single port device.
- Despite the high attenuation in water, the sensor detection range was

determined to be up to 1.5m. This finding implies that when a dig is required for repair, the detected fault is within 1.5m relative to the sensor head saving in the number of dry digs where excavations do not result in finding the asset let alone pinpointing the fault.

- Results taken with the final prototype in the 12m rig comprising various pipe types and conditions, showed accurate detection of the Ø118mm pipe from the Ø170mm pipe, the leaking pipe from the non-leaking pipe and the cross that simulates on unrecorded branch in the network.

Sourcing potable water requires energy, and wasting this water through leakage increases costs due to pumping and treatment, therefore water companies will see a direct financial benefit from the introduction of this sensor as more previously unrecorded branches are discovered and added to their assets. This novel non-destructive electromagnetic sensor will improve detection rates and reduce costs and benefit the end customer as the down time in case of failure is shortened. The use of the sensor will also require minimal training of the operators due to the simple graphical user interface which displays the test results in real-time allowing for faster planning and repair.

7.1 Future work

To improve the detection rate and the accuracy of this novel electromagnetic sensor prototype, some recommendations for future work were identified.

The amplitude of the detected signal by the power detector currently in the range of 2dB, showed the need to investigate the introduction of an amplifier before the detector in order to improve the detection rate by emphasising changes to the

electromagnetic signal which are used in the correlation with the stored samples.

As the file containing the recorded samples grows, a more advanced storing method will be required using popular platforms such as the open source database MySQL[73] to improve speed and data analysis which will require more sophisticated queries to sort the considerable volume of data.

The frequency range of the voltage controlled oscillator is limited to a 350MHz span while a wider span of 450MHz would provide more comparison points between signatures. To remedy this, direct digital synthesising (DDS) signal generation with sweeping capability should be explored. DDS such as the AD9858[17] would significantly improve speed and accuracy as the frequency range is digitally stored as profiles with up to 32 bits resolution. Furthermore, it will introduce flexibility in modifying the signal parameters by simply loading the required profile. This will also allow the use of an on-board battery to supply power taking the sensor ultimately to an un-tethered version with an on-board storage module.

[17] 1 GSPS Direct Digital Synthesizer. www.analog.com

References

[1] United Utilities Water Limited, “Access Code for use of the Water Supply System for combined supply licensees,” 2014.

[2] J. (CBC N. C. Davison, “City water leaks wasting millions of tax dollars.” [Online]. Available: http://www.cbc.ca/news/canada/city-water-leaks-wasting-millions-of-tax-dollars-1.1048035.

[3] P. Beuken, R., Lavooij, C., Bosch, A., and Schaap, “Low Leakage in the Netherlands Confirmed,” in *Water Distribution Systems Analysis Symposium 2006*, pp. 1–8.

[4] Strategic Management Consultants, “Review of the calculation of sustainable economic level of leakage and its integration with water resource management planning,” 2012. [Online]. Available: http://www.ofwat.gov.uk/sustainability/waterresources/leakage/rpt_com121012smcsell.pdf.

[5] OFWAT, “Ofwat: Regulating the Industry: How do companies perform?: Companies’ performance 2012-13: Reliability and availability,” 2013. [Online]. Available: http://www.ofwat.gov.uk/regulating/reporting/rpt_los2012-13reliability.

[6] OFWAT, “Water Companies in England and Wales: Summary of performance 2010-2011,” 2011. [Online]. Available: http://www.ofwat.gov.uk/regulating/prs_web201110perf_summ. [Accessed: 26-Jul-2013].

[7] A. C. Twort, D. D. Ratnayaka, and M. J. Brandt, *Water Supply*, 5th ed. London: Arnold, 2000, p. 676.

[8] S. B. B. Costello, D. N. N. Chapman, C. D. F. D. F. Rogers, and N. Metje, “Underground asset location and condition assessment technologies,” *Tunn. Undergr. Sp. Technol.*, vol. 22, no. 5–6, pp. 524–542, Sep. 2007.

[9] J. Parker, “Briefing : The real cost of street works,” *Proc. Inst. Civ. Eng. Transp.*, no. November 2008, pp. 175–176, 2010.

[10] Water UK Sustainability Network, “sustainable water: wtate of the water sector report,” London, 2008.

[11] Lord Mitchell, Lord Paul, and Lord Winston, “Water Management,” 2006.

[12] Z. Y. Wu, “Innovative Optimization Model for Water Distribution Leakage

Detection," *Methods*. Marbella (Spain), pp. 1–8, 2008.

[13] Department for Transport, "Street Works (Charges for Unreasonably Prolonged Occupation of the Highway) (England) Regulations 2011." [Online]. Available: http://www.legislation.gov.uk/ukia/2012/23/pdfs/ukia_20120023_en.pdf. [Accessed: 29-Apr-2012].

[14] Department for Culture Media and Sport, "Microtrenching and Street Works: An advice note for Local Authorities and Communications Providers," 2011. [Online]. Available: https://www.gov.uk/government/uploads/system/uploads/attachment_data/file/77427/Microtrenching_guidance_NOV2011.pdf. [Accessed: 01-May-2014].

[15] J. Parker and U. K. W. I. Research, *Minimising Street Works Disruption: An Overview of the VISTA Project*. UK Water Industry Research Limited, 2010, p. 35.

[16] N. Baker, *The Street Works (Charges for Occupation of the Highway) (England) Regulations 2012*. UK: Department for Transport, 2012.

[17] N. Metje, P. Atkins, M. Brennan, D. Chapman, H. Lim, J. Machell, J. Muggleton, S. Pennock, J. Ratcliffe, and M. Redfern, "Mapping the Underworld – State-of-the-art review," *Tunn. Undergr. Sp. Technol.*, vol. 22, no. 5–6, pp. 568–586, Sep. 2007.

[18] R. L. Sterling, "Utility Locating Technologies: A Summary of Responses to a Statement of Need Distributed by the Federal Laboratory Consortium for Technology Transfer Utility Locating Technologies: A Summary of Responses to a Statement of Need Distributed by the Federal," 2000.

[19] M. R. Nakhkash, M. and Mahmood-Zadeh, "Water leak detection using ground penetrating radar," in *Ground Penetrating Radar, 2004. GPR 2004. Proceedings of the Tenth International Conference on*, 2004, pp. 525–528.

[20] A. Cataldo, G. Cannazza, E. De Benedetto, and N. Giaquinto, "A TDR-based system for the localization of leaks in newly installed, underground pipes made of any material," *Meas. Sci. Technol.*, vol. 23, no. 10, p. 105010, 2012.

[21] T. Inari, K. Takashima, M. Watanabe, and J. Fujimoto, "Optical inspection system for the inner surface of a pipe using detection of circular images projected by a laser source," *Measurement*, vol. 13, no. 2, pp. 99–106, Apr. 1994.

[22] K. Reber, M. Beller, H. Willems, and O. A. Barbian, "A new generation of Ultrasonic In-Line Inspection Tools for Detecting , Sizing and Locating Metal Loss and Cracks in Transmission pipelines 2002 IEEE ULTRASONICS SYMPOSIUM-666," *Ultrasonics*, vol.

00, no. c, pp. 665–671, 2002.

[23] A. Kadri, A. Abu-dayya, D. Trinchero, R. Stefanelli, and P. Torino, “Autonomous sensing for leakage detection in underground water pipelines,” in *Sensing Technology (ICST), 2011 Fifth International Conference on*, 2011, pp. 639–643.

[24] Pure Technologies Ltd, “SmartBall | Water Main Leak Detection.” [Online]. Available: http://www.puretechltd.com/products/smartball/smartball_leak_detection.shtml. [Accessed: 22-Oct-2012].

[25] J. H. Goh, A. Shaw, J. D. Cullen, a. I. Al-Shammaa, M. Oliver, M. Vines, and M. Brockhurst, “Real Time Water Pipes Leak Detection Using EM Waves for the Water Industry,” *2009 Second Int. Conf. Dev. eSystems Eng.*, no. 5, pp. 431–436, Dec. 2009.

[26] G. S. S. Regulations, W. Supply, S. Services, C. S. Standards, and T. Gss, “1 . The guaranteed standards scheme,” 2009.

[27] OFWAT, “Water meters – your questions answered,” 2013. [Online]. Available: http://www.ofwat.gov.uk/mediacentre/leaflets/prs_lft_101117meters.pdf. [Accessed: 03-May-2014].

[28] Worcester-Bosh Group, “Pressure to perform under new water restrictions - Worcester, Bosch Group UK homeowner site,” 2006. [Online]. Available: http://www.worcester-bosch.co.uk/homeowner/our-company/news/pressure-to-perform-under-new-water-restrictions-. [Accessed: 10-Jan-2012].

[29] Manchester Evening News, “Hear we go to stop leaks! - Manchester Evening News.” [Online]. Available: http://www.manchestereveningnews.co.uk/news/greater-manchester-news/hear-we-go-to-stop-leaks-897090. [Accessed: 20-May-2012].

[30] ADI Leak Detection, “Water Leak Detection London - 0800 731 3843.” [Online]. Available: http://adileakdetectionlondon.co.uk/blog/. [Accessed: 15-Mar-2012].

[31] T. W. Miller, B. Borchers, J. M. H. Hendrickx, S. Hong, L. W. Dekker, and C. J. Ritsema, “Effects of soil physical properties on GPR for landmine detection,” in *Fifth International Symposium on Technology and the Mine Problem*, 2002.

[32] Complete Detection Ltd, “Pipe Tracing | Water Leak | Auckland | Complete Detection.” [Online]. Available: http://www.completedetection.co.nz/pipe-tracing.php. [Accessed: 13-Mar-2012].

[33] Concrete Imaging Australia Pty Ltd, “Ground Penetrating Radar Surveys (GPR)

« Concrete Imaging Australia Pty Ltd.” [Online]. Available: http://www.concreteimaging.com.au/services/ground-penetrating-radar-surveys. [Accessed: 15-Jun-2012].

[34] R. K. Miller, A. A. Pollock, D. J. Watts, J. M. Carlyle, A. N. Tafuric, and J. J. Y. Jr, “A reference standard for the development of acoustic emission pipeline leak detection techniques,” *NDT E Int.*, vol. 32, no. 1, pp. 1–8, Jan. 1999.

[35] O. Hunaidi, “Detecting Leaks in Water-Distribution Pipes,” *Construction*, no. 40, 2000.

[36] Q. Wan, D. B. Koch, and K. W. Morris, “Multichannel spectral analysis for tube leak detection,” *Power*, no. 4–7 Apr 1993, p. 4, 1993.

[37] J. Yang, Y. Wen, and P. Li, “Leak acoustic detection in water distribution pipelines,” *2008 7th World Congr. Intell. Control Autom.*, pp. 3057–3061, Jun. 2008.

[38] M. Bimpas, A. Amditis, and N. Uzunoglu, “Detection of water leaks in supply pipes using continuous wave sensor operating at 2.45 GHz,” *J. Appl. Geophys.*, vol. 70, no. 3, p. 226, 2010.

[39] A. C. Twort, D. D. Ratnayaka, and M. J. Brandt, *Water Supply*. Butterworth-Heinemann, 2000, p. 676.

[40] Saint-Gobain PAM UK, “Product Catalogues: Pipes & Fittings ,” *Catalogue*, 2012. [Online]. Available: http://www.saint-gobain-pam.co.uk/assets/docs/ws/Pipes_Fittings_ProductGuide.pdf. [Accessed: 08-Feb-2013].

[41] R. Netting, “Electromagnetic Waves - different waves, different wavelengths,” *NASA*, 2007. [Online]. Available: http://science.hq.nasa.gov/kids/imagers/ems/waves3.html. [Accessed: 11-Jul-2013].

[42] D. K. Cheng, *Field and wave electromagnetics*. Addison-Wesley, 1989, p. 703.

[43] K. F. Sander and G. A. L. Reed, *Transmission and propagation of electromagnetic waves Electronics texts for engineers and scientists*, 2, illustr. CUP Archive, 1986, p. 458.

[44] Y. Huang and K. Boyle, *ANTENNAS from theory to practice*, Illustrate. John Wiley and Sons, 2008, p. 363.

[45] ANSYS, “ANSYS HFSS.” ANSYS, Inc. Southpointe, 275 Technology Drive Canonsburg,

PA 15317 USA, 2010.

[46] C. A. Balanis, *Advanced Engineering Electromagnetics*. New York: John Wiley & Sons, Inc., 1989, p. 981.

[47] R. Schmitt, *Electromagnetics Explained: A Handbook for Wireless/RF, EMC, and High-speed Electronics*. Newnes, 2002, p. 359.

[48] ROHDE&SCHWARZ, "R&S®ZVL3 Vector Network Analyzer - Overview - Rohde & Schwarz." [Online]. Available: http://www.rohde-schwarz.com/en/product/zvl3-productstartpage_63493-9015.html. [Accessed: 30-Jan-2014].

[49] J. H. Goh, A. Shaw, J. D. Cullen, A. I. Al-Shamma'a, M. Oliver, M. Vines, and M. Brockhurst, "Water pipe leak detection using electromagnetic wave sensor for the water industry," in *2011 IEEE Symposium on Computers & Informatics*, 2011, pp. 290–295.

[50] M. Hiebel, *Fundamentals of Vector Network Analysis*. Rohde & Schwarz, 2011, p. 420.

[51] T. S. Editor-, T. Bird, and T. S. Bird, "Definition and Misuse of Return Loss," no. 1, pp. 166–167, 2009.

[52] J. H. Goh, "Real time water pipes leak detection using electromagnetic waves for the water industry," Liverpool John Moores University, 2011.

[53] john D. Kraus and Ronald J Marhefka, *Antennas: For All Applications*, Third. New York: McGraw-Hill Education, 2002, p. 938.

[54] C. A. Balanis, *Antenna Theory: Analysis and Design*, vol. 2012. New Jersey: John Wiley & Sons, 2005, p. 1117.

[55] J. D. Kraus, *Antennas*. McGraw-Hill Education, 1988, p. 892.

[56] KELAN, "Double sided copper clad epoxy glass FR4." [Online]. Available: http://uk.farnell.com/kelan/14339/pcb-plain-d-s-100x160mm/dp/149058. [Accessed: 04-Feb-2014].

[57] ROHDE&SCHWARZ, "R&S®SMB-B103 RF and Microwave Signal Generator." [Online]. Available: http://www.rohde-schwarz.co.uk/en/products/test_and_measurement/Signal_Generators/SMB100A-%7C-Overview-%7C-100-%7C-6136.html. [Accessed: 27-May-2014].

[58] HAMEG Instruments GmbH, "HAMEG HMS-3G." [Online]. Available:

http://www.hameg.com/h014_hoo100000.0.html?&no_cache=1&L=0.

[59] Ensinger Ltd, “White Nylon Rod, 500mm x 80mm Diameter.” [Online]. Available: http://docs-europe.electrocomponents.com/webdocs/0bae/0900766b80bae13c.pdf. [Accessed: 28-May-2013].

[60] “AT502-50 - ADVANCE TAPES - TAPE, ALUMINIUM, 50MM | Farnell UK.” [Online]. Available: http://uk.farnell.com/advance-tapes/at502-50/tape-aluminium-50mm/dp/627434. [Accessed: 29-Jan-2014].

[61] Ofwat, “Your water supply and drought.” [Online]. Available: http://www.ofwat.gov.uk/consumerissues/conservingwater/supply/. [Accessed: 01-Oct-2013].

[62] R. Watt-Pringle, “IBM: smarter water for crowded cities - Water Technology.” [Online]. Available: http://www.water-technology.net/features/featureibm-smarter-water-project-smart-cities/. [Accessed: 24-Feb-2014].

[63] National Intruments, “What’s New in NI LabVIEW 2013 - National Instruments,” 2013. [Online]. Available: http://www.ni.com/labview/whatsnew/. [Accessed: 29-May-2014].

[64] David Ray Anderson, Dennis J. Sweeney, and Thomas Arthur Williams, *Statistics: Concepts and applications*. St Paul: West Publishing Company, 1986, p. 687.

[65] CadSoft, “EAGLE (Easily Applicable Graphical Layout Editor).” .

[66] Maxim Integrated, “MAX5312 ±10V, 12-Bit, Serial, Voltage-Output DAC - Maxim.” [Online]. Available: http://www.maximintegrated.com/en/products/analog/data-converters/digital-to-analog-converters/MAX5312.html. [Accessed: 02-May-2014].

[67] Arduino, “Arduino Pro Mini.” [Online]. Available: http://arduino.cc/en/Main/ArduinoBoardProMini. [Accessed: 23-Jan-2014].

[68] Dassault Systèmes, “Student Software 3D MCAD Tools from SolidWorks.” [Online]. Available: http://www.solidworks.co.uk/sw/products/student-software-3d-mcad.htm. [Accessed: 15-Jun-2014].

[69] Ensinger Ltd, “Grey Polyvinyl Chloride (PVC) Rod, 1000mm x 70mm Diameter.” [Online]. Available: http://docs-europe.electrocomponents.com/webdocs/0de8/0900766b80de8d58.pdf. [Accessed: 28-Aug-2013].

[70] Water Regulations Advisory Scheme, “WRAS Material Guidance,” *Version 2.0*,

2013. [Online]. Available: https://www.wras.co.uk/downloads/documents/8.4.2.3_-_wras_materials_guidance_3.44.pdf/. [Accessed: 01-Oct-2014].

[71] National Instruments, “NI cDAQ-9172 - National Instruments.” [Online]. Available: http://sine.ni.com/nips/cds/view/p/lang/en/nid/202545. [Accessed: 30-Jan-2014].

[72] HUE HD, “HUE HD0002.” [Online]. Available: http://www.amazon.co.uk/HUE-HD-red-camera-Windows/dp/B001KPAINS. [Accessed: 18-May-2014].

[73] Oracle Corporation, “MySQL Editions,” 2014. [Online]. Available: http://www.mysql.com/products/. [Accessed: 24-Feb-2014].

Appendices

Appendix 1: VCO with DAC sensor schematic

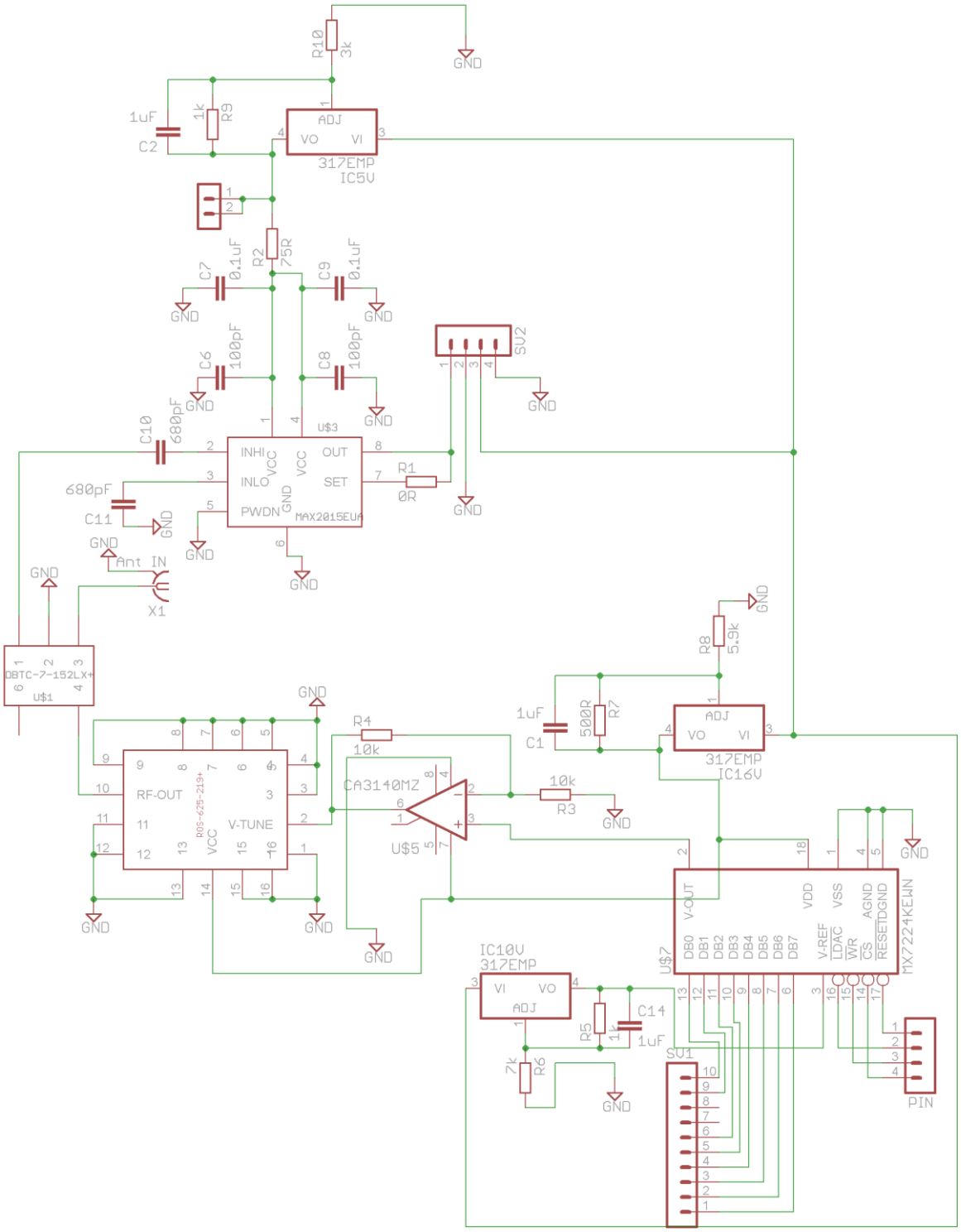

Appendix 2: Arduino 1.0.5.rs sketch used

```
#include <SPI.h>

const int ldacPin = 3;

const int clrPin = 7;

const int uniPin = 8;

const int ssPin = 10;

//pin 11(MOSI) on Arduino connected to pin 2(DIN) on DAC

const int sclkPin = 13;

int VoltDetected = A0; //To read the output from the detector

int val = 0; //Store A0

int timer = 1;

int x = 1;

int command = 0b0100000000000000; // 0100  Load input and DAC registers from shift register;
DAC output updated.

int commandPlusData;

int iB = 0;

void setup() {

 SPI.begin();

 Serial.begin(115200);

 pinMode(ssPin,OUTPUT);

 digitalWrite (ssPin, HIGH);

 pinMode(clrPin,OUTPUT);

 digitalWrite (clrPin, HIGH); //To clear DAC

 pinMode(ldacPin,OUTPUT);

 digitalWrite (ldacPin, HIGH);

 pinMode(uniPin,OUTPUT);

 digitalWrite(uniPin, HIGH); //Needed to set DAC to unipolar mode pin 8 on the dac

}
```

```
void loop() {
 val = analogRead(VoltDetected);// Show data in the terminal window
 Serial.println(">"); //Indicate ready and waiting loop start
 while(1)
 {
  while(iB!=83){ //Capital S to start the DAC sequence
   iB = Serial.read();  //Send space to start back the loop
  }
  iB = 0;
  /*
 The data value set at 2710 generate upto 591.66MHz with 16V supply to the sensor
   */
  for (int data=0b0000000000000000; data < 2710; data = ++x)  // Increment upto data<xxxx
  {
   commandPlusData = command | data;
   digitalWrite (ssPin, LOW); // pin 10 - initiate serial communication
   SPI.transfer (highByte (commandPlusData));
   SPI.transfer (lowByte (commandPlusData));
   digitalWrite (ssPin, HIGH);
   Serial.print(data); //Show data in the terminal window
   Serial.print(",");
   delay(timer);
   Serial.println(val);//Show in the terminal window the saved input to the analog pin
}
  Serial.println("#"); //Indicate end of loop as Serial.write(35) but newline after
};
}
```

Appendix 3: LabView block diagram

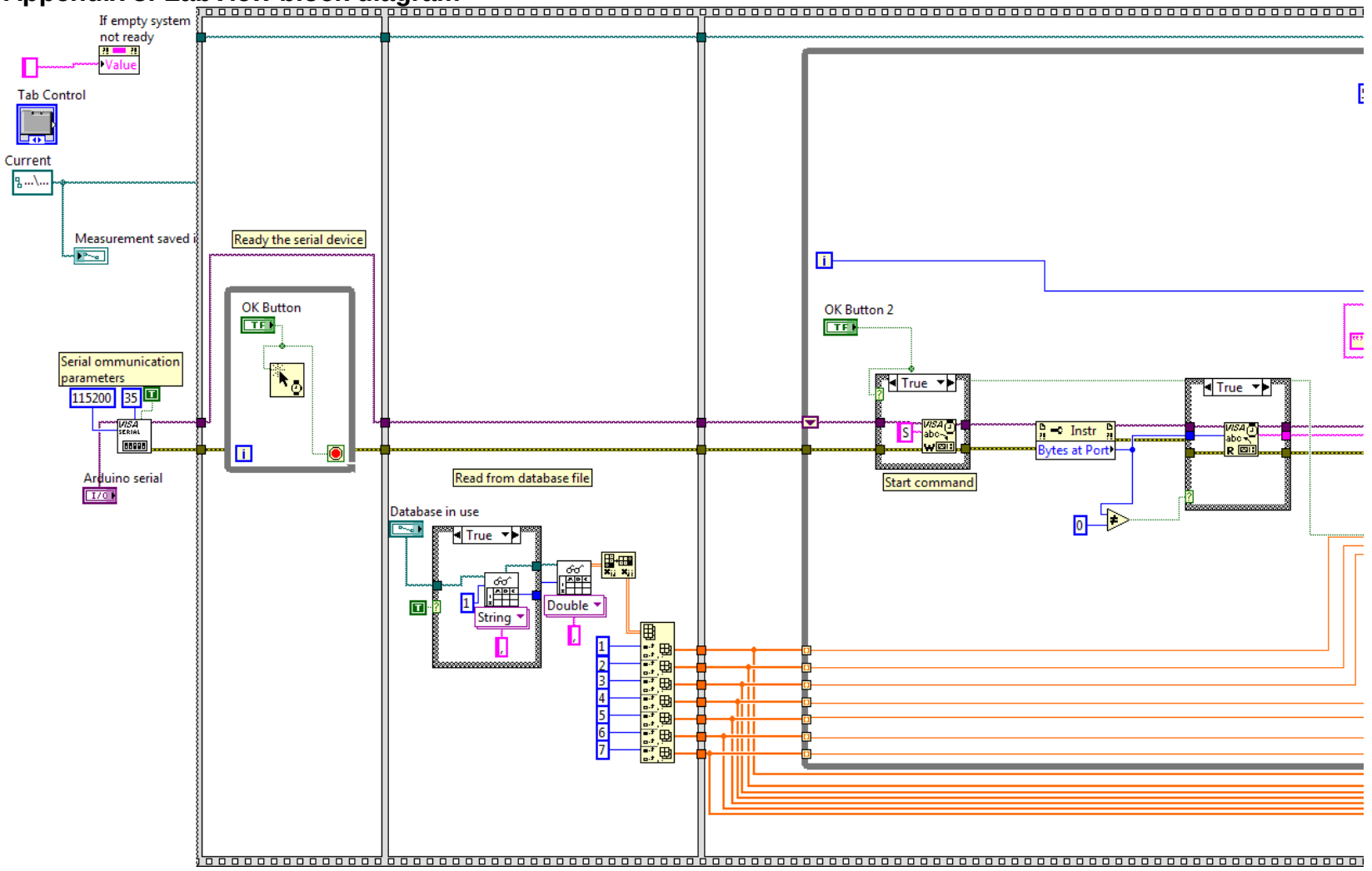

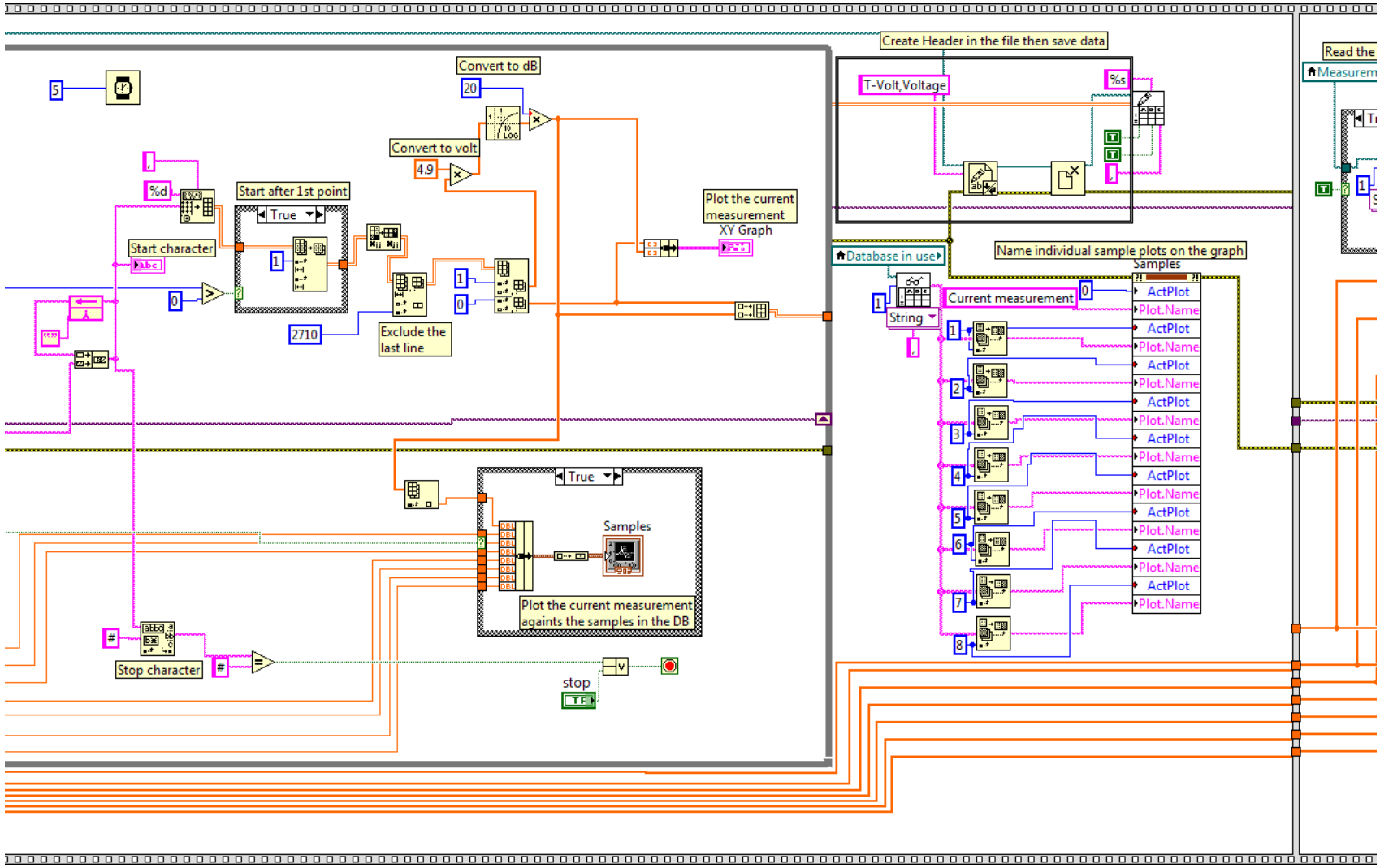
Create Header in the file then save data
T-Volt,Voltage
%s
Convert to dB
20
Convert to volt
4.9
Start after 1st point
True
%d
Start character
Plot the current measurement XY Graph
2710
Exclude the last line
Database in use
String
Name individual sample plots on the graph
Samples
Current measurement
ActPlot
Plot.Name
True
Samples
Plot the current measurement againts the samples in the DB
Stop character
stop
Read the

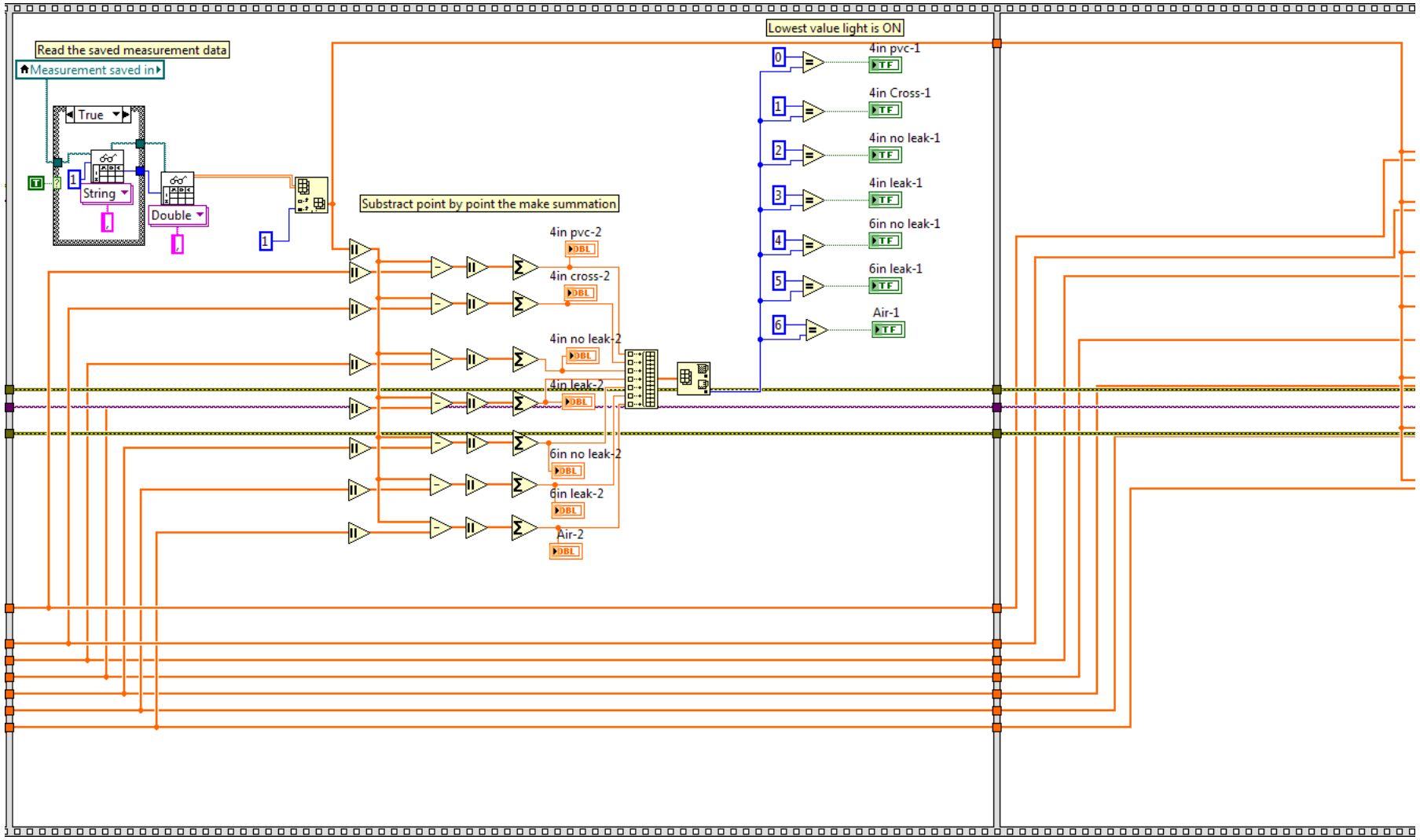
Read the saved measurement data
Measurement saved in
True
String
Double
Substract point by point the make summation
4in pvc-2
4in cross-2
4in no leak-2
4in leak-2
6in no leak-2
6in leak-2
Air-2
Lowest value light is ON
4in pvc-1
4in Cross-1
4in no leak-1
4in leak-1
6in no leak-1
6in leak-1
Air-1

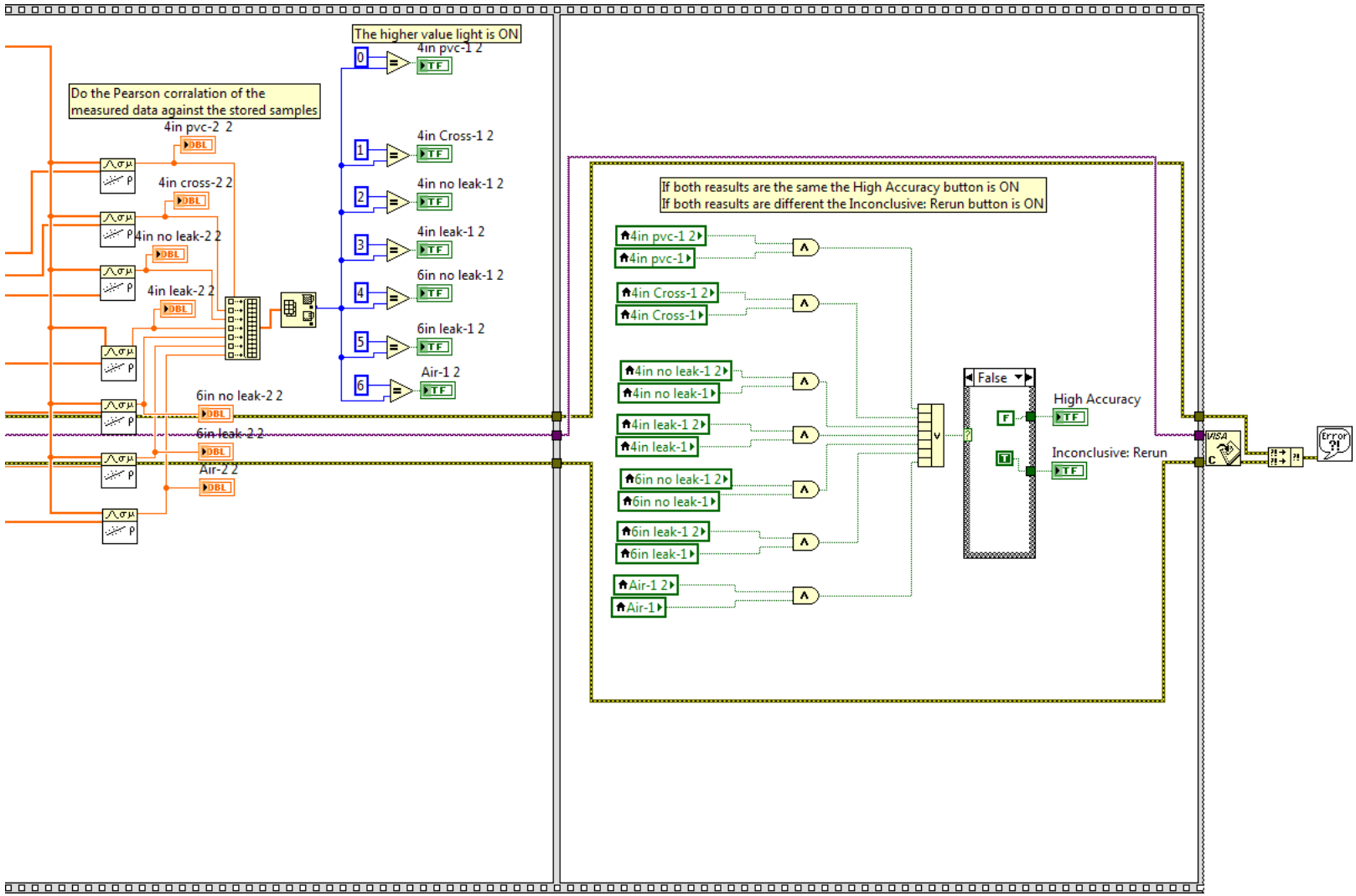
The higher value light is ON
Do the Pearson corralation of the measured data against the stored samples
4in pvc-2 2
4in cross-2 2
4in no leak-2 2
4in leak-2 2
6in no leak-2 2
6in leak-2 2
Air-2 2
4in pvc-1 2
4in Cross-1 2
4in no leak-1 2
4in leak-1 2
6in no leak-1 2
6in leak-1 2
Air-1 2
If both reasults are the same the High Accuracy button is ON
If both reasults are different the Inconclusive: Rerun button is ON
4in pvc-1
4in Cross-1
4in no leak-1
4in leak-1
6in no leak-1
6in leak-1
Air-1
False
High Accuracy
Inconclusive: Rerun
VISA
Error

Appendix 4: Materials in the sensor manufacturing and use in contact with drinking water

Part	Material	Supplier	Order code	WRAS approval number	WRAS section that may apply?
PVC casing	Grey Polyvinyl Chloride	rs	700-9859		5300 5305
Seal	PTFE Tread seal	The bss group ltd	79024607	1306531	
Pipe Jointing compound	Boss White Universal paste	The bss group ltd	84410700	1312504	
Screw	nylon metric screw	rs	524-095		5175 5180
Cable Access Kit 10m	Glass-reinforced plastic	Screwfix	82483		5120
	Brass connectors				
Transparent camera cover	Acrylic Sheet	rs	824-654		
Straight 3/8in Coupling Body	Acetal	rs	325-0315		5010 5015